

A SENSOR FOR CONTINUOUSLY MONITORING THE BATCH
ANNEALING OF COLD WORKED STEEL STRIP

Simon J.P. Durham

A Thesis Submitted to The Faculty of Graduate Studies
and Research in Partial Fulfillment
of the Requirements for the Degree
Master of Engineering

Department of Mining and Metallurgical Engineering

McGill University

Montreal, Canada

© November 1984

ACKNOWLEDGEMENTS

I would like to thank Prof. W.M. Williams and Dr. R.A.L. Drew for their support and assistance throughout my degree.

I appreciate the assistance of the staff of the Mining and Metallurgical Engineering Department, and would particularly like to thank F. Van Gils, M. Knoepfel, and B. Grondin for their invaluable technical assistance.

Lastly, special thanks go to Linda Zarnon who had the patience to type this Thesis.

To all those who have made me feel so welcome in Montreal

ABSTRAIT

Un capteur résistif a été construit pour étudier les changements métallurgiques qui se produisent lors du recuit en four d'acier au carbone à basse teneur. Le capteur, qui fonctionne sur courant alternatif, a été conçu pour mesurer la chute de tension (ΔV) pendant le recuit entre un échantillon traité à froid et un échantillon du même matériau préalablement recuit. En utilisant cette technique, il est possible de surveiller de façon continue les étapes de recristallisation récupérative et la croissance des grains pendant le procédé. Un microprocesseur a été utilisé pour l'acquisition des données, et d'en tracer les graphes en temps réel, ainsi que pour la manipulation des données. L'étape importante de recristallisation est accentuée en traçant le dérivé de la différence en tension ΔV pendant le traitement à chaleur. Il est également possible de surveiller de la même façon des grains mais la technique doit être raffinée pour améliorer la fiabilité des résultats. Des suggestions sont offertes, l'une d'elles étant l'incorporation de capteur dans un système de contrôle en feedback du recuit de l'acier en four.

ABSTRACT

A resistivity sensor has been designed to follow the metallurgical changes that occur during the batch annealing of low carbon steel. The sensor utilizes an A.C. technique designed to measure the difference in voltage (ΔV) between a cold worked sample of the material being annealed and an annealed reference standard made of the same material. It is possible using this technique, to continuously monitor the recovery, recrystallization, and grain growth stages during annealing. A microprocessor system has been used for data acquisition, enabling real time plotting and data manipulation. The important recrystallization stage is highlighted by arranging for the plotting of the derivative of ΔV during heat treatment. It was also possible to monitor grain growth continuously, but the technique needs further refinement to improve the reliability of the results. Suggestions are made as to how the sensor could be incorporated in a feedback control system for the batch annealing of steel.

CONTENTS

	PAGE
<u>CHAPTER 1</u>	
1.1 INTRODUCTION	1
1.1.1 LATTICE DEFECTS	1
1.1.2 THE ROLE OF DISLOCATIONS IN WORK HARDENING	6
1.1.3 PRECIPITATION HARDENING	8
1.1.4 RECOVERY, RECRYSTALLIZATION AND GRAIN GROWTH	16
1.1.4.1 RECOVERY	18
1.1.4.2 RECRYSTALLIZATION	18
1.1.4.2.1 HOMOGENEOUS NUCLEATION	19
1.1.4.2.2 HETEROGENEOUS NUCLEATION	20
1.1.4.3 GRAIN GROWTH	22
1.2 INDUSTRIAL ANNEALING	24
1.2.1 INTRODUCTION	24
1.2.2 BATCH ANNEALING	25
1.2.3 CONTINUOUS ANNEALING	26
1.2.4 COMPARISON BETWEEN BATCH AND CONTINUOUS ANNEALING	29
1.2.5 BATCH ANNEALING: ADVANCES AND CURRENT PRACTICES	35
1.2.5.1 GAS VELOCITY	36
1.2.5.2 BURNER EFFICIENCY	36

1.2.5.3	INCREASED COOLING RATES	38
1.2.5.4	PROTECTIVE GAS CIRCULATION	40
1.2.5.5	FURNACE CONTROL AND OPTIMISATION	43
1.3	SUMMARY	47

CHAPTER 2

2.1	OBJECTIVES OF THE PRESENT RESEARCH	48
-----	------------------------------------	----

CHAPTER 3

3.1	DESIGN OF AN ANNEALING SENSOR BASED ON ELECTRICAL RESISTIVITY	50
3.2	ELECTRICAL RESISTIVITY OF METALS	51
3.3	EXPERIMENTAL METHODS FOR DETERMINING ELECTRICAL RESISTIVITY	52
3.4	THE DIFFERENTIAL A.C. TECHNIQUE	54
3.5	APPLICATION OF THE DIFFERENTIAL RESISTIVITY METHOD TO THE ANNEALING OF LOW CARBON STEELS	58
3.6	SENSOR DESIGN	61
3.7	ANNEALING OF REFERENCE STANDARDS	65
3.8	FURNACE CONTROL	68
3.9	ATMOSPHERE CONTROL	70
3.10	EXPERIMENTAL PROCEDURE	70
3.11	DATA ACQUISITION SYSTEM	71
3.12	METALLOGRAPHY AND HARDNESS MEASUREMENTS	74
3.13	MATERIAL SELECTION	75

CHAPTER 4

4.1	INTRODUCTION	77
4.2	GENERAL DISCUSSION OF ANNEALING OF LOW CARBON STEELS	78
4.3	RECOVERY STAGE	84
4.3.1	EXPLANATION OF THE ANOMALOUS RECOVERY BEHAVIOUR	91
4.4	RECRYSTALLIZATION	96
4.5	GRAIN GROWTH	96
4.5.1	CORRELATION OF GRAIN GROWTH WITH DIFFERENTIAL RESISTIVITY MEASUREMENTS	105
4.6	SIMULATION OF BATCH ANNEALING	109
4.7	APPLICATION TO INDUSTRIAL ANNEALING	110

CHAPTER 5

5.1	CONCLUSIONS	116
-----	-------------	-----

CHAPTER 6

6.1	SUGGESTIONS FOR FURTHER WORK	117
-----	------------------------------	-----

APPENDIX I	118
------------	-----

APPENDIX II	123
-------------	-----

APPENDIX III	125
--------------	-----

REFERENCES	127
------------	-----

CHAPTER 1

1.1 INTRODUCTION

For many centuries, the heat treatment of cold worked metals has been used to soften them prior to further fabrication or deformation. This is as true today as it ever was. For example, many metals today are produced in the form of cold rolled strip. At particular stages in the production of the strip, there comes a time when further deformation of the metal will either be very difficult or may even damage it. The strip will have hardened because of the deformation it received and it can only be softened by annealing it at a suitable temperature. Further deformation can then be carried out, for instance, by a pressing or deep drawing process, or by further rolling.

To explain the hardening and softening behaviour of metals due to deformation and annealing, it is necessary to consider how the microstructure of a metal affects its mechanical properties.

1.1.1. LATTICE DEFECTS

An ideal crystalline material has no defects, and the atoms are arranged in an ordered and regular array.

Plastic deformation of a perfect crystal can occur by the sliding of one set of atoms in a plane over the atoms in an adjacent plane. This is called glide, the cooperative movement of all the atoms in a plane from one position of perfect registry to a neighbouring position. The shear stress required to produce this was first calculated by Frenkel¹. In the situation illustrated in Figure 1, it is assumed that the shearing force required to move the top row of atoms across the bottom row is given by the sinusoidal relation:

$$\tau = \frac{b}{2a} \sin \frac{2\pi x}{b} \quad (1)$$

where τ is the shear modulus; b , the interatomic spacing in the direction of shear stress; a , the spacing between the rows of atoms; and x , the distance from the low energy equilibrium position. The theoretical shear stress is thus reduced to:

$$\tau = \frac{b}{a} G \quad (2)$$

Since $b \approx a$, a theoretical shear stress is only a small fraction of the shear modulus. Using a more realistic expression for the theoretical shear stress force as a function of displacement, a value of:

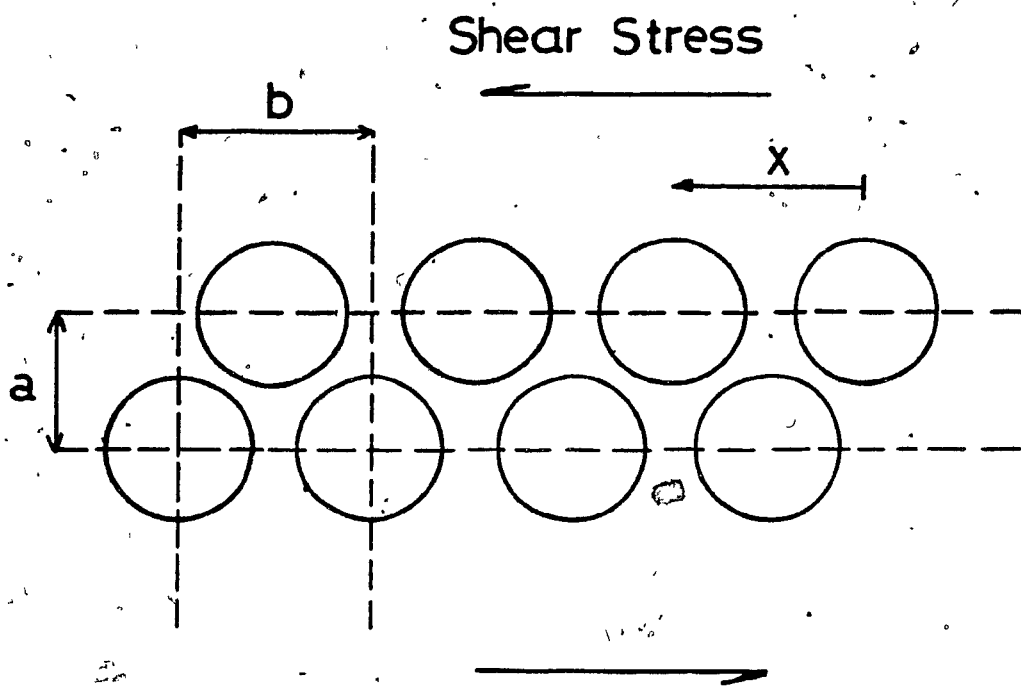


Figure 1.

$$\tau = G/30$$

(3)

for copper, silver, and gold has been obtained.

Although these calculations are only approximate, the shear stresses involved are many orders of magnitude higher than those values obtained experimentally from real materials. It is now generally acknowledged that it is the "defects" present in the material, known as dislocations, that account for the striking difference between theoretical prediction and experiment.

A dislocation is a linear lattice imperfection which is the interface between a fully slipped region of the lattice and an unslipped region. The slipped region may grow at the expense of the unslipped region by the advance of a dislocation through it.

There are two basic types of dislocations: edge and screw dislocations. An edge dislocation can be considered as an additional plane of atoms in an otherwise regular lattice, shown by the line XX' in Figure 2(1). Figures 2(2) and 2(3) illustrate how an edge dislocation moves through the lattice, helping the nucleation and growth of slip deformation in the lattice. The net result, in this case, is the displacement of one plane of atoms over another by one lattice spacing in the direction of movement of the dislocation. Figure 3a shows the region around a typical right hand screw dislocation in a

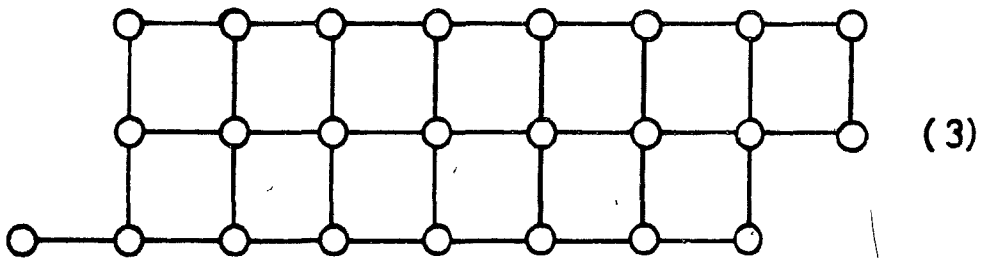
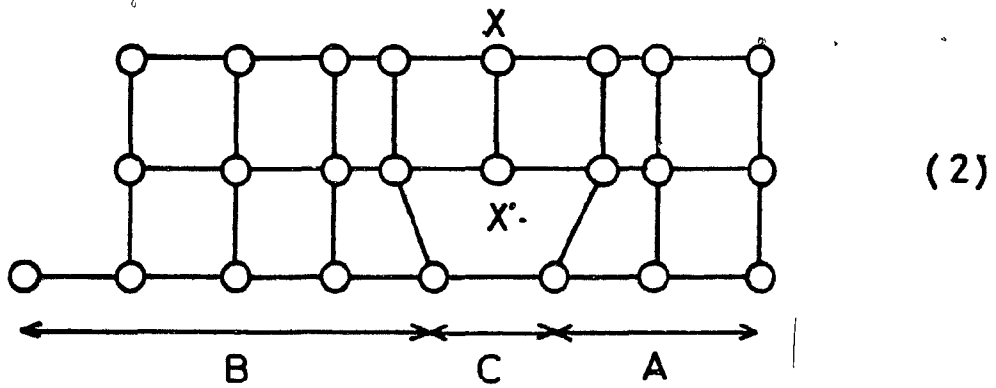
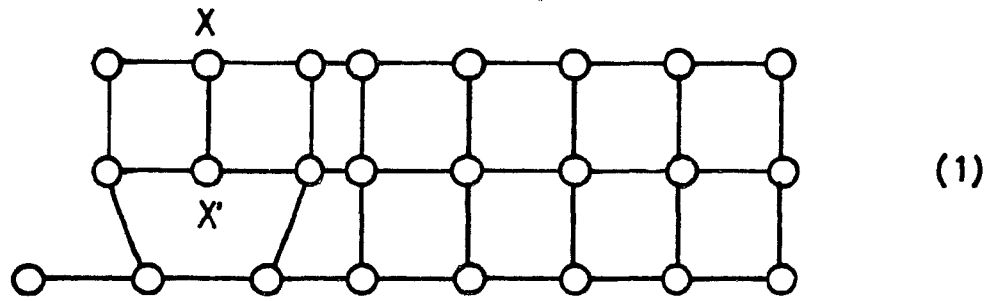


Figure 2. The Movement of a Dislocation through a Regular Lattice.

simple lattice. Unlike the edge dislocation, the planes intersected by the dislocation are no longer a family of separate parallel planes. They are all joined up into a single helicoidal surface -- hence the name screw dislocation. Figure 3b shows the result of the passage of a screw dislocation XX' through a crystal lattice. In this case, the displacement is one lattice spacing perpendicular to the direction of dislocation movement.

1.1.2. THE ROLE OF DISLOCATIONS IN WORK HARDENING

Hardening by plastic deformation is an important means of strengthening certain metals and alloys. For rapid work hardening to occur, plastic deformation on two or more intersecting glide systems is necessary. In cubic structures, there are two distinct stages. The first stage is the "easy glide" of planes over one another. At this point, there is little work hardening before the characteristic rapid rise of the second stage begins. It is during this second stage that the greatest rate of work hardening occurs. The greatest rate of work hardening in pure single crystals, measured over strains which are large compared with the elastic strain, is of the order of $d\sigma/d\varepsilon = \mu/150$. The rate of work hardening rises linearly, but above a certain resolved shear stress, which depends on the temperature, it falls off in a parabolic

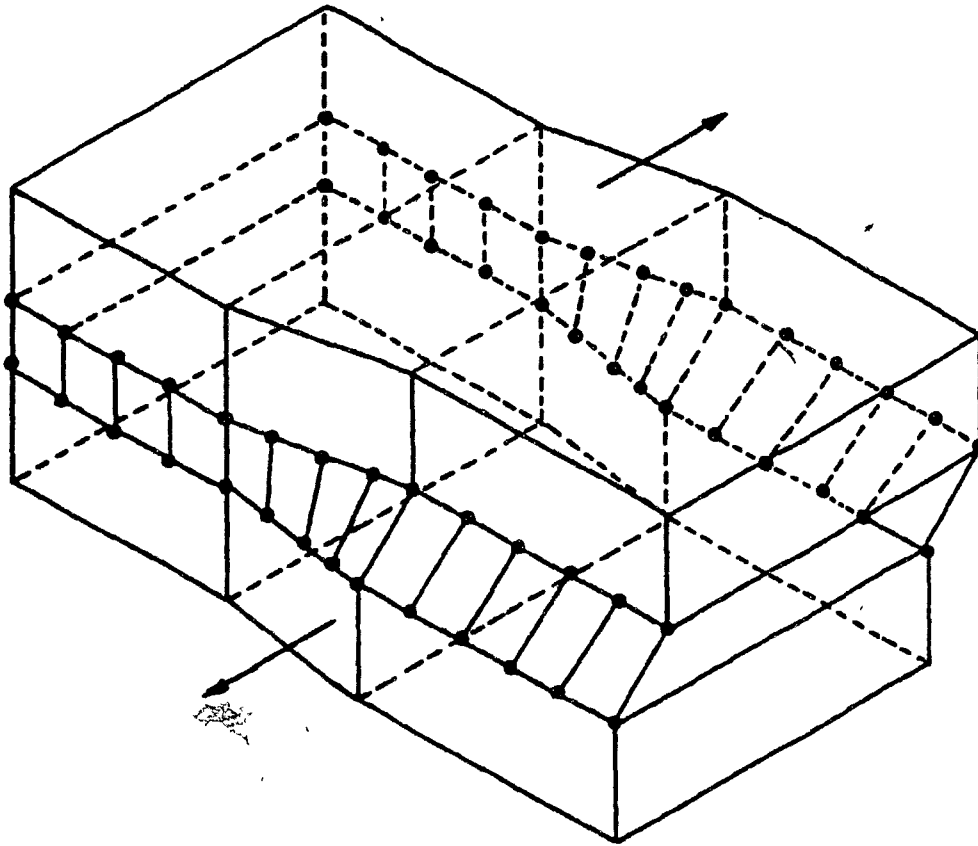


Figure 3a. Typical Right Hand Screw Dislocation

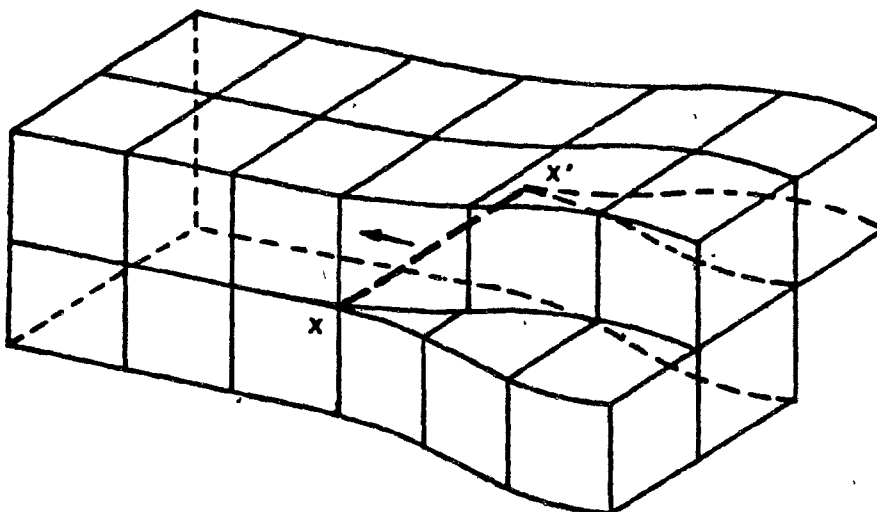


Figure 3b. Movement of a Screw Dislocation through a Regular Lattice.

manner. Figure 4 depicts this relationship for a selection of metals.

Electron microscopy has confirmed that the mechanism of work hardening involves the production of more dislocations, and their mutual obstruction by gliding along intersecting planes. There are several means by which dislocations may influence or pin one another: by their internal stress fields, caused by the distortion of the lattice structure; by penetration of one another's glide planes, like trees in a forest which have to be cut through for glide to continue; by intersecting one another, they may become locked and unable to move in the conventional manner of conservative movement. This mutual entanglement and subsequent immobilization of dislocations on intersecting glide systems is the basis of work hardening.

1.1.3. PRECIPITATION HARDENING

The above description applies to pure metals only; however, there are many metals and alloys in which work hardening occurs by the pinning of dislocations with precipitated second phase particles and impurities. One example of this is the solution of carbon in iron, where the carbon atoms pin the dislocations in the matrix. In addition to the effect of interstitial carbon atoms,

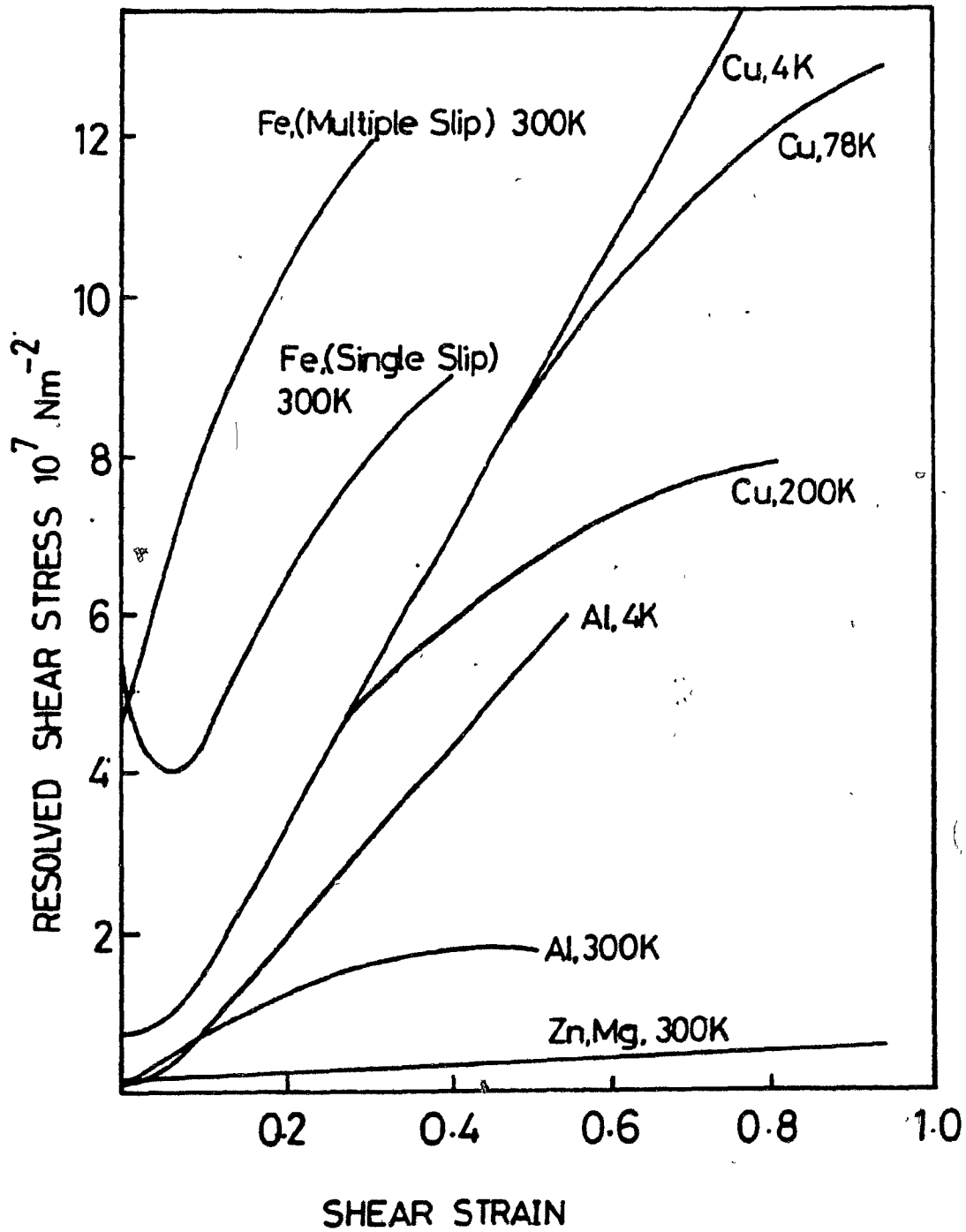


Figure 4. Resolved Shear Stress/Strain Curves for a Selection of Metals.

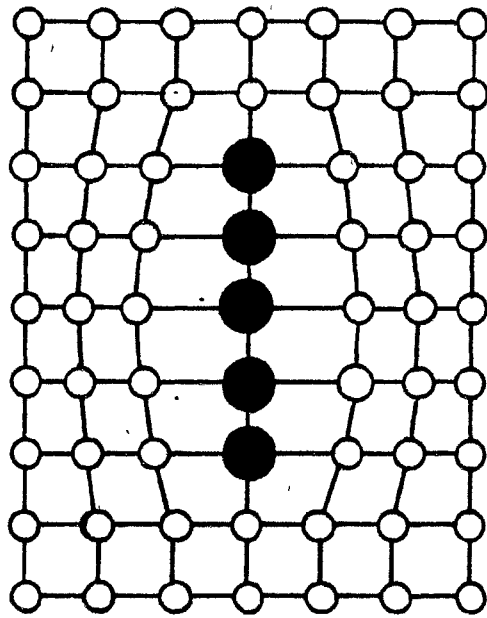
there is the effect of the precipitated second phase of iron carbide. The importance of these precipitates lies in their size and their subsequent degree of coherency or incoherency. Figure 5 is a schematic representation of precipitate zones² which give rise to coherency strains, caused by the enforced accommodation of the precipitate within the solvent matrix. The elastic strains around the precipitates can be relieved in two ways: by the formation of a dislocation interface around the precipitate zone to produce a semi-coherent boundary, or by bulk diffusion which creates a high angle boundary around the precipitate. The latter makes the grain precipitate incoherent.

Substitutional solute atoms can produce three basic hardening effects due to:

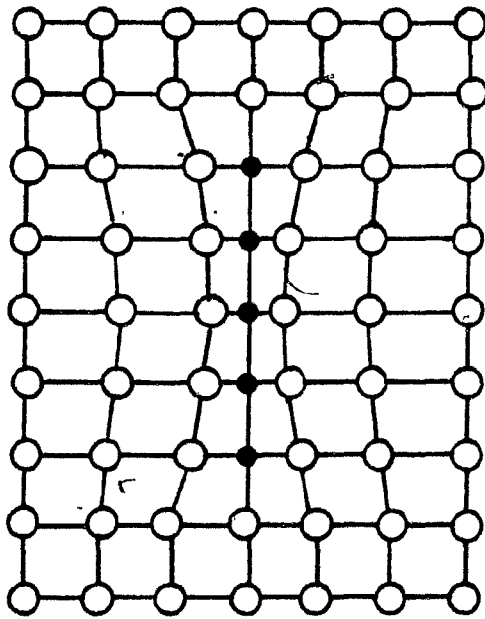
1. substitutional solid solution
2. formation of coherent precipitates or zones
3. formation of incoherent precipitates or zones

In all of the above cases, the moving dislocations engendered by cold working processes must overcome the resistance provided by these barriers. The ease with which a dislocation does this depends on the size and distribution of the precipitates.

Consider a perfectly straight dislocation line lying in a crystal with randomly distributed solute atoms,



(a)



(b)

Figure 5. Two Forms of Precipitate Zone Giving Rise to Coherency Strains.

as illustrated in Figure 6. When the dislocation is close to a solute atom, its strain field will interact with that of the solute atom and the dislocation will be attracted or repelled, according to the orientation of the dislocation. Providing the dislocation remains straight, there will be no net force on the dislocation, since the algebraic sum of all the interaction energies will be zero, and the strain fields of the solute atoms will provide no resistance to the passage of the dislocation. However, the dislocations are flexible and will take up lower energy positions by bending around regions of large interaction energy. Hence, the position of a dislocation and, therefore, the type of interaction will depend on the average spacing, L , of the particles.

Figure 7 illustrates the effect of three different particle sizes and distributions on the movement of flexible dislocations in a material. In Figure 7a the particle spacing, L , is small and the local stress fields of the precipitates are not sufficient to bend the dislocation around each particle. The dislocation therefore overrides the strain field of the particles and can pass through the material. In Figure 7b the dislocations are able to bend around the particles so that their radius of curvature, ρ , is equal to L . Glide occurs by each dislocation loop overcoming the interaction

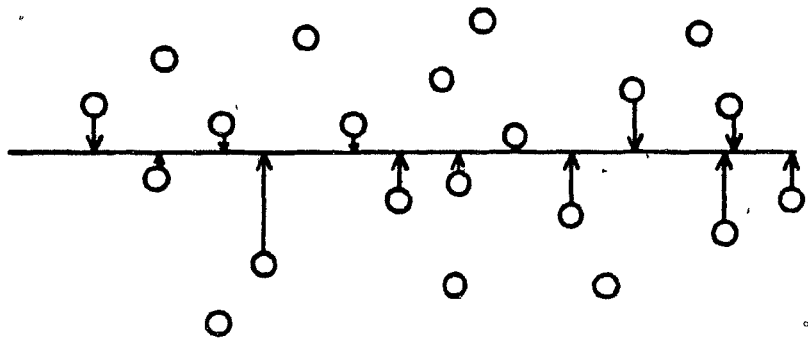


Figure 6. Interaction of a Dislocation with Solute Atoms.

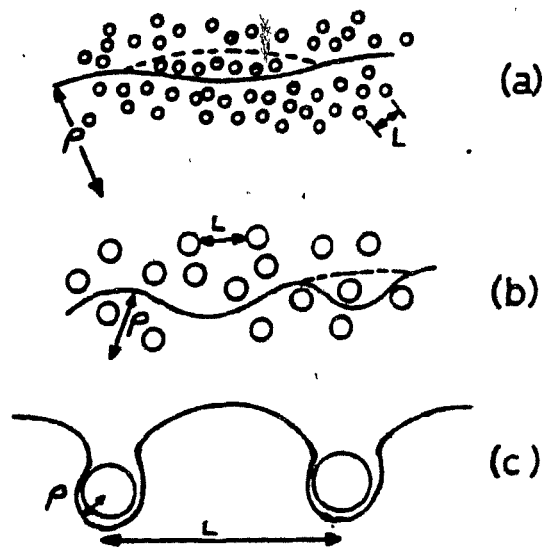


Figure 7. Effect of the Size of Solute Atoms on the Movement of Flexible Dislocations.

energy of the particle, a major contribution being provided by the work done in shearing through the particle. When the crystal is in this condition, it is at its maximum hardness and yield strength. In Figure 7c the distance between the particles is much larger, and dislocations can bow around the particle leaving a loop of dislocation around it. In this case, the dislocations are able to pass through the crystal lattice with relative ease since there is no work involved in shearing through the particle.

Thus, there is an optimum precipitate distribution offering the greatest resistance to dislocation movement, resulting in a maximum attainable yield stress by precipitation hardening. Figure 8 sums up the change in yield stress with increasing particle distribution, with points a, b, and c corresponding to the particle dispersions in Figure 7.

A practical example of precipitation hardening can be illustrated by the aging of a single crystal of Al-Cu alloy at 190°C. The variation of the shear stress with aging time is similar to that seen in Figure 8 (aging time being linked to particle size.) In commercial alloys, the resolved shear strength rises from approximately 10μ in the as-quenched condition, to 10μ in the fully hardened condition, where μ is the shear modulus. The

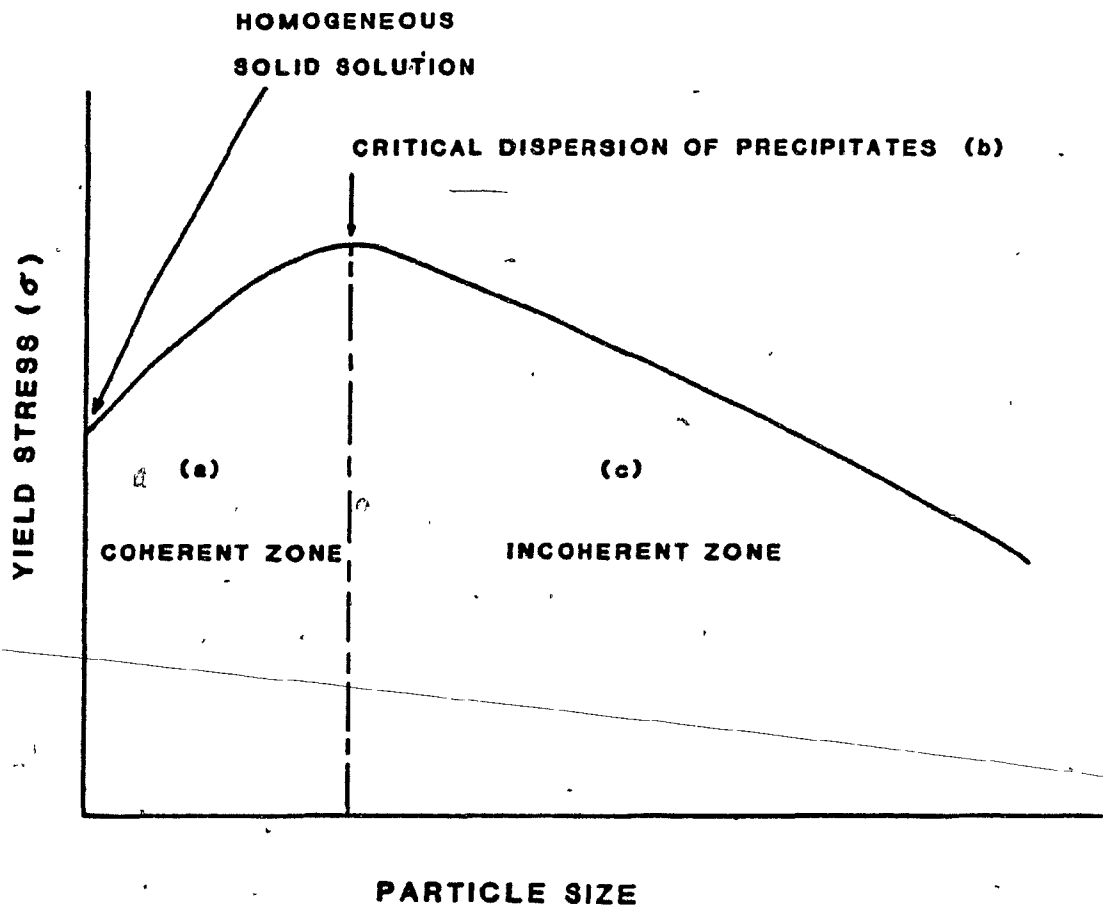


Figure 8. The Change in Yield Strength with Increasing Particle Size.

maximum hardening corresponds to a particle spacing of 100 Å to 1000 Å. Particles smaller than 100 Å do not harden the alloy much because thermal energy fluctuations are able to "push" the dislocations through them. If the particle distributions are greater than 2000 Å, the hardness of the alloy is lower because the dislocations bow around the precipitates leaving loops of dislocations around the particles, as has already been explained.

1.1.4. RECOVERY, RECRYSTALLIZATION AND GRAIN GROWTH

It was illustrated in Figure 4 that there is a limit to the degree of useful work hardening that can be produced in a metal or alloy. For further cold fabrication to take place, the structure of the material must be returned to a more deformable state, which is brought about by a reduction in the dislocation density. The cold worked state is mechanically stable and can remain in such a state almost indefinitely; however, it is not thermodynamically stable. Approximately 5% of the total energy of plastic deformation is stored within the dislocation structure of the material. (the remaining energy being dissipated as heat during deformation.)

Heating up the metal allows the dislocations to move out of their slip planes, thus enabling them to move along new sets of glide planes. The way in which

dislocations are able to do this depends on the type of dislocation involved. Screw dislocations move by cross-slip, which generally occurs at relatively low temperatures. At higher temperatures, edge dislocations, unable to move at low temperatures, are able to climb past their pinning obstacles.

Thus the annealing of cold worked metals occurs through a number of processes which may occur concurrently or consecutively during heat treatment. These are:

1. The reactions of point defects and point defect agglomerates (especially the annihilation of these defects).
2. The annihilation of dislocations of opposite sign and the shrinking of dislocation loops.
3. The rearrangement of dislocations to form energetically more favourable configurations, a process usually called polygonization.
4. The absorption of point defects and dislocations by grain boundaries migrating through the material.
5. The reduction of total grain boundary area.

Points 1 and 2 are discussed under the heading Recovery; Points 3 and 4 under Recrystallization; and Point 5 under Grain Growth.

1.1.4.1. RECOVERY

The hardness of a metal is one of the best indicators of the degree of deformation that the metal has received. During the recovery stage of annealing, there is little or no reduction in the hardness of a cold worked metal. Thus the recovery process is thought to be the "tidying-up" or reorganizing of the dislocation structure prior to the nucleation of recrystallization. Minor changes may occur in some of the physical properties of a metal, e.g. the resistivity and the amount of stored lattice energy.

1.1.4.2. RECRYSTALLIZATION

Recrystallization is characterized by a very drastic softening that commonly occurs at temperatures of $0.3 T_m$ for pure metals and $0.5 T_m$ for impure metals and alloys, where T_m is the melting point of the metal. The "recrystallization temperature" may be taken as the approximate temperature at which a sufficient amount of energy has been supplied to activate substantial recrystallization in a heavily cold worked metal in a matter of hours. A particular quantity of energy is required to form the strain-free nuclei from which a fully recrystallized structure can grow in a defect lattice. What is not fully understood is exactly how nucleation

takes place, since the nucleus formation requires an increase in the total free energy of the material, in opposition to the general "downtrend" in free energy demanded by thermodynamics.

From experimental observations of the connection between deformed structures and recrystallized regions within those structures, it has however been concluded that nuclei do spring up in regions where stored energy is locally concentrated or when there is strong lattice curvature. There have been two general explanations of these experimental observations. The first is based on the idea that nucleation is a spontaneous, and random process; the second assumes that there is a continuous sequence of reactions of lattice defects, ultimately leading to a recrystallized region large enough to be capable of continuous growth. The latter explanation leads to the more general assumption that nucleation consists of the development or ripening of lattice regions already present after deformation.

Two models have been suggested for each concept:

1.1.4.2.1. Homogeneous Nucleation

a) The classical model is similar to the classical phase transition theory, in which a nucleus of a critical size must be formed before growth can occur. In this case, it is assumed that the nucleus is formed as a result of

thermal fluctuations of a number of atoms. However, when applied to a homogeneously deformed material, the critical nucleus size and the activation energy required to form it is much greater than actually observed. If the deformation is assumed to be heterogeneous, i.e. localized regions of high strain energy exist throughout the metal, better agreement is obtained. However, the estimate of the local dislocation density is very high when compared with what is generally observed. The dislocation density that would be required for such high lattice strains is of the order of 10^{14} to 10^{15} cm^{-2} , whereas the values usually observed for cold worked metals is more like 10^{10} to 10^{12} cm^{-2} .

b) The martensitic model assumes that there are lattice regions of specific mutual orientation and specifically orientated interfaces that occasionally lie next to each other. Both of these regions combine with each other in a new third orientation by a martensitic-like process, due to the reaction of partial dislocations. The lattice region formed in this way is the nucleus which has achieved a suitable size for growth to continue. There has been some recent circumstantial evidence which would justify such a mechanism. ^{4, 5, 6}

1.1.4.2.2. Heterogeneous Nucleation

a) Subgrain coarsening is a form of heterogeneous nucleation in regions of high dislocation density. This applies mainly to metals having second phase boundaries at which lattice mismatch strains have brought about regions of high dislocation density. These regions grow by slow gradual recovery and rearrangement of lattice defects, especially dislocations. At first small angle grain boundaries are formed, from which mobile large angle grain boundaries grow. The transition of the former to the latter is a controversial point still under discussion. There are two possible ways which could bring about such a transformation: subgrain growth and subgrain coalescence. For subgrain growth, large angle boundaries are thought to be formed by the migration of subgrain boundaries during annealing; for subgrain coalescence, the disintegration of some subgrain boundaries is thought to have the same effect. In either instance, large subgrains are formed in which parts of the subgrain boundaries are large angle boundaries. Evidence for both processes has been obtained from electron microscopy studies.^{7, 8, 9, 10}

b) The bulging mechanism takes into account the fact that a cold worked metal has large angle boundaries present in the structure. These large angle boundaries bow out in

areas of locally higher stored energy, and create a nucleus of dislocation-free lattice which is then free to grow. Evidence for the bulging mechanism has also been obtained repeatedly.^{11, 12}

In summary, the experimental evidence suggests that nucleation during recrystallization may occur in a number of different ways, but the specific conditions which account for the occurrence of one mechanism in preference to another are not yet understood.

1.1.4.3. GRAIN GROWTH

Recrystallization is complete once the moving grain boundaries impinge upon one another and the cold worked structure has been completely consumed leaving a new grain structure. With continued heating, the larger grains will continue to grow at the expense of the smaller so that the mean grain diameter gradually increases. There are two major modes of grain growth: normal (or continuous) grain growth, where the grain diameter remains uniform throughout the specimen; and discontinuous grain growth, often referred to as secondary recrystallization. In the latter case, a small number of grains grow much more rapidly than the others, a phenomenon which has been variously ascribed to the surface energy of the metal and/or differences in specific boundary energy between neighboring grains.

In the initial stages of grain growth, the process appears discontinuous but, on continued annealing, the grain growth becomes normal, especially if the initial grain size distribution is broad. Normal grain growth ceases when the mean grain diameter is approximately the same as the specimen dimension, e.g. the sheet thickness or wire diameter (a grain size generally much greater than this is not needed commercially). The grain boundaries then become pinned at the surface by "thermal grooving." In exceptional cases where the pinning force is small enough to be overcome by the grain boundary, a tertiary recrystallization process is sometimes initiated. The driving force in this process results from the difference in surface energy between adjacent grains of different orientation.

Normal grain growth, which is the mode of grain growth most important commercially, has been extensively investigated. For very pure metals, the grain size follows the relationship:

$$D - D_0 = Kt^{1/2} \quad (4)$$

where D_0 is the initial grain size, K is the rate constant, and t is the annealing time. However, for alloys and commercial purity metals, the rate of growth is slower and the power of t is nearer to 0.3 than 0.5. This

is because grain boundaries and dislocations are pinned by second phase precipitates of insoluble inclusions, as has been explained in Section 1.1.3. As the grain size increases, the driving force per unit area decreases, and eventually a stable grain size is reached at which the anchoring forces balance the driving forces. From an estimate of these forces Smith¹³ has deduced that this stable grain size is about $4r/3\alpha$ in a metal which contains a volume fraction, α , of inclusions of radius r . (The grain size of metals can be controlled using controlled generation of inclusions as in the production of Aluminum-killed steels).

1.2 INDUSTRIAL ANNEALING

1.2.1. INTRODUCTION

The causes of work hardening in metals and the way it can be removed by annealing have been discussed. It remains to be seen how annealing is carried out on an industrial scale. Since the research work to be described later is concerned with developing an annealing sensor for low carbon steel, particular reference will be made to current annealing practices in the steel industry.

Before cold rolled steel strip can be fabricated, it must be annealed. The sole purpose of annealing is to

soften the steel so that it can be used in severe cold working operations, such as pressing and deep drawing without tearing.

An example of how important the annealing stage is in the production of steels for fabrication can be seen from some approximate world steel production figures: In 1983 total world output was approximately 800 million tonnes¹⁴. About 60% of this production was in the form of cold rolled strip, most of which has to be annealed, i.e. more than half the world's steel requires annealing before shipment.

There are basically two processes available for annealing of cold rolled strip: Batch and continuous annealing. Each has its advantages and disadvantages.

1.2.2. BATCH ANNEALING

The most common batch annealing furnace used in industry is the gas powered bell furnace. The bell is a hood which is placed over the charge of tightly wound steel coils, and then either filled with a protective gas or totally evacuated. A protective atmosphere furnace is principally used for the bright annealing of cold rolled low carbon steel strip, whereas the annealing of high carbon and alloy steels is carried out using a combination of vacuum and inert gas methods.

Figure 9 is a cutaway diagram of a typical bell type furnace, the details of which are enumerated in Figure 10.

The furnace, consisting of the gas burners and hot gas recuperators, can be lifted on or off the bells, so that the charge can be cooled or loaded more rapidly. During the cooling cycle, the furnace can be replaced by a fan-driven cooling hood which directs cool air on to the bells. The furnace, meanwhile, can be transferred to another loaded base where heating can be resumed. Small single stack batch annealing furnaces are designed to work on a carousel system, i.e. to rotate from one base to another from a fixed central column.

The amount of steel in a large batch annealing furnace can be as much as 250 tonnes, consuming about 175 kcal of heating gas per kilogram of steel. This is a very large energy requirement, due to the high heat capacity of steel, so a lot of the heat is required to ensure that all parts of all the coils reach the annealing temperature.

1.2.3. CONTINUOUS ANNEALING

Continuous annealing is a relatively new process (although the first installations were made about 50 years ago), and will be dealt with purely as a contrast to batch

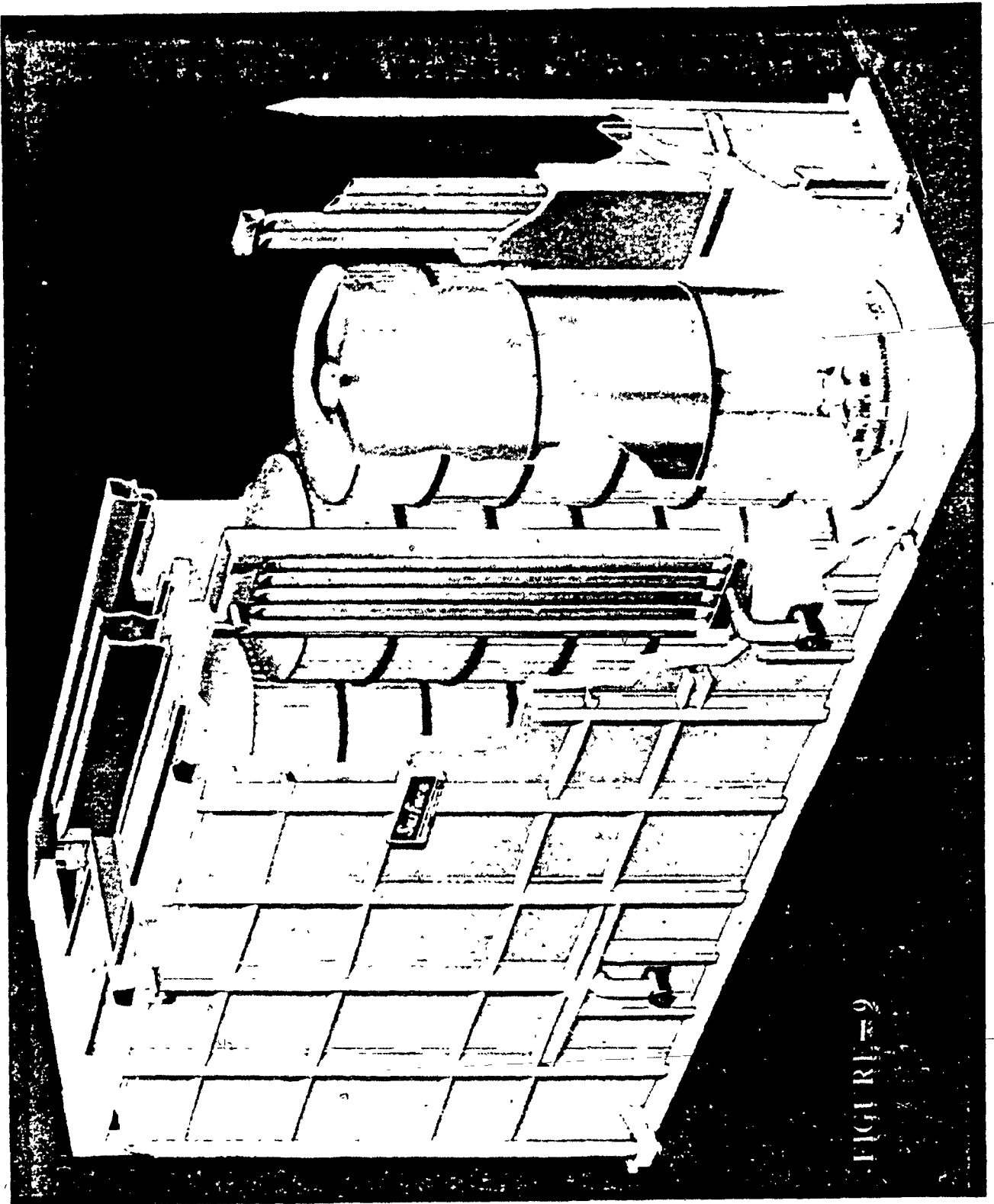
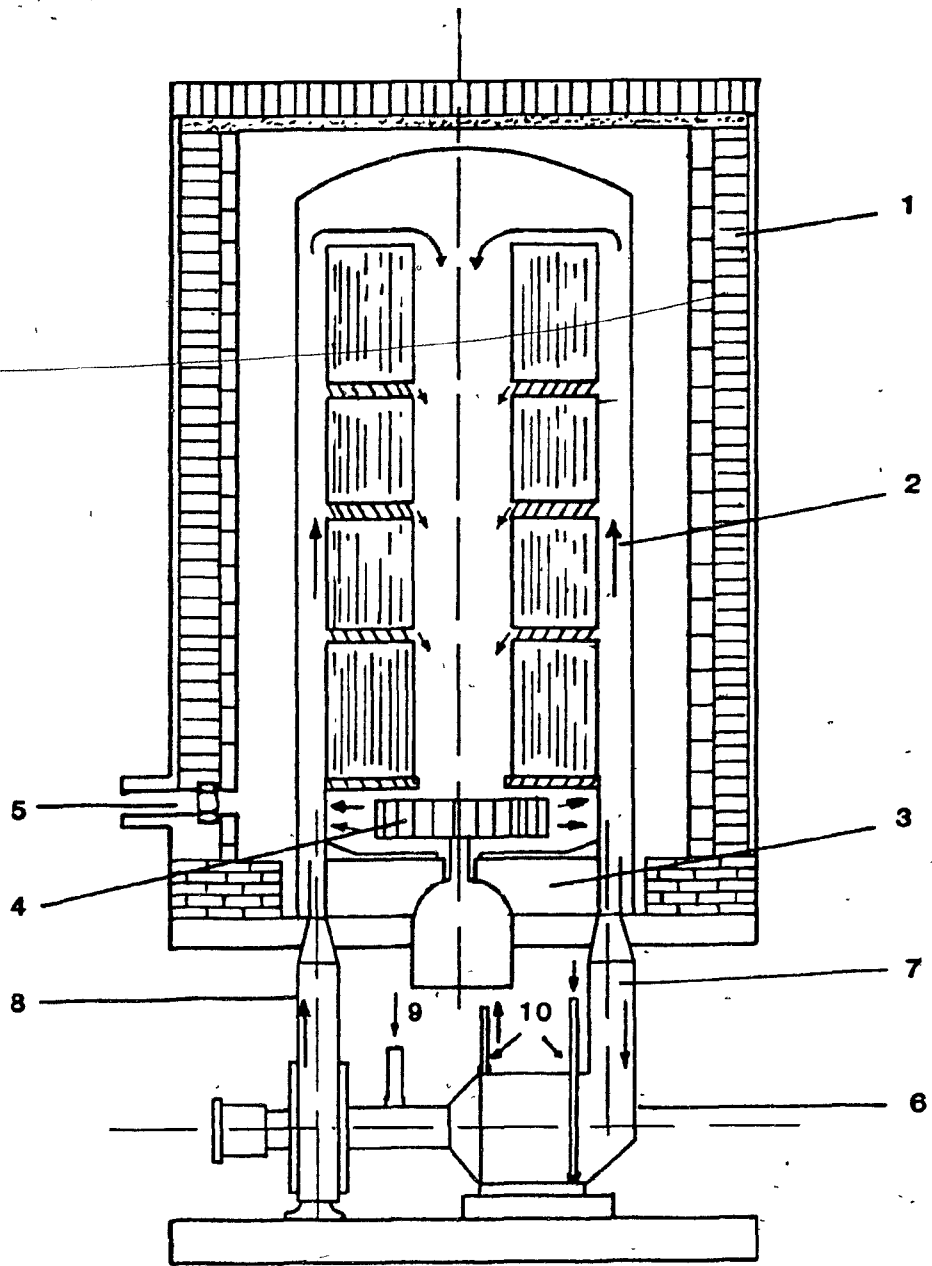


FIGURE 9



- | | |
|----------------------------|--------------------------|
| 1. Gas Heated Bell Furnace | 6. Gas Cooling Unit |
| 2. Annealing Bell | 7. Hot Gas In |
| 3. Charging Support Base | 8. Cooled Gas Out |
| 4. Gas Agitation Fan | 9. Protective Gas In |
| 5. High Velocity Burner | 10. Cooling Water In/Out |

Figure 10. Section Diagram of a Bell Annealing Furnace.

annealing. In continuous annealing, the coil is gradually unwound and the strip passes through a furnace, thus being rapidly heated to the annealing temperature. During its passage through the furnace, it is held at the annealing temperature for a short period, and then rapidly cooled. The total annealing time for any one section of the strand is from four to eight minutes. Figure 11¹⁵ shows the comparison of the heat treatment cycles for continuous and batch annealing. The quick conclusion from this comparison is that the continuous process would be the more desirable. However, there are serious disadvantages to continuous annealing which will be discussed in the next section.

Modern continuous annealing furnaces have been incorporated into full processing lines, e.g. the installation at N.K.K.¹⁶ (Figure 12.) Pickling, electrolytic cleaning, and temper rolling are all combined into one process.

1.2.4. COMPARISON BETWEEN BATCH AND CONTINUOUS ANNEALING

Continuous and batch annealing are two very different processes: Batch annealing is a very simple but lengthy process which is difficult to control; continuous annealing is a short but complex set up that is relatively easy to control. From a metallurgical viewpoint, the

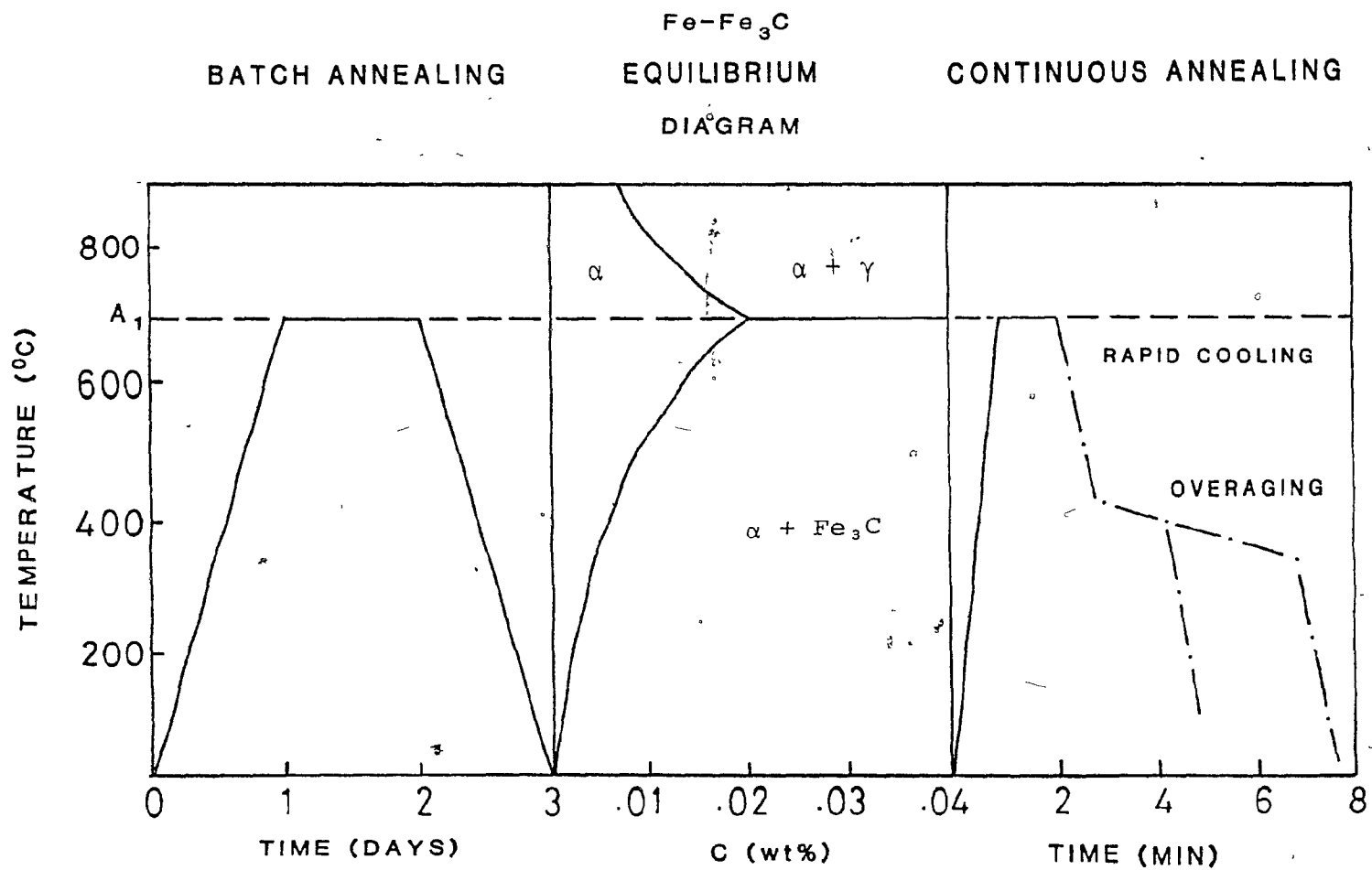
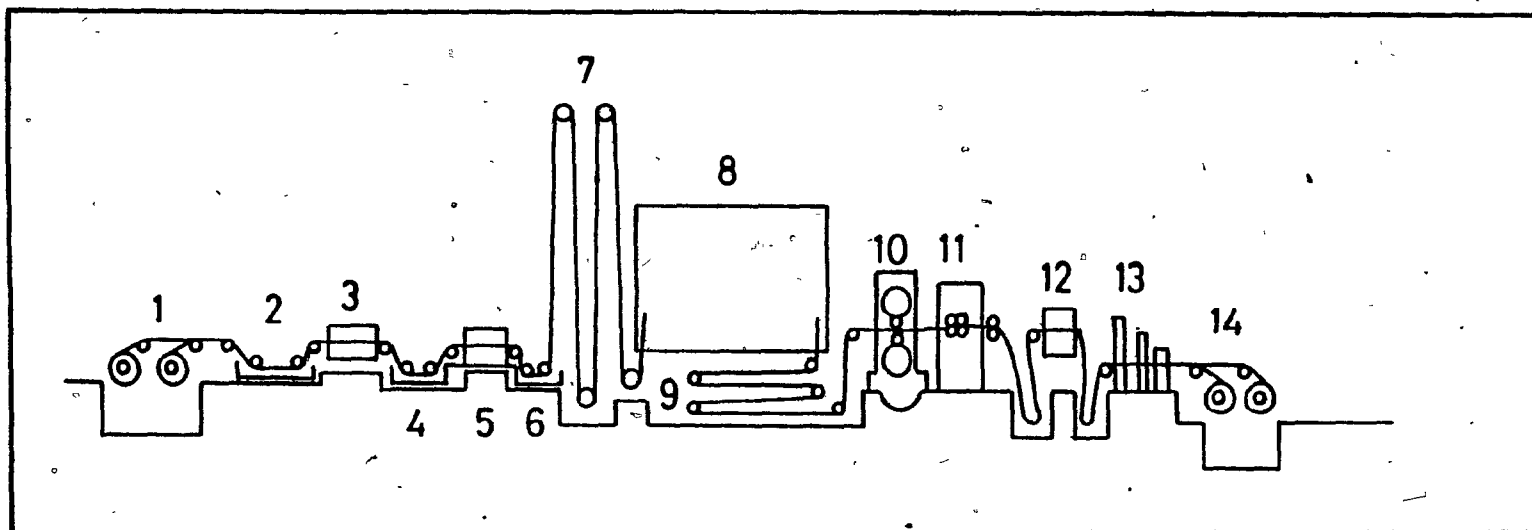


Figure 11. Comparison of Batch and Continuous Annealing Schedules.



- | | | |
|----------------------|------------------|-----------------------|
| 1. Two Pay-Off Reels | 6. Rinse Tank | 11. Tension Leveler |
| 2. Hot Caustic Tank | 7. Looping Tower | 12. Side Trimmer |
| 3. Brush Scrubber | 8. Furnace | 13. Oiler |
| 4. Electrolytic Tank | 9. Exit Loop | 14. Two Tension Reels |
| 5. Brush Scrubber | 10. Temper Mill | |

Figure 12. N.K.K. Continuous Annealing Line.

large time difference between the two processing cycles has important effects on the structure of the final product.

The aim of industrial annealing is to obtain a satisfactory grain size that will provide the material with the desired mechanical properties suitable for further fabrication processes. Low carbon steels, especially Drawing Quality Specially Killed (DQSK) steels, usually require the grain size to be a minimum of 30 μm and a maximum of 40 μm . The upper limit is usually defined by the appearance of the "orange peel" effect, caused by the steel having so large an average grain size that, when cold worked, it produces a roughened and objectionable surface similar to that of the peel of an orange.

Forty μm is a large grain size, and is not easily achieved in a typical low carbon steel. For instance, a steel with a carbon content of about 0.05 w/o has approximately 0.03 w/o of carbon out of solution at an annealing temperature of 700°C. Also, there can be some complex oxides -- mainly alumina spinels -- and sulfides present which, together with the undissolved carbon, prevent the movement of grain boundaries. For this reason, low carbon steels need long soak periods at temperature so that the desired grain size can be

achieved. The annealing time for the continuous process is very short and allows no time for grain growth to occur; hence, aluminum-killed steels are not annealed on a continuous annealing line because of the presence of insoluble inclusions which prevent grain growth. Batch annealing, however, can provide the soak times that are needed for low carbon steels with a high inclusion content. Grain growth rates can be increased in the continuous process by raising the annealing temperature above the A_1 temperature (approximately 720°C.) This is possible because the short annealing times do not allow the carbide precipitates to coarsen by a significant amount, a phenomenon which would otherwise decrease the formability of the steel. Batch annealing on the other hand is restricted to temperatures below A_1 because, not only would the carbide precipitates coarsen at higher temperatures with the long soak periods, but also, adjacent wraps in the coils would tend to stick together.

Drawing quality specially killed (DQSK) steels not only have to have a suitable grain size, but also must have isotropic mechanical properties. The batch process is the preferred method for annealing these steels, because precipitation of aluminum nitride during early recrystallization promotes the growth of grains having suitable crystallographic textures for good deep

drawability. In continuous annealing, aluminum nitride is undesirable because, like the aluminum oxide inclusions in killed steels, the nitride particles restrict grain growth.

Another factor affecting grain growth is the heating rate. Slow heating rates, like those used in batch annealing, are thought to act to reduce the number of active recrystallization nuclei, and so increase the final grain size.

The quality of the heat treatment received by the steel can differ greatly between the two processes. The heat treatment of a single strand is easier to control and monitor than that of a large number of stacked coils. Therefore, the annealing of steel by the continuous method is more uniform and repeatable than the batch process. The heat treatment received by a coil in the batch process is very dependent upon the position of the coil within the furnace. Coils at the top of the furnace tend to heat more quickly and reach a higher temperature than those at the bottom. Ways of minimizing this have been developed by controlling the direction of gas flow around the furnace, and will be discussed in more detail in Section 1.2.5.4.

The greatest advantage that all batch operations have over continuous ones is that they can allow for a

great deal of process flexibility. Continuous processes, once installed, cannot be dramatically altered to suit a widely varying product requirement, because of the high capital cost incurred by altering the process. Batch annealing furnaces can deal with the wide variety of steel compositions and heating/cooling cycles required by different customers. Batch annealing furnaces are therefore still widely preferred because of the process flexibility in spite of their disadvantages outlined above.

Batch annealing furnaces are therefore unlikely to be superseded by the continuous annealing line, particularly in view of the high capital cost of the latter; but it is probable that larger quantities of steel are going to be processed by the continuous process as new alloys are developed.

1.2.5. BATCH ANNEALING: ADVANCES AND CURRENT PRACTICES

Modern batch annealing practice is governed by two major factors: a need for greater heating efficiency brought about by escalating fuel costs; and technological advancements in all phases of steel-making which have increased the rate of production. For instance, heats of 45 minutes in the basic oxygen furnace, computerized slabbing and hot mills, and high speed tandem mills have all forced an increase in the turn-around time for the batch annealing process.

1.2.5.1. GAS VELOCITY

The heating efficiency and heating rate are both very dependent upon the volume and velocity of the heating and protective gases. The latter is directly controlled by the gas agitation fan at the base of the furnace (Figure 10). To reach the most even temperature distribution possible within the stack, the fan should be able to deliver the protective gas at particularly high temperatures and velocities. Should the gas velocity be too low, the heat treatment received by the coils can be very variable. In a similar way, the combustion gases within the combustion chamber should have a high velocity to give the best possible temperature distribution over all the protective bells. This is achieved by positioning the burners in the combustion chamber so as to create a swirling motion (Figure 13.) This reduces the number of burners and associated hardware that are required, and also means that the burner flames do not directly impinge on any of the bells, a circumstance which would create localized hot spots that set up thermal stresses, ultimately causing the bells to rupture.

1.2.5.2. BURNER EFFICIENCY

Burner efficiency has been increased by preheating the fuel/air mixture prior to combustion, and maintaining

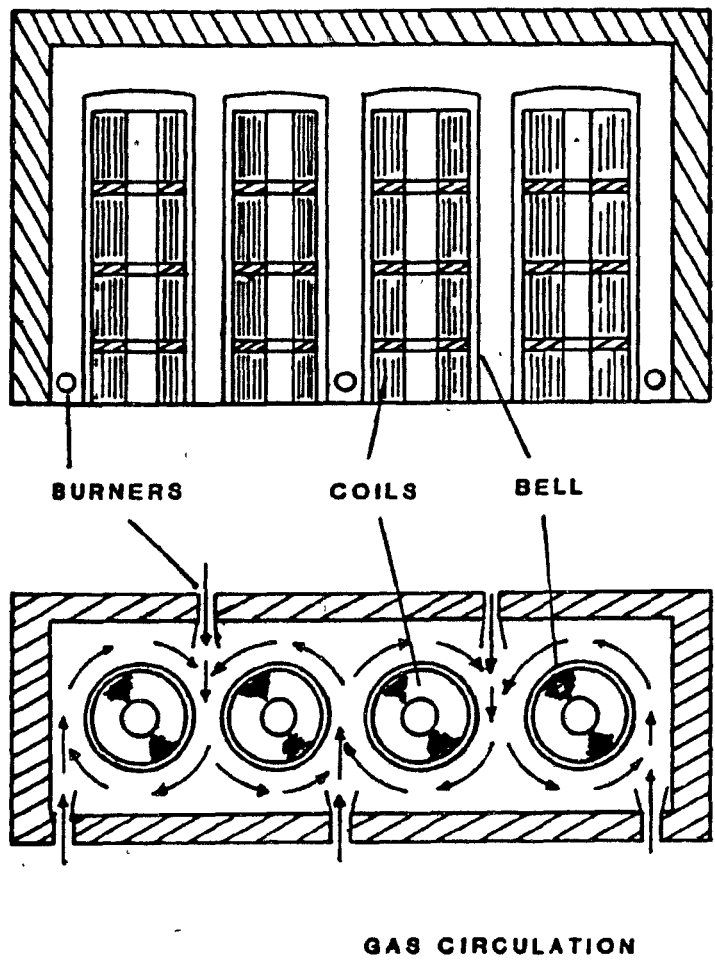


Figure 13. Four-Stand Bell Furnace and 5 High Momentum Burners.

the correct fuel/air ratio throughout the heating cycle. The combustion mixture is preheated, using recuperators situated within the furnace. As the preheat temperature increases, so the energy wasted in heating the combustion gases by direct combustion decreases, and the fuel/air ratio has to be changed accordingly (Figure 14¹⁷). The correct ratio is automatically maintained, regardless of preheat temperature, by a simple arrangement of diaphragm regulated pressure valves. If the proper fuel/air ratio is not maintained, fuel savings gained from recuperation would be lost due to inefficient combustion.

1.2.5.3. INCREASED COOLING RATES

On fixed base annealing plants in cold rolling mills operating with protective gases, equipment to accelerate cooling is used either to save space or to speed up production. This has permitted the base to furnace ratio to be lowered from 3:1 to 2:1, giving lower capital outlay, but increasing operating and maintenance costs.

Accelerated cooling rates are achieved using built-in water-cooled cooling units in the base of the furnace (Figure 10). One version of this system has been developed under the trade name "Intra Kool" by Surface Div., Midland Ross Corp.¹⁷ During the heating cycle,

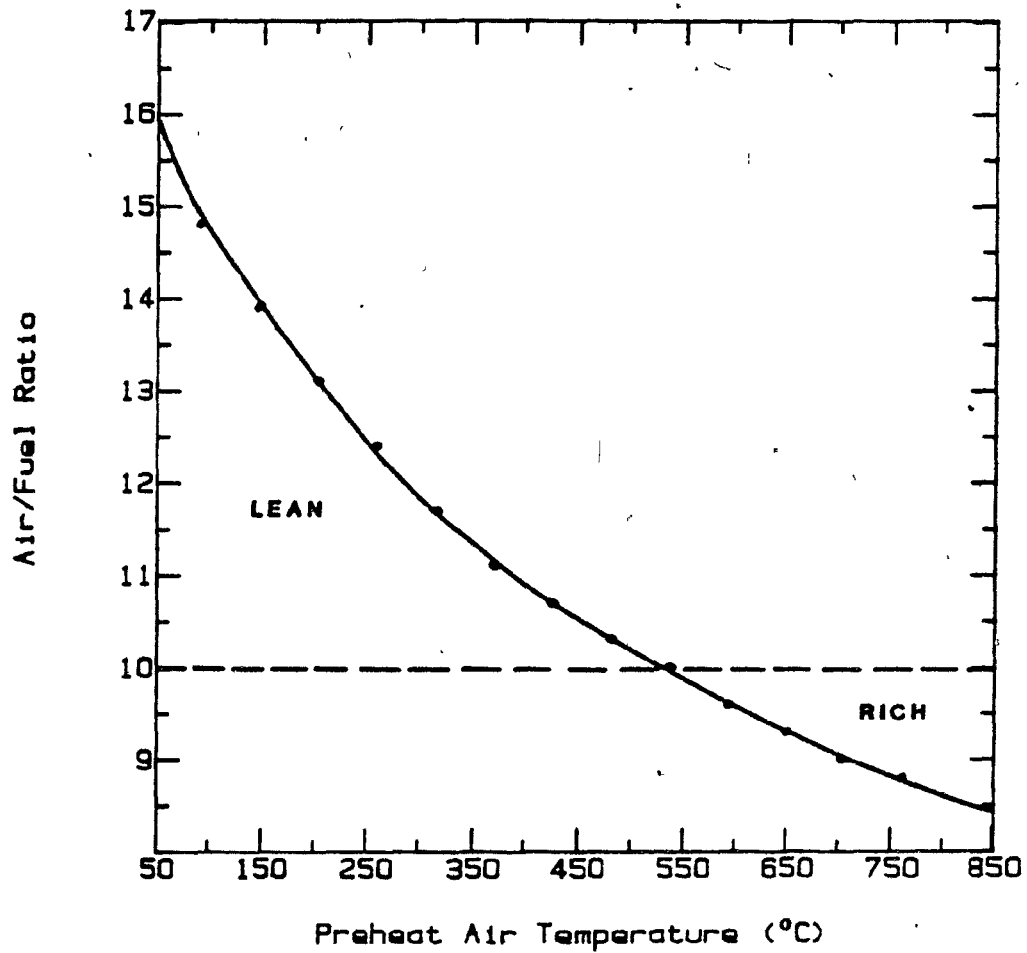


Figure 14. Control of Air/Fuel Ratio as a Function of Preheated Air Temperature.

the system is dry; on cooling, water is introduced when the temperature has decreased to the 600 to 550°C range. This results in rapid cooling of the gas atmosphere recirculating within the bell. The cooled gas, in turn, cools the load by forced convection from the gas agitation fan. Using the "Intra Kool" system, a 250 tonne charge can be uncapped in 30 to 35 hours, compared with 60 to 65 hours in normal practice. By this means, up to 50% more tonnage can be produced from a given floor area when compared with conventional cooling techniques. There have been difficulties using the Intra Kool technique because the cooling spirals are subject to distortion, mechanical restraint, corrosion, and atmosphere collapse. These problems are being resolved with better design and materials selection for the spirals and support brackets, as well as improved installation techniques.

1.2.5.4. PROTECTIVE GAS CIRCULATION

Without the presence of a forced circulation of protective gas, the temperature distribution within the furnace would be very uneven, since the heat transfer would depend only on the protective gas convection currents. Studies carried out on heat transfer models of the batch annealing process have brought about profound changes in the gas flow systems within the furnaces.

The temperature distribution within any particular coil in a batch annealing furnace has been studied by Terzic¹⁸, who mathematically modelled the change in temperature contours through vertical sections of the coils. It was shown that the radial transmission of heat is not negligible, and may have a value of 5 kcal/mh°C which, in the longitudinal direction, amounts to 32 kcal/mh°C. As a consequence of the radial heat transmission, the cold spot during heating, or hot spot during cooling, is offset towards the axis of any particular steel coil. If a charge of coils is to have a uniform heat treatment in a batch annealing furnace, then the heat transfer from the circulating gas to the coils must also be uniform. It has already been stated in Section 1.2.5.1. that the overall heat transfer is highly dependent on the pressure and velocity of the gas but, more recently, the flow pattern around the coils has been found to be equally significant. Harries and Guthrie¹⁹ used laboratory water models to model the gas flow in a production annealing stack, and found that the system had very poor flow characteristics. Approximately 70% of the flow was channelled around the outside of the coil and down the axis, with 15% flowing through each of the spaces between the coils (Figure 15a). In conventional furnaces the coils at the top of the stack heat up more quickly

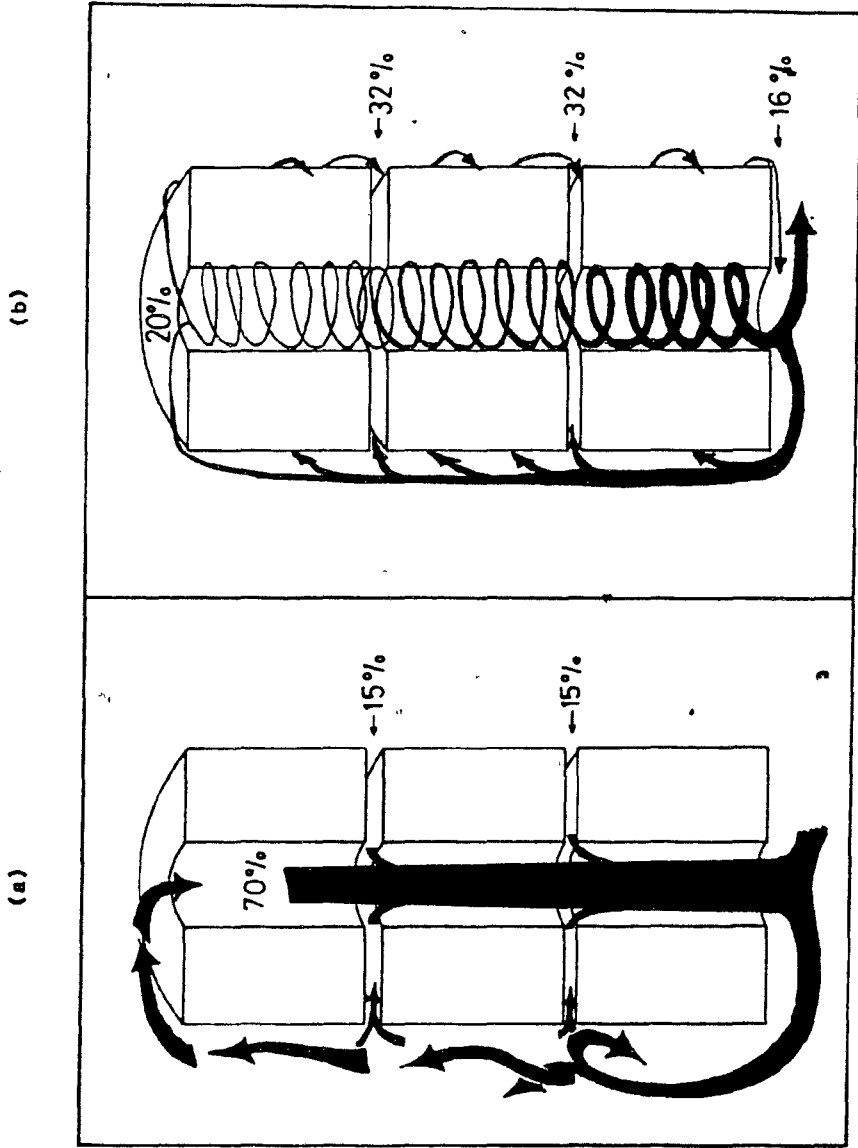


FIGURE 15.- IMPROVEMENTS IN HEAT TRANSFER BY IMPROVED GAS FLOW CONDITIONS

than the coils at the bottom. Often the coils at the top become overheated long before the bottom coils reach the soak temperature. This is an unnecessary waste of energy caused by poor gas flow and inefficient heat transfer. A plexiglass water model was used to model the gas flow around a stack of coils. The best flow system was found to be a swirling motion caused by a series of diffusers and spacers placed in the base and in between the coils (Figure 15b). This evened out the flow throughout the stack; 32% of the flow was channeled in between each of the coils, 20% down the axis and 16% in through the base. The result of this was a decrease in the overall annealing time by 12 hours between the original flow system and the new system: an improvement of 10-15%.

1.2.5.5. FURNACE CONTROL AND OPTIMIZATION

By far the largest customer for annealed steels is the automotive industry, the required tonnage products being DQSK steels. The invariance of the product and its heat treatment means that the control system itself can be fairly simple.

The batch annealing facility at North Annealing¹⁷ anneals these steels at a standard cold spot temperature of 704-715°C, the standard furnace temperature being 815°C. The parameters have been based on past experience in the annealing of DQSK steels.

The control system, made by Leeds and Northrup, records the furnace temperature, as well as each individual stack temperature. Control is effected by using the furnace temperature reading and one of the stack temperatures as a second control reference.

The batch annealing process, like many other processes, can of course be adapted to computer or microprocessor control. This has already been accomplished in the cold rolling mill at Krupp Stahl A G, Bochum in Germany ²⁰, with the introduction of microprocessors, each microprocessor controlling one furnace installation in accordance with preset parameters for the annealing and cooling cycles.

A great deal of work has been done in the U.S.A. with the aim of reducing the annealing cycle times using computer control. Midland Ross ¹⁷ have developed an "on-line" real time monitoring and control system which uses feedback information from four thermocouples in each stack (Figure 16). These readings are used to predict the thermal gradients within the coolest coils, using a heat transfer analysis model. Such information can be used to automatically trim individual burners in order to control the overall furnace temperature, as well as any irregularities in temperature distribution in each stack.

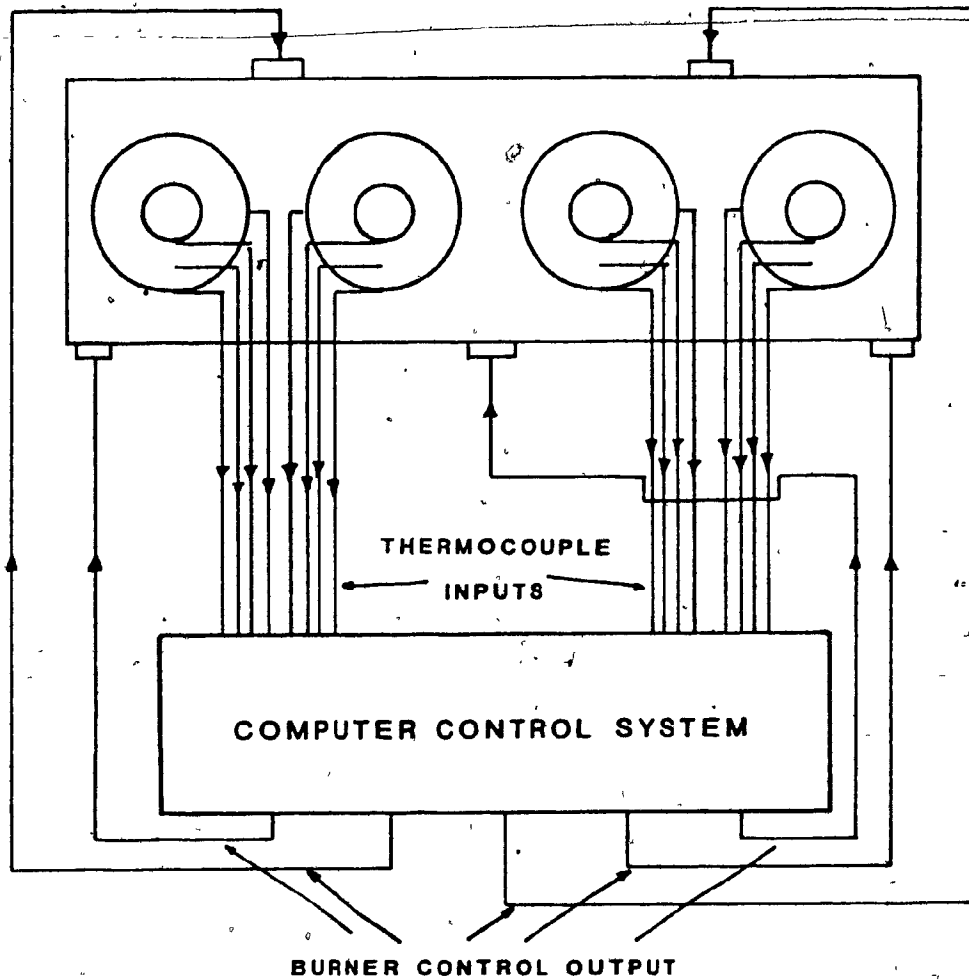


Figure 16. Diagram of Computer Control System for Batch Annealing.

Thus there are three major benefits from the use of a computer-controlled system:

- 1) Improved reliability and process repeatability
- 2) Energy savings through reduction of excess heating time
- 3) Increased productivity

The use of the computer in the future will no doubt be extended to include inventory control and calculation of optimum load, based on priority, coil size, cycle time, and stack heights.

An example of the successful application of computerization in the annealing of steels is the computer program developed by the Engineering Corporation of America¹⁷, used to predict firing time on charges. This program has allowed the firing of coils in each charge according to their nature, rather than to an average time, with a safety margin added. The use of the program brought about savings of 15% on firing time, 9% on atmosphere gas, and 8% on natural gas.

1.3. SUMMARY

1. The properties of metals, which are dramatically changed by the generation and movement of dislocations during cold work, may be restored by annealing.
2. Industrial annealing of cold rolled low carbon steels is carried out in batch and continuous annealing furnaces.
3. The development of more efficient burners, and better gas flow within the batch furnace, have greatly improved efficiency of the process, as well as reproducibility of properties of the annealed steel.
4. Microprocessors and computers have recently been adapted to control batch annealing.

CHAPTER 2

2.1 OBJECTIVES OF THE PRESENT RESEARCH

The batch annealing cycle time is very long; this leads to high costs. However, there is little to gain economically from minor reductions in the process time. For any incentive for change, it is desirable to achieve reductions in time of an order of magnitude.

There is little information in the literature to indicate that the operating parameters for batch annealing furnaces are based on anything more than previous annealing experience. The advent of computer modelling and control has improved the situation by taking into account the physical properties of the steel. Although the application of computer modelling and control has made the process more efficient and reproducible, more precise control of the furnace, and hence the final product, could be effected if there were some means of taking a direct measurement of a mechanical or physical property of the steel that would exactly follow the progress of annealing.

The present research project was designed to develop a sensor capable of continuously monitoring recrystallization and grain growth during the annealing of

low carbon steels. An important factor in designing a sensor was its potential adaptability to the currently used batch process and equipment in order to be an acceptable means of control. Other factors which influence sensor design include the size, cost, ease of manufacture or replacement, and adaptability to instrumentation and control under industrial conditions.

The next chapter will outline a new technique which was thought to be capable of following all of the annealing stages, and of fulfilling the requirements outlined above for a batch annealing sensor.

CHAPTER 3

3.1 THE DESIGN OF AN ANNEALING SENSOR BASED ON ELECTRICAL RESISTIVITY

There are many properties of cold worked metals which could be used to follow the changes that take place during annealing. Some of the techniques and physical phenomena which have been or could be used to follow such changes are the hardness test²¹, density measurements²², electron and optical metallography²³, calorimetry²⁴, ultra-sonic attenuation²⁵, eddy current changes²⁶, and even more sophisticated methods such as X-ray topography²⁷, and positron annihilation²⁸. All these methods are capable of identifying the changes which occur during the several stages of annealing. However, they are generally much better suited to laboratory investigations than to industrial monitoring, where the needs for accuracy, robustness, reliability, and adaptability to control procedures are all influential considerations.

After reviewing the various possibilities, the physical parameter that appeared to be best suited to eventual industrial application as a sensor was electrical resistivity. Being a quantity that is very sensitive to structural change, it can be measured with great accuracy, and is amenable to instrumentation.

3.2 THE ELECTRICAL RESISTIVITY OF METALS

The resistance to the flow of thermal and electric currents in any metal is caused by scattering of the conducting electrons. The two principal sources of electron scattering are thermal vibrations of the lattice, and defects in the lattice. The latter can take the form of impurity atoms and lattice defects, such as dislocations and vacancies, which limit the mean free paths of the electrons, thereby increasing the resistance of the metal. It is also assumed that the resistivities due to thermal vibrations and lattice imperfections are both additive. This was the basis for Matthiessen's Rule of 1884, which states that the electrical resistivity, ρ , of a metal at temperature, T , can be expressed as:

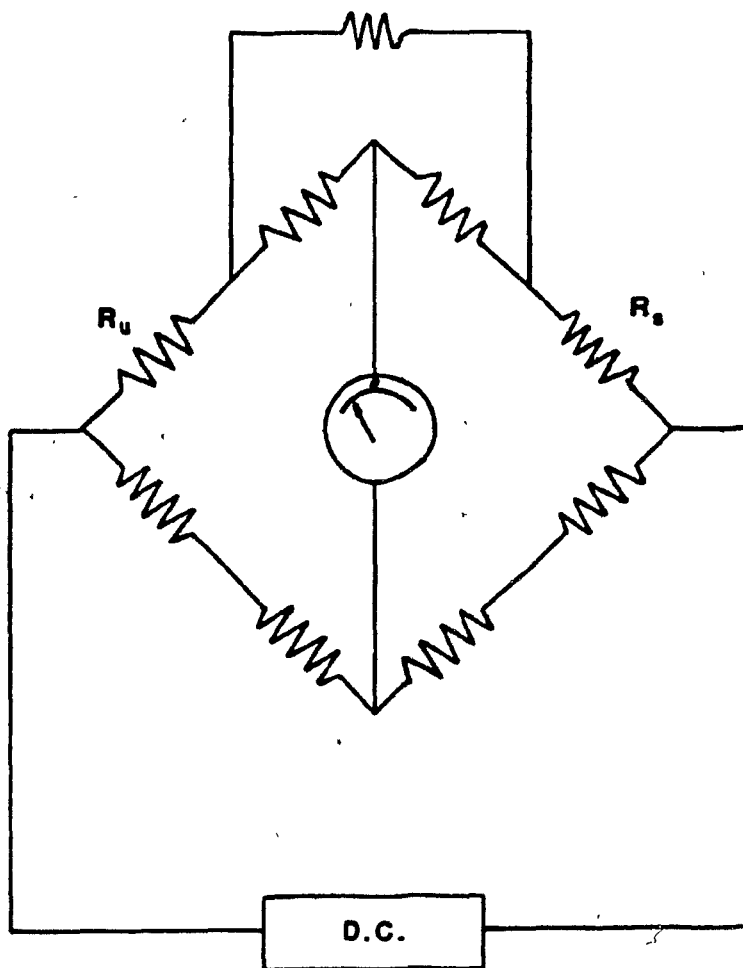
$$\rho(T) = \rho_i + \rho_T + \rho_{CW} + \rho_{GB} \quad (5)$$

where ρ_i is the residual resistivity due to impurities; ρ_T is the residual resistivity due to lattice vibration scattering; ρ_{CW} is the residual resistivity caused by lattice imperfections (viz dislocations and vacancies); ρ_{GB} is the residual resistivity due to scattering at grain boundaries. ρ_{GB} is very much smaller than ρ_{CW} , and in the case of a single crystal, $\rho_{GB} = 0$. For a fully annealed metal with a relatively large grain size, it can be assumed that $\rho_{GB} \approx 0$ and $\rho_{CW} = 0$.

3.3 EXPERIMENTAL METHODS FOR DETERMINING ELECTRICAL RESISTIVITY

For many decades, the standard approach to the measurement of low resistivity materials has been to use a D.C. method, such as the Hoopes or Kelvin Bridge (Figure 17). For example, the D.C. method has been the standard procedure for measuring the electrical resistivity of copper for industrial quality control since the ASTM B-193 specification was first published in 1944. It is reported that the method provides an accuracy of plus or minus 0.3% for materials having a resistance of $10\mu\Omega$ or more. The drawback of techniques such as the Kelvin bridge is that a correction must be made for the temperature at which the measurement is taken, due to the temperature component of resistivity. To measure the absolute resistivity of a metal to a high degree of accuracy, the measurement must be taken at 4K. At this low temperature, it is assumed that $\rho_T \approx 0$, and that the value of resistivity is entirely due to impurities and lattice defects present in the material.

Two classical approaches to following annealing processes using resistivity measurements are (i) to quench samples from the heat treatment temperature after various times of annealing and then measure the resistivity at the temperature of liquid nitrogen²⁹, or (ii) to measure



R_u UNKNOWN R_s STANDARD

Figure 17. Hoopes or Kelvin Bridge.

the resistivity of quenched samples at room temperature and then make temperature corrections to the readings so that they can all be considered to have been taken at exactly the same temperatures. These techniques are, of course, unsuitable for continuous measurements at high temperatures. If the microstructural and physical changes that occur during annealing are to be studied, it is essential to eliminate the contributions to the electrical resistivity due to temperature and impurities present in the lattice. Fortunately, a very sensitive differential A.C. technique has recently been developed by Drew et al.³¹ that was thought to be adaptable to the special requirements of the annealing of steels.

3.4 THE DIFFERENTIAL A.C. TECHNIQUE

If the resistance of a cold worked metal is measured during annealing, the change in ρ_{CW} is small compared to ρ_T and, therefore, any changes due to recrystallization are masked. However, if it were possible to measure directly the difference in resistivity ($\Delta \rho$) between a cold worked sample and a previously fully annealed specimen (i.e. a reference standard) of the same material, then:

$$\Delta \rho = \rho_{CW} + \rho_{GB} \quad (6)$$

assuming that ρ_i and ρ_T are not influenced by cold work, and that ρ_{CW} and ρ_{GB} can both be regarded as zero

for a fully annealed sample. Thus, $\Delta\rho$ is a direct indication of the progress of annealing, regardless of temperature or temperature fluctuations.

The circuit originally proposed by Muir and Strom-Olsen³² can be modified to measure the difference in resistance of two specimens (Figure 18a). The lock-in amplifier has a differential input which may be switched to read either V_1 or V_2 (the voltages across each sample), or $\Delta V = V_1 - V_2$. Since the resistances of the samples are of the order of a few milliohms, the 500 ohm ballast resistor converts the signal generator into a constant current source. If the change in the resistance is very small (of the order of 0.05 milliohm), then the change in the voltage across the cold worked specimen is correspondingly small. This change is magnified by two commercially available, high quality, shielded 30:1, audio transformers, T_1 and T_2 , which are identical in performance to within 0.1%.

This arrangement also had to be adapted to monitor the change in electrical resistivity of metals during annealing. This was done by building a probe that could be inserted into a furnace and, in particular, hold specially designed specimens of the metal.

In order to determine $\Delta\rho$ from the measured voltage, ΔV , the geometry of the specimens must be known.

Since the same current flows through both the cold worked and annealed specimens, then:

$$\Delta V = R_1 - R_2 = \rho_1 \left[\frac{L_1}{A_1} \right] - \rho_2 \left[\frac{L_2}{A_2} \right] \quad (7)$$

where L and A are the length and cross-sectional area, respectively, of the specimens. If the specimens are identical, then:

$$\Delta \rho = \frac{\Delta V}{I} \left[\frac{A}{L} \right] \quad (8)$$

(i.e. $\Delta \rho$ is directly proportional to ΔV).

Specimens of identical geometry were produced (Figure 18b) using a die and punch, which enabled them to be matched more closely. Mismatch of the specimens results in a deviation from that of matched pairs by an amount proportional to:

$$\rho_m \times \left[\frac{L_1}{A_1} - \frac{L_2}{A_2} \right] \quad (9)$$

A similar but more erratic error occurs if there is a difference in temperature between the specimens. In order to equalize the temperature between the cold worked sample and the standard, the specimens were tightly held in

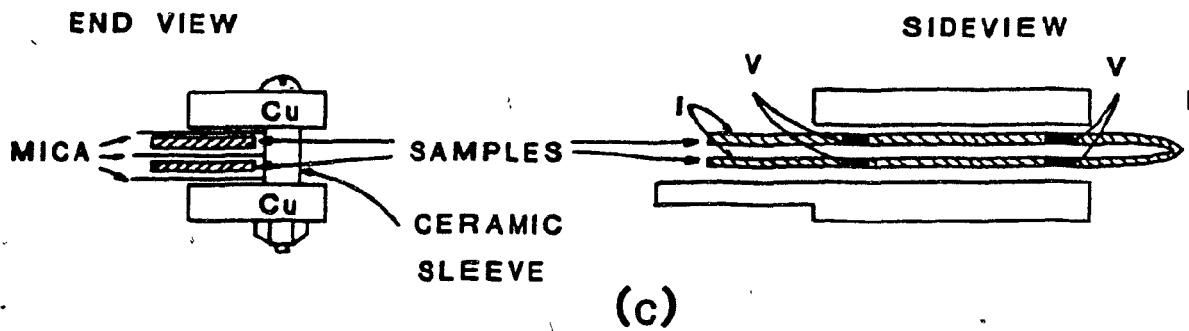
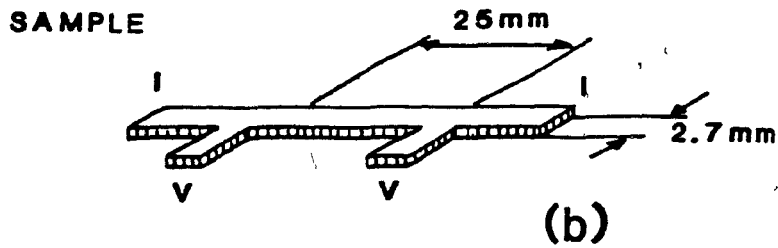
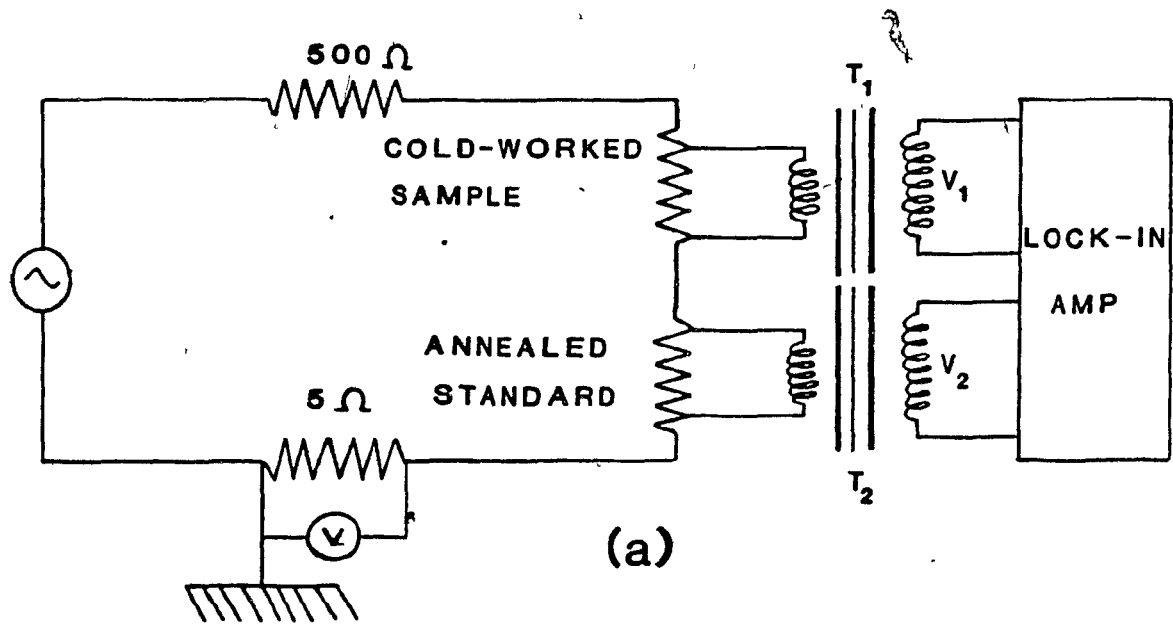


Figure 18. Circuit, Sample Design and Sample Holder.

a copper holder (Figure 18c), and insulated from each other with thin sheets of natural mica.

The leads to the specimen were insulated from each other by small diameter, twin bore, ceramic thermocouple tubes. The current leads (I) were separated from the potential leads (V) by approximately 1cm, to minimize any inductive coupling between them.

The voltage, ΔV , and temperature were recorded continuously on a floppy disc, using a microcomputer system. This system will be described in greater detail later.

The great advantage of the differential A.C. technique over D.C. methods is that the effects due to thermally generated emf's produced in the current and potential leads are completely eliminated. This enables measurements to be taken continuously and "in situ" for the complete duration of the annealing cycle.

3.5 APPLICATION OF THE DIFFERENTIAL RESISTIVITY METHOD TO THE ANNEALING OF LOW CARBON STEELS

The differential resistivity technique described in the previous section was first successfully used by Drew et al³¹ to follow the progress of annealing of cold rolled α -brass and copper, both single-phase materials. The purpose of the present research was to develop and

refine this method so that it could be used to follow the progress of annealing in cold worked low carbon sheet steel. This was expected to be difficult since the recrystallization temperature (and therefore the industrial annealing temperature) of low carbon steel is approximately 400°C higher than that of copper or α -brass. Steel, being at least a two-phase material, is also a more complex material.

Another difficulty arises from the fact that, unlike copper, the rate of increase of the resistivity of steel is not proportional to the increase in temperature. Figure 19 shows the reduced resistivity (ρ_T / ρ_{RT}) for plain carbon steel³³ and copper³³, plotted as a function of temperature, where ρ_T is the electrical resistivity at temperature T, and ρ_{RT} is the electrical resistivity at room temperature. The data for plain carbon steel correspond closely to those for the steel used in the present research; further information on this steel will be given later.

The increase in the reduced resistivity for copper from room temperature to 700°C is of the order of 3:1. In contrast, the value of ρ_T / ρ_{RT} for plain carbon steels varies much more strongly with temperature, increasing by about 9:1, from room temperature to 700°C. The effect of this, when measuring the differential resistivity during the annealing of steel, is to increase

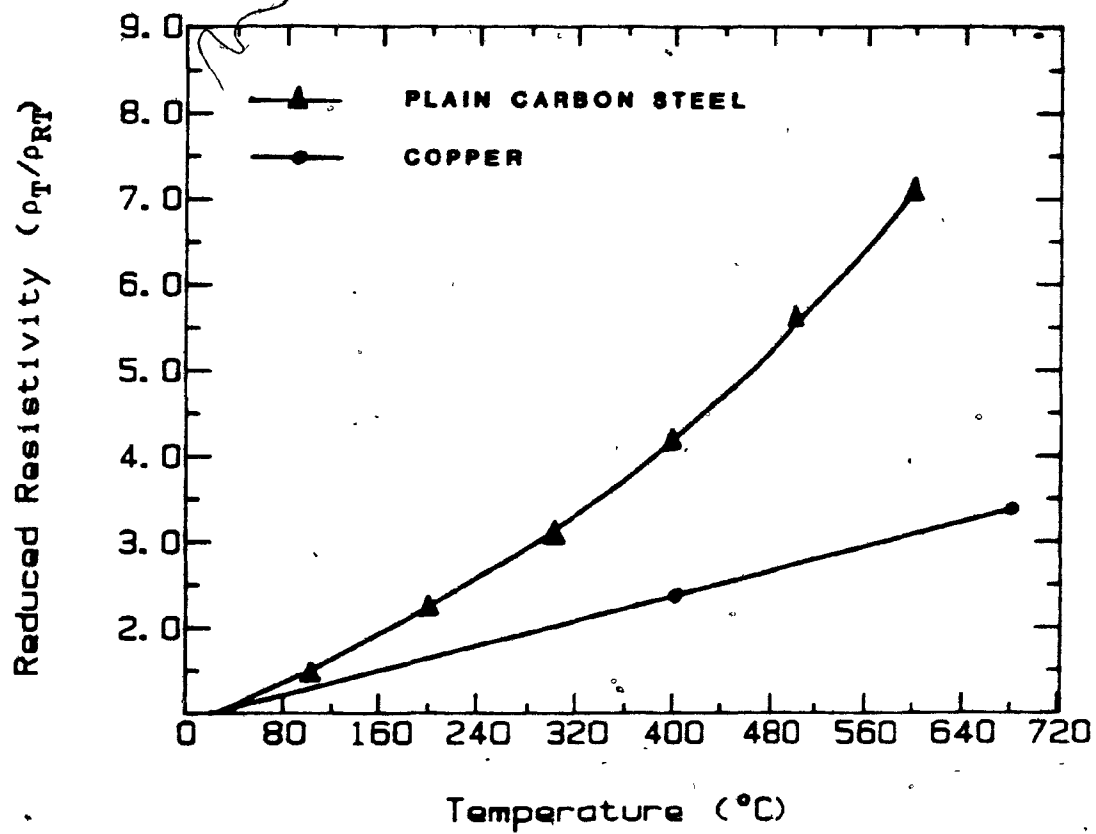


Figure 19. Variation of Reduced Resistivity with Temperature for Copper and Plain Carbon Steel.

the accuracy of the measurement. This is because there is a larger increase in voltage across each steel sample than in the case of copper or α -brass (In general, the larger the voltage drop, the more accurately it may be measured). Although this makes measurement at high temperatures more accurate, if the two specimens differ in temperature by more than about $\pm 0.5^\circ\text{C}$, the accuracy of measurement of ΔV decreases to an unacceptable level. It is for this reason that the two specimens must be clamped tightly together in a copper holder to minimize thermal gradients. The net result is that the accuracy of measurement of ΔV for iron and steel is about $\pm 4\%$, much lower than that for copper ($\pm 1\%$), or α -brass ($\pm 0.5\%$)³¹.

Since steel is (at least) a two-phase system, the solution (or precipitation) of carbon was also expected to influence the accuracy of measurement. However, with the use of a differential method - assuming the composition of the samples to be identical - these effects turned out to be of minor importance, and did not affect the accuracy of measurement.

3.6 SENSOR DESIGN

The samples prepared by Drew et al.³¹ in the study of copper and α -brass were machined from plate or strip metal to the dimensions seen in Figure 18c. Apart

from being a long and tedious process, machining did not provide the precise dimensional control required for sample matching. In Section 3.4 it was explained how differences in the dimensions affected the final results. In the present work, all the samples were made using a specially designed punch and die, which improved the dimensional precision to better than 1%.

Another difficulty arose due to the variation in the thickness of the sheet across the rolling direction, a consequence of poor roll quality. To solve this problem, a small jig was designed (Figure 20) which enabled the differential resistivity of two cold worked specimens to be measured at room temperature. One specimen was used as a reference, against which about 20 to 25 others were compared. Samples were then matched up by pairing off those with the most similar readings against the reference. One of the specimens in each matched pair could then be annealed to the required heat treatment.

Electrical connections for the voltage and current leads were made by spot welding constantan wire to the tags on the matched pairs. The cold worked and annealed samples were then spot welded together at one end (Figure 21). Constantan wire is an ideal material for electrical leads: it spot welds easily to steel, does not undergo any phase changes in the annealing temperature range (near

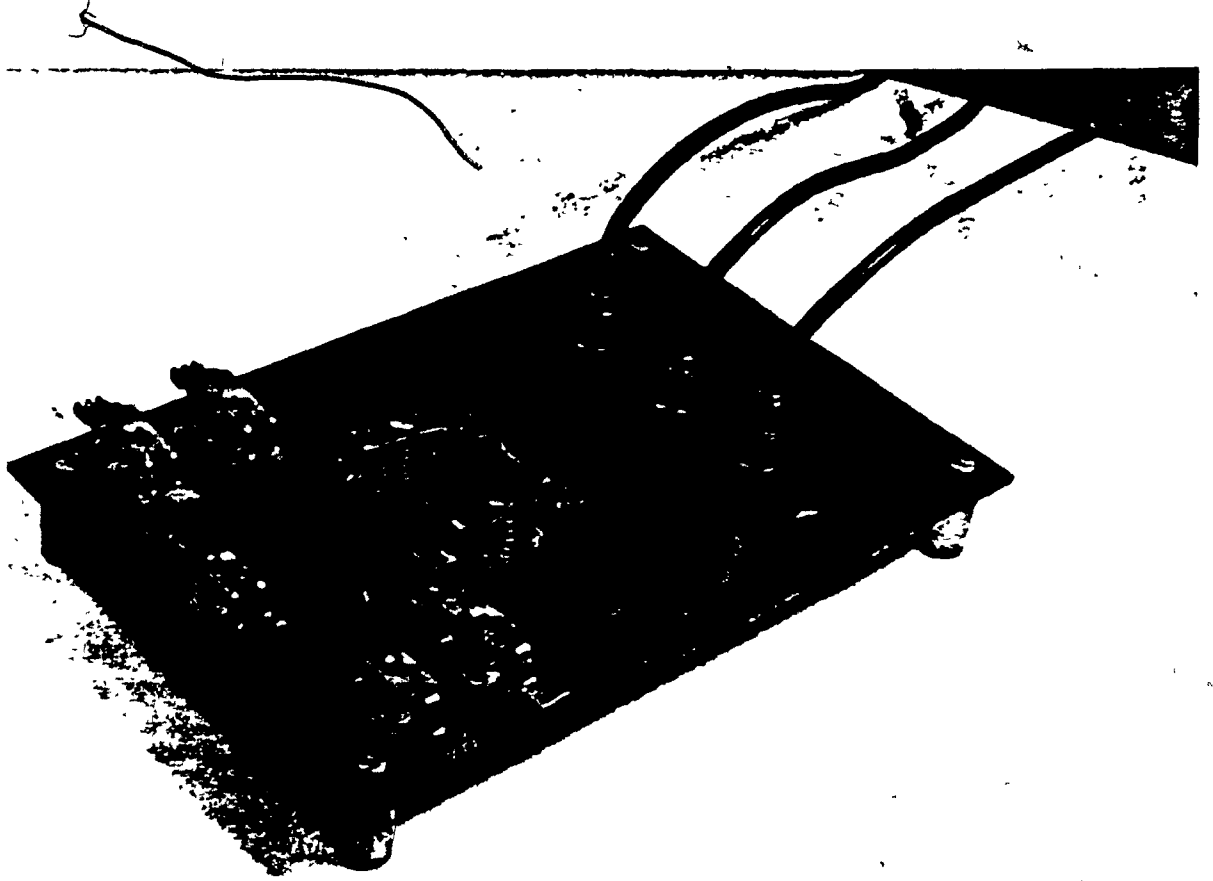


Figure 20. Matching Jig.

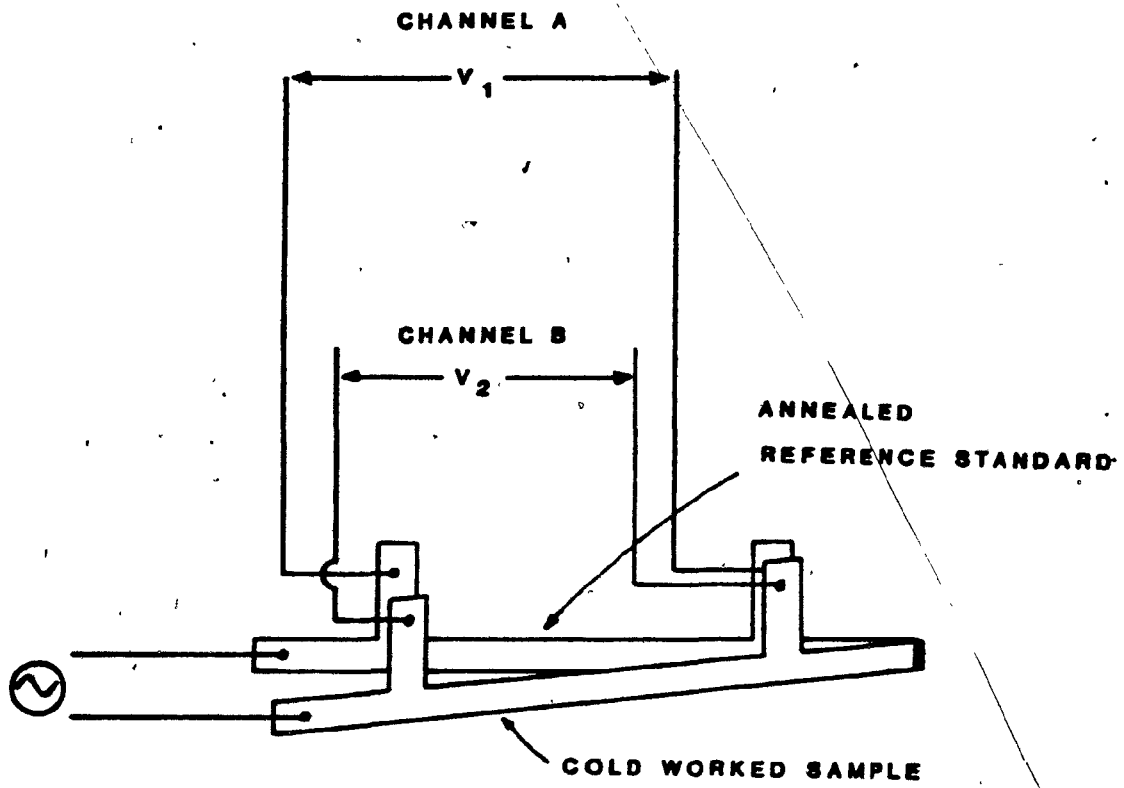


Figure 21. Specimen Arrangement.

700°C), and has a low temperature coefficient of resistivity over that range.

3.7 ANNEALING OF REFERENCE STANDARDS

The steel reference standards were annealed in a high vacuum to protect them from oxidation. Table I shows the five heat treatments that were used. Figure 22 shows the typical grain structures and grain sizes obtained by these heat treatments.

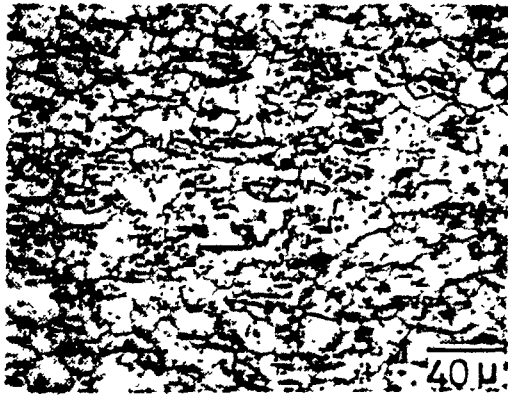
The object of heat treatment A was to obtain a reference standard that retained as much carbon as possible in solution at low temperatures. Standards treated in this way were stored at -20°C to prevent aging (i.e., precipitation of carbides) at room temperature prior to being used.

Heat treatments B and C aimed to achieve a minimum and maximum grain size at a temperature of 700°C. Figure 23 shows the increase in grain size with annealing time at 700°C. From this graph it is clear that a minimum grain size of 5.81 μm is obtained after 15 minutes annealing time and the maximum of 8.78 μm after 64 hours. By allowing the standards to cool slowly in the furnace from the annealing temperature, it was hoped that their carbon compositions would be in equilibrium on reaching room temperature.

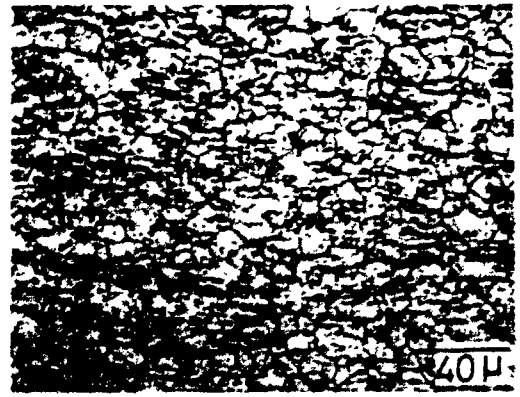
TABLE I

HEAT TREATMENTS USED TO PRODUCE REFERENCE STANDARDS

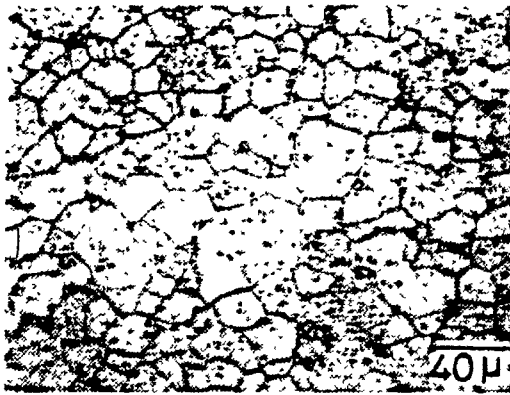
HEAT TREATMENT	TIME/TEMPERATURE	COOLING METHOD
A	15 minutes @ 700°C	water quench
B	15 minutes @ 700°C	furnace cooled
C	64 hours @ 700°C	furnace cooled
D	0.5 hours @ 1100°C	furnace cooled
E	0.5 hours @ 1100°C + 64 hours @ 700°C	furnace cooled



(a) GS=5.1μ



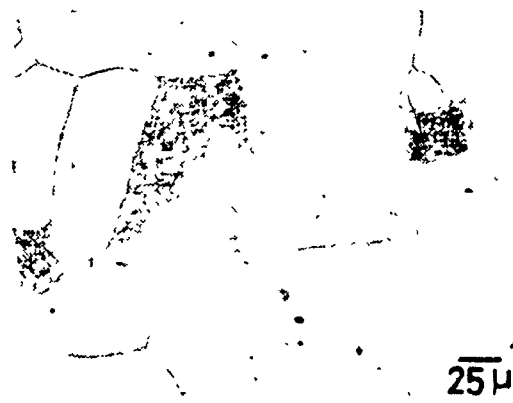
(b) GS=5.9μ



(c) GS=8.8μ



(d) GS=30.3μ



(e) GS=31.2μ

FIGURE 22.-TYPICAL GRAIN STRUCTURES

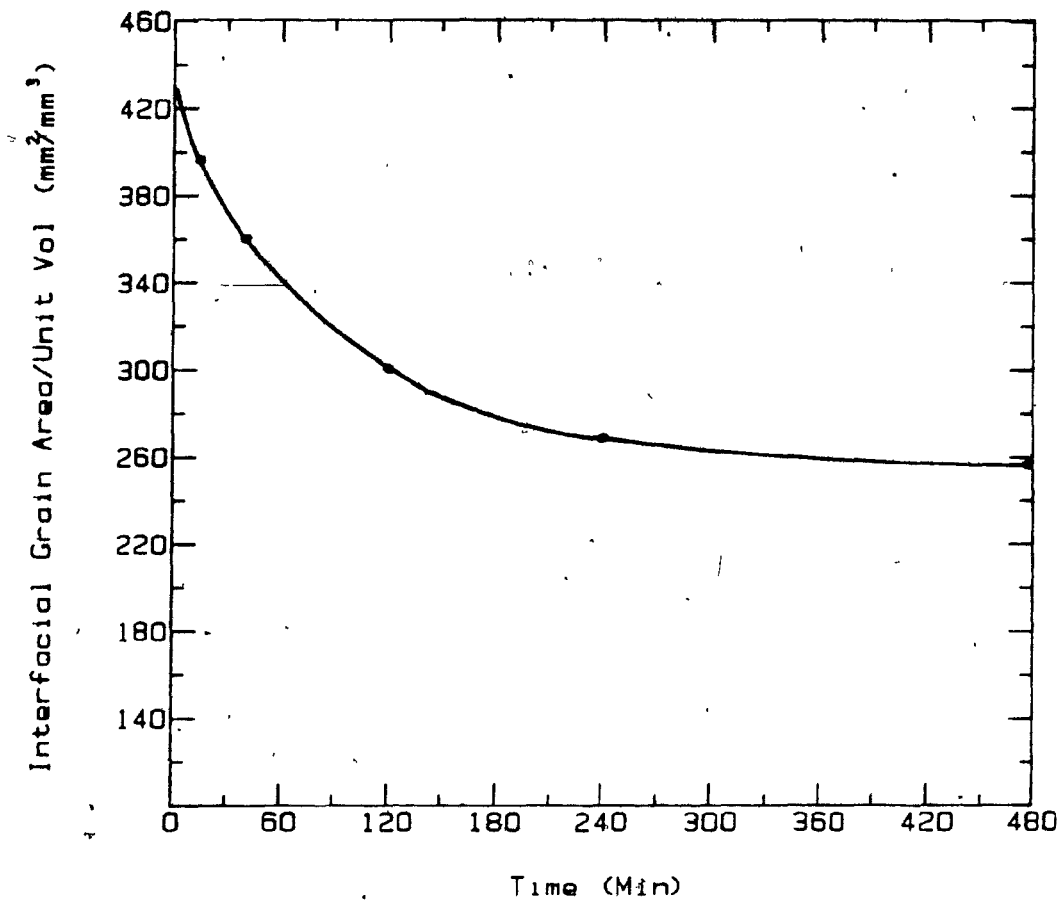


Figure 23. Increase in the Grain Size of the Steel with Annealing Time at 700°C.

By heating the standards to 1100°C (into the austenite range), as in heat treatments D and E, and then slowly cooling from this temperature, a very large grain size of 30.3 μ was obtained, with about 35% of the grain structure being pearlite. Further heating at 700°C for 64 hours, as in heat treatment E, ensured that the pearlite became spheroidized.

The reference standards used in heat treatments D and E were slowly cooled in the furnace to room temperature in order to ensure that they were in equilibrium.

3.8 FURNACE CONTROL

The furnace used for the main study of in-situ changes in resistivity during annealing was made up of a 40 cm long, 2.5 cm inside diameter mullite tube. Kanthal A-1 resistance wire was wound around the tube in a bifilar manner to avoid electrical induction in the samples. The coils were also wrapped around the tube in such a way that the coils at the ends were closer together than in the middle. This made the hot zone as long as possible (approximately 10 cm). The maximum variation in temperature within this zone was $\pm 2^\circ\text{C}$. The furnace was heated by a regulated D.C. power supply, controlled by a proportional gain control, and pre-programmed ramp

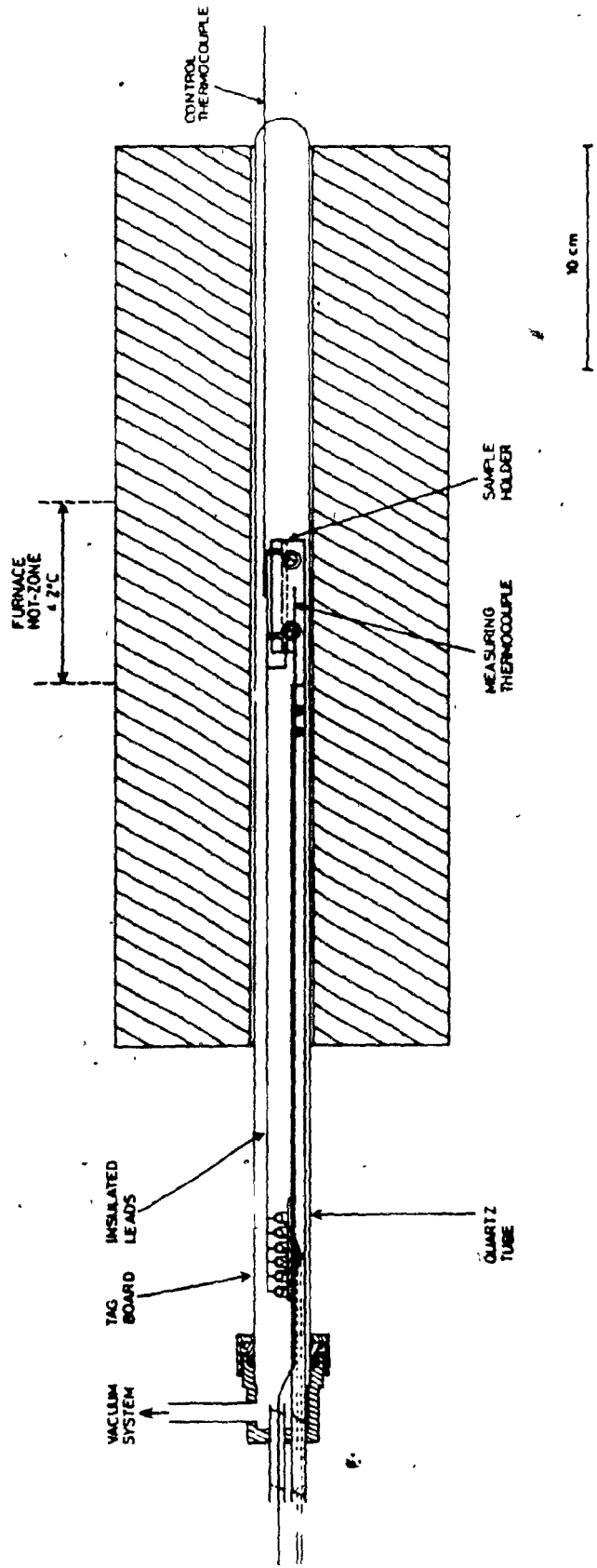


FIGURE 24 - EQUIPMENT SET-UP

generator. The ramp generator was capable of providing a range of constant heating or cooling cycles of 30 minutes to 128 hours, to the required temperature in increments of a factor of two:

3.9 ATMOSPHERE CONTROL

All experiments were carried out under vacuum, using a rotary and diffusion pump system capable of achieving a vacuum of 10^{-5} torr. There was also provision for the introduction of a protective gas. To ensure that oxidation of the samples was reduced to an absolute minimum, a few small pieces of titanium sponge were placed in the hot zone to act as an oxygen getter.

3.10 EXPERIMENTAL PROCEDURE

The basic arrangement of the annealing probe as used in the experimental furnace is shown in Figure 24. The probe, with the copper holder and samples clamped tightly within it, was placed in a quartz tube sealed at one end. The seal between the probe and the quartz tube was provided by an "O" ring, squeezed against the quartz tube to make the seal. All the electrical leads and thermocouples were sealed into the probe with high-vacuum sealing wax.

Both the control and measuring thermocouples were of the "E" type because, in the range of 0 to 1000°C, the "E" type thermocouple gives the highest voltage output of all the thermocouple types, and, therefore, the most accurate reading, and is also suitable for use in a vacuum. The tip of the measuring thermocouple was pressed against the centre of the copper holder to give the best reading of the sample temperature. The control thermocouple passed between the quartz tube and the furnace wall so that the control action and response times could be as fast as possible. In addition, both thermocouples were compensated for room temperature, using Omega-CJ cold junction compensators.

All cables to and from the sensor were shielded with coaxial cable to prevent any spurious A.C. interference arising from other devices in the vicinity of the experiment.

3.11 DATA ACQUISITION SYSTEM

In the previous work done by Drew et al³¹, the data were plotted continuously with an X-Y chart recorder. This proved to be an awkward means of treating the data because there were a number of subsequent calculations which had to be carried out and which, when done by hand, were very time-consuming. The decision was therefore made

to employ a microcomputer which could handle data acquisition, manipulation, storage, and real time plotting.

Figure 25 is a schematic illustration of the system that was used. The central component was the Gimex (6809) microprocessor, which was able to control the various peripherals like the floppy disc drives, the graphics plotter, and the μ MAC-4000 analogue-to-digital converter. The computer worked with a low level assembler language, simultaneously with a high level Basic language. The assembler program which, for copyright reasons, cannot be published here, was supplied by S.A. Argyropoulos.³⁴ This activated, controlled, and received data from the μ MAC-4000, and stored these values on a temporary spot on the computer memory. The Basic programme (Appendix I) then took these data and performed several functions:

1. The thermocouple temperature reading was converted from millivolts to degrees celsius by a polynomial conversion. The Basic programme computed and directed this result, with the ΔV reading to be stored on a floppy disc drive.
2. The temperature and ΔV data were then used to calculate the derivative of the data. This was accomplished by completing a regression analysis over

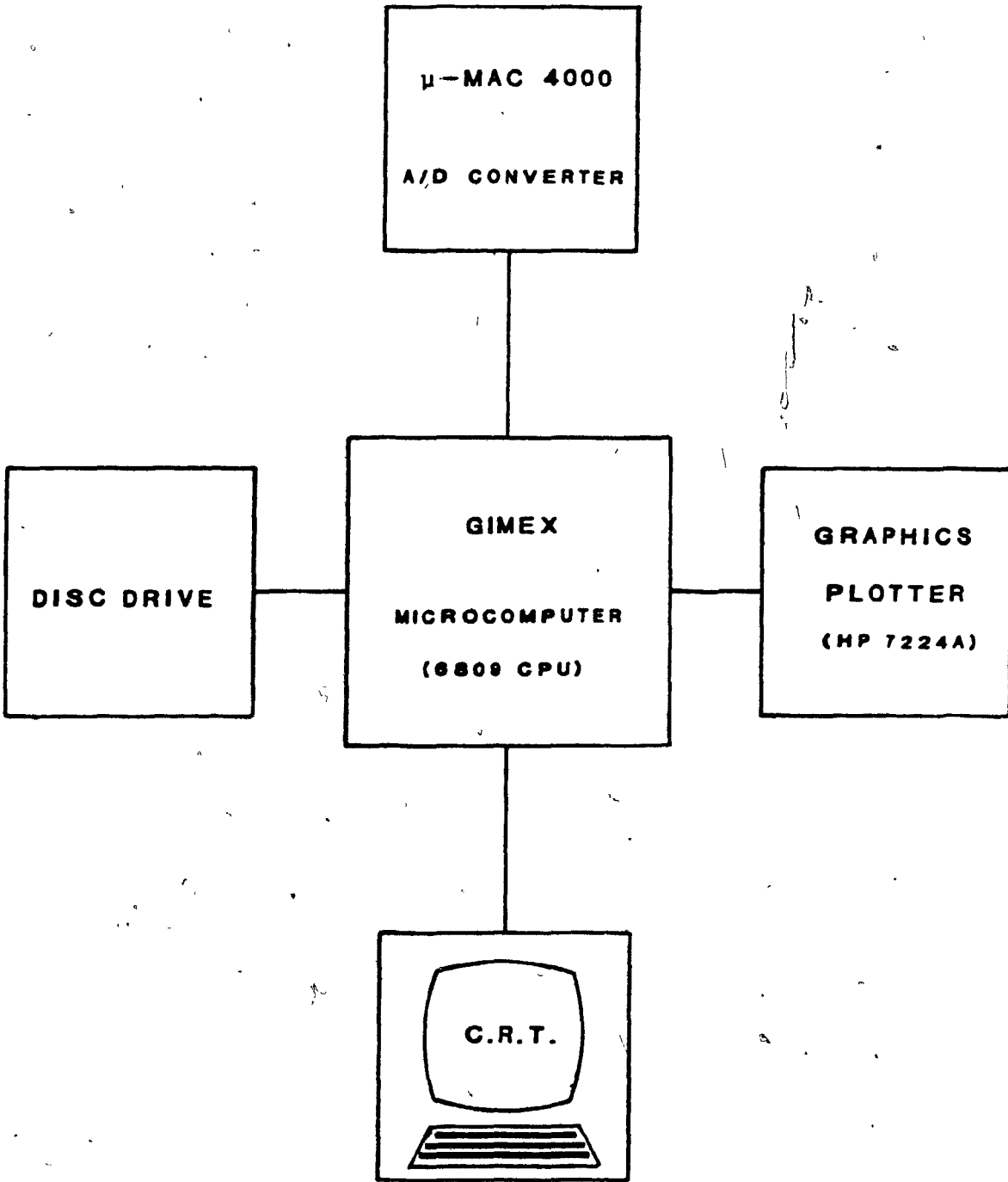


Figure 25. Data Acquisition System.

twenty points -- a temperature span of approximately 2°C. From this, the slope at a particular temperature was obtained and, once again, directed to a separate file on a floppy disc. This data group was then advanced by five readings, and the whole operation repeated.

3. The Basic programme also controlled and relayed both sets of data directly to a Hewlett Packard 7224A graphics plotter so that the data could be plotted on a real time basis. This meant that both sets of data could be plotted simultaneously during the experiments.

3.12 METALLOGRAPHY AND HARDNESS MEASUREMENTS

Metallography and hardness measurements were required on samples of the steel under study in order to compare them with the results obtained from the differential resistivity measurements. Samples of steel were prepared to correspond to different stages of the annealing cycle. Each sample was heated to the required temperature at the same rate as was used in all the experiments, and then cooled rapidly (but still in vacuum) outside the furnace.

Hardness tests were carried out immediately after heat treatment, in order to eliminate any age hardening

that might otherwise occur. A Vickers hardness tester was used to take the measurements using a load of 2.5 kg.

Metallographic specimens of the same heat treated samples were polished in stages from 240 to 600 mesh silicon carbide papers, and then from 6 micron down to 0.25 micron with diamond polishing wheels.

Photomicrographs were taken of the specimens on a Neophot metallograph. Grain size measurements were made directly on the micrographs using the grain boundary linear intercept method.

3.13 MATERIAL SELECTION

The steel used in this work was a commercial grade of steel, of the type commonly supplied to the automobile industry, and made available by Stelco Inc.

The chemical analysis of the steel was carried out on an emission spectrometer, and showed it to be a run-of-the-mill, low carbon steel (Table II). Table III details the amount of cold reduction received by the steel, its thickness, final hardness, and room temperature resistivity. These properties are similar to those expected of a low carbon cold rolled steel sheet of an AISI-SAE grade 1020 steel.

TABLE II

Chemical Analysis

C	Mn	P	S	Si	Cu	Ni	Cr	Mo
0.175	0.590	0.005	0.016	0.010	0.028	0.019	0.128	0.002

TABLE III

Physical Analysis

Prior Cold Reduction (%)	Cold Rolled Thickness (mm)	Vickers Diamond Pyramid Hardness (VHN)	Room Temperature Resistivity ($n\Omega m$)
82	0.41	234	172

CHAPTER 4

RESULTS AND DISCUSSION

4.1 INTRODUCTION

The discussion of the experimental work described in this thesis will be in the following sequence.

- a) The first section will deal with typical results obtained with the differential resistivity technique for the low carbon steel whose properties were detailed in Chapter 3. The three stages of annealing (recovery, recrystallization and grain growth) will be discussed in detail. Special use will be made of the derivative plots of the resistivity/temperature curves, which illustrate more dramatically than straight plots the changes in resistivity that occur upon annealing.
- b) The second section will point out some anomalous behavior in the resistivity/temperature relationships during the recovery stage of annealing. This behavior will be explained using the results of subsidiary heat treatment experiments.
- c) The third section will examine how the differential resistivity technique might be improved to monitor and measure grain growth at the annealing temperatures normally used in steel processing (650 - 725 °C).

CHAPTER 4

RESULTS AND DISCUSSION

4.1 INTRODUCTION

The discussion of the experimental work described in this thesis will be in the following sequence:

- a) The first will deal with typical results obtained with the differential resistivity technique for the low carbon steel whose properties were detailed in Chapter 3. The three stages of annealing, recovery, recrystallization, and grain growth will be discussed in detail. Special use will be made of the derivative plots of the resistivity/temperature curves, which illustrate more dramatically than straight plots the changes in resistivity that occur upon annealing.
- b) The second section will point out some anomalous behavior in the resistivity/temperature relationships during the recovery stage of annealing. This behavior will be explained using the results of subsidiary heat treatment experiments.
- c) The third section will examine how the differential resistivity technique might be improved to monitor and measure grain growth at the annealing temperatures normally used in steel processing (650 - 725°C).

- d) The fourth section will be concerned with experiments on the simulation of industrial batch annealing.
- e) The final section will discuss the potential adaptation of the technique to the monitoring and control of a large (250 tonne) industrial batch annealing furnace.

4.2 GENERAL DISCUSSION OF ANNEALING OF LOW CARBON STEEL

It was previously explained in Chapter 3.4 that ΔV is directly proportional to the differential resistivity ($\Delta \rho$). Since all of the measurements recorded in each experiment were in terms of the voltage (ΔV), henceforward, all references to the differential resistivity will be referred to as ΔV .

Figure 26 shows a typical plot of ΔV versus temperature obtained for the low carbon sheet steel detailed in Chapter 3. The cold worked sample was matched with a reference standard annealed to heat treatment B (Table 1). The lines OM and MF represent the change in ΔV with temperature during the heating and cooling cycles respectively. V_{SAMP} and V_{RS} indicate the directions that an increase in the resistivity of the sample or reference standard would have on the value of ΔV .

The three stages of annealing are identified in Figure 26. Recovery (Stage 1), which occurred between room temperature and 530°C, resulted in a decrease of 60% in ΔV . Recrystallization (Stage 2) resulted in a 40% decrease in ΔV between 530 and 600°C. The change in ΔV resulting from grain growth (Stage 3) between 600 - 700°C was very small in this case, and could not be accurately quantified. However, further investigation into grain growth was carried out and will be described later.

The overall percentage decrease in ΔV at room temperature resistivity is given by:

$$\frac{\Delta \rho_T}{\rho_{RS}} \times 100 = \frac{\Delta V_T}{V_{RS}} \times 100 \quad (10)$$

where $\Delta \rho_T$ and ΔV_T are the total differential resistivity and voltage changes after annealing, and ρ_{RS} and V_{RS} are the resistivity and voltage across the reference standard at room temperature.

The overall percentage decrease in room temperature resistivity resulting from annealing was 4.5% (this decrease corresponding to the change from an 80% cold rolled state to a fully annealed one). This compares with decreases of 13% and 2% reported previously³¹ for 60% cold worked α -brass and 50% cold worked copper respectively. The magnitude of the decrease in ΔV during

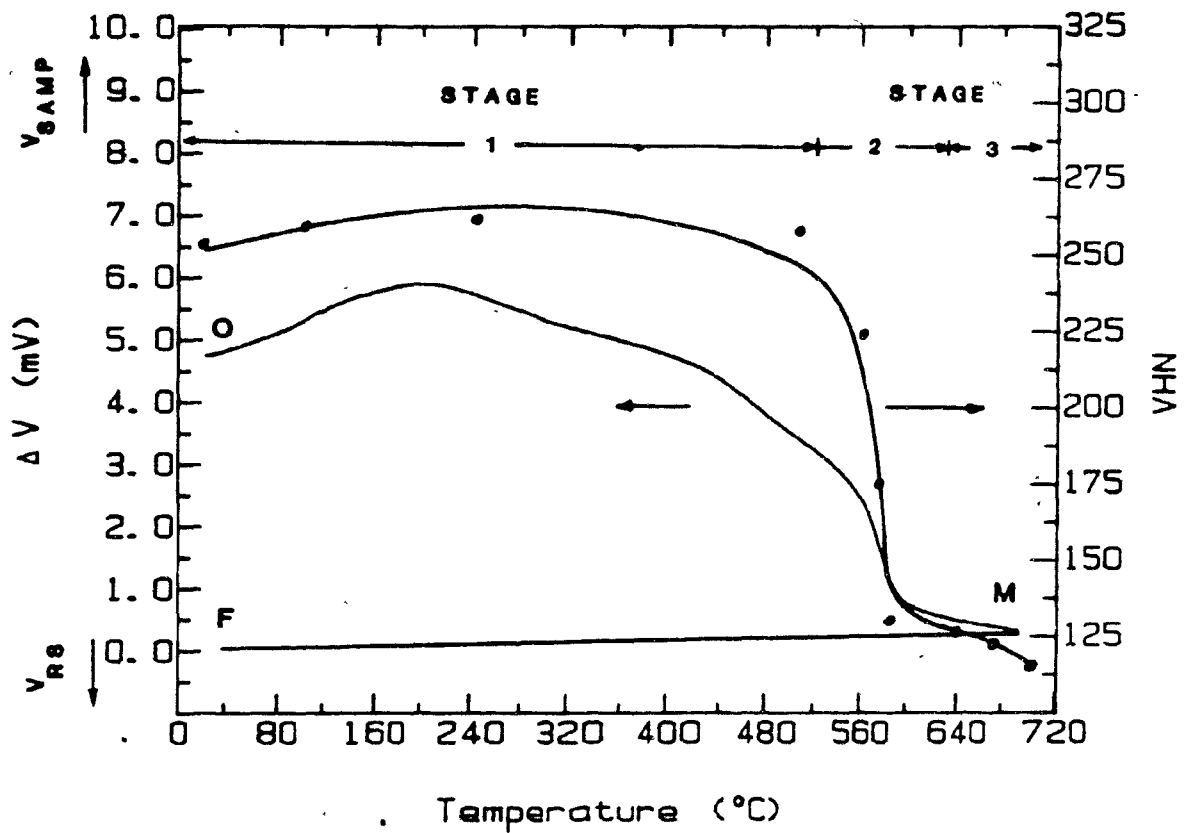


Figure 26. The Change in ΔV and Hardness with Steadily Increasing Temperature (heat treatment B). (Reference Standard = heat treatment B)

recrystallization is an intrinsic property of the metal being tested, as well as being dependent on the degree of cold work.

Also shown in Figure 26 is the change in hardness that resulted from annealing. Good correlation was observed between ΔV and hardness data; as expected, the largest change in hardness occurred during recrystallization (Stage 2, 530°C) with only a minor decrease in hardness resulting from grain growth (Stage 3).

Figure 27 illustrates the metallographic changes that occurred during stages 2 and 3. Micrograph (a) illustrates the microstructure at about 50% recrystallization, and (b) after complete recrystallization. Very little grain growth occurred between 640°C and 700°C (micrograph (c)), which explains the relatively small changes in ΔV and hardness that were observed in Stage 3.

Figure 28 shows the plot of ΔV and the derivative of ΔV , $(d(\Delta V)/dT)$, as a function of temperature for the annealing heating cycle (line OM in Figure 26). Both graphs were plotted simultaneously by the microprocessor during the experiment.

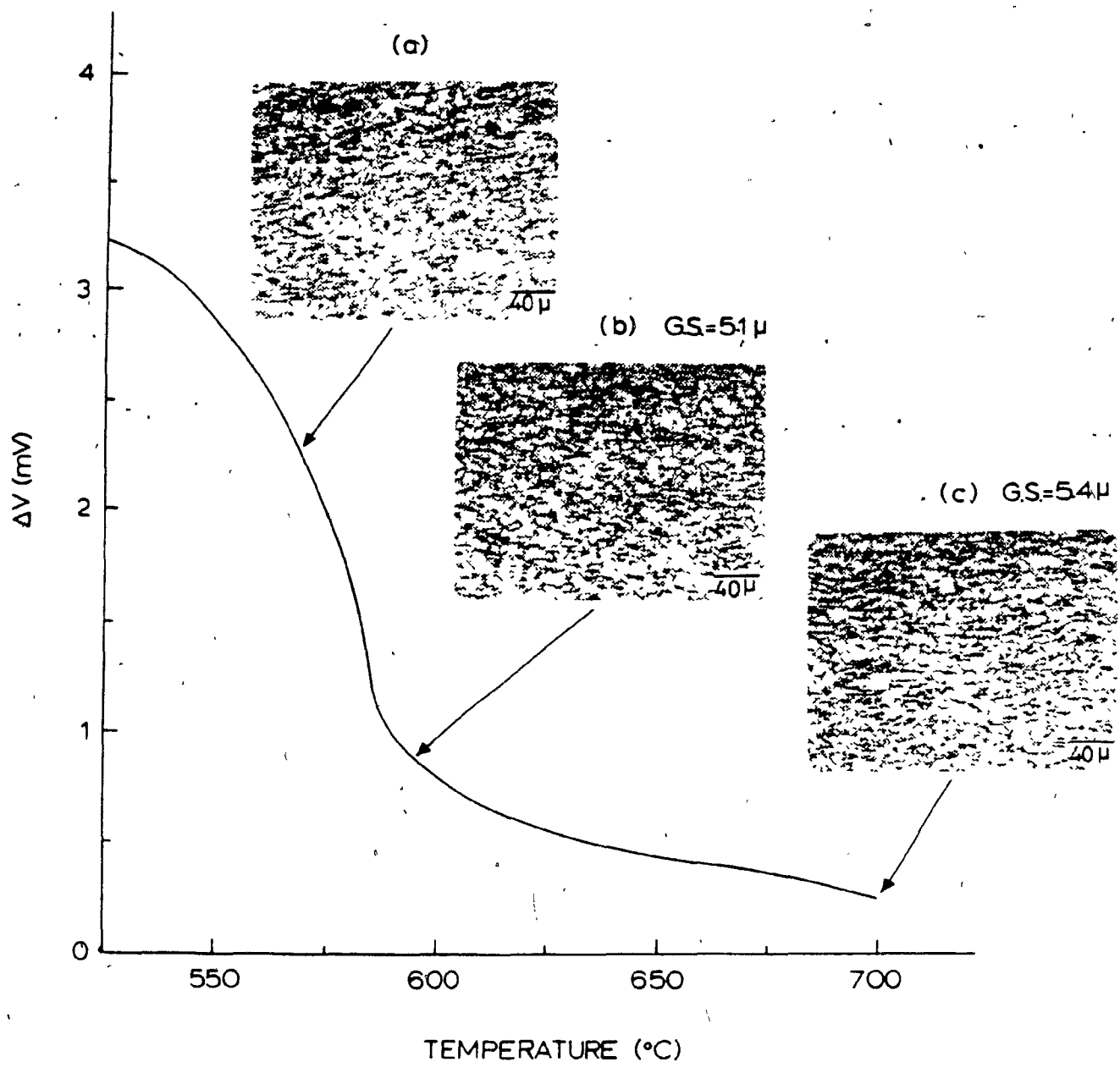


FIGURE 27. - ΔV vs T DURING RECRYSTALLIZATION AND GRAIN GROWTH

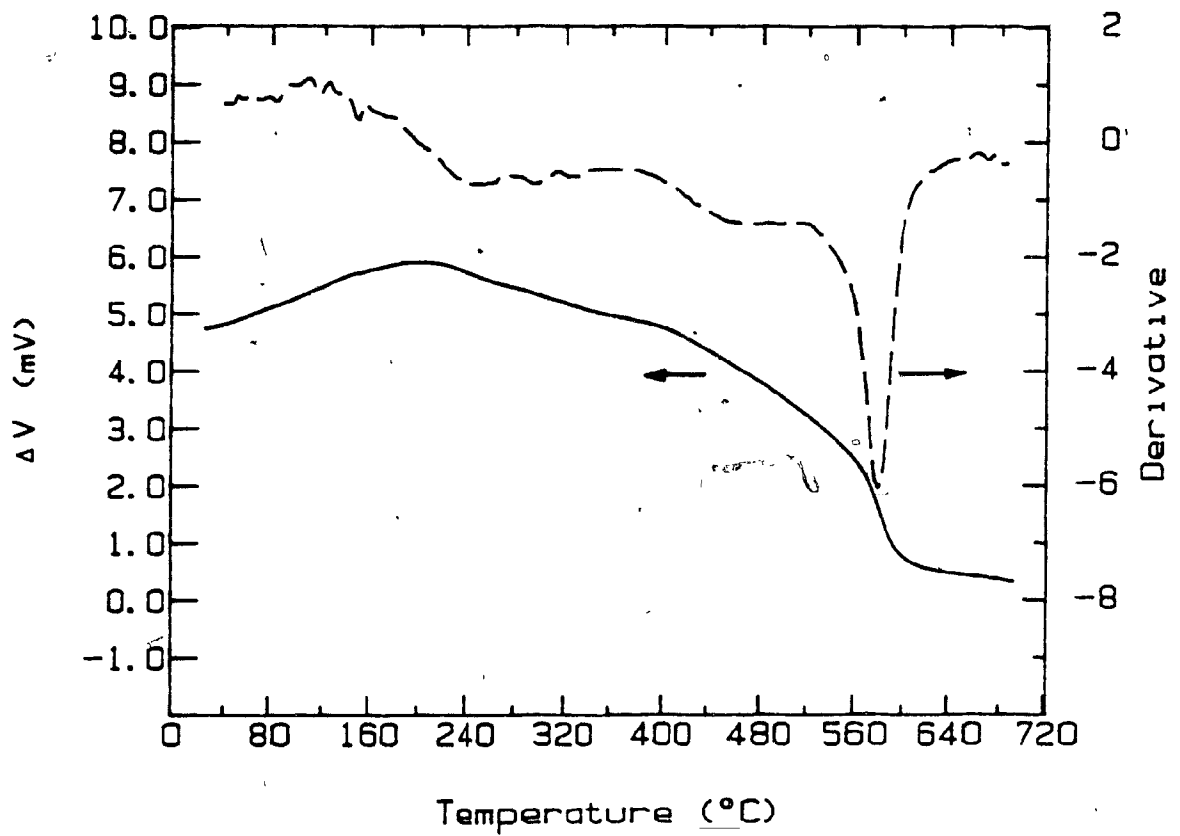


Figure 28. Plot of ΔV and the Derivative of ΔV ($d(\Delta V)/dT$) as a Function of Temperature. (Reference standard = heat treatment B)

The derivative curve clearly defines the recrystallization stage as a large peak which is much more obvious than the slope change in the conventional ΔV versus temperature plot. The beginning, middle, and end of recrystallization can easily be identified in this way. For this particular experiment, the midpoint of recrystallization (i.e. the point where nucleation and growth rates are clearly at a maximum) was at 570°C. This method of portraying results (using the derivative of ΔV is also important from an operational viewpoint: the technique, backed up by the microprocessor and instrumentation already described, thus allows continuous monitoring of what is happening at any moment within the steel itself. Observations are free of inference or "experience" or personal judgement. The resistivity probe plus microprocessor and plotter is indeed an accurate, direct sensor of the microstructural state of the metal.

4.3 RECOVERY STAGE

The previous section pointed out that the three stages of annealing (recovery, recrystallization, and grain growth) can clearly be identified using the differential resistivity technique. The recovery stage (Stage 1) in Figure 26 showed an unexpected (but repeatable) increase in ΔV . This was followed by a

decrease prior to recrystallization. It was assumed that the resistivity of the reference standard increased continuously (only as a result of ρ_T) with the increase in temperature. The increase in ΔV was therefore ascribed to a physical change occurring in the cold worked sample that was not occurring in the reference standard. An increase in the resistivity has to be a result of the increase in the number of electron scattering points (such as interstitial atoms). Such an increase would be inconsistent with previous observations of the changes in the resistivity of metals during recovery^{22, 29, 35}, which have all shown that the resistivity decreases and approaches its original value (prior to cold work). This, it is argued, would be expected, since recovery is presumed to be a rearrangement of the structure of the cold worked lattice before recrystallization. The problem, however, is that recovery is an overall change that occurs as a result of a combination of processes, which have to be studied individually to determine their effects. It is generally accepted that recovery is: (1) the ordering and annihilation of dislocations to form dislocation cells; (2) the production and annihilation of point defects; and (3) the precipitation of interstitial atoms around dislocations. These re-ordering processes are presumed to result in a decrease in the number of

electron scattering points and consequently result in a decrease in resistivity.

The anomalous behaviour recorded in the recovery stage in the previous experiments is probably made more visible because the differential resistivity technique is an "in situ" method, which is very accurate and, in this case, is measuring changes in voltage between the matched pairs of specimens as small as 1 in 400 mV (0.25%) at these temperatures. Previous investigations^{22, 29, 30, 35} relied on measurements taken on specimens quenched from the annealing temperature. As a consequence, previous results could have been subjected to uncertainties and inaccuracies related to, for example, the quench rate, which would otherwise overshadow small (real) changes in resistivity during recovery.

It has already been stated that recovery is the rearrangement of dislocations and the annihilation of vacancies prior to recrystallization. Since the structure becomes more ordered, it is not possible to reverse the process of recovery, therefore any physical properties affected by recovery would also be irreversible. Hence, if the profile of the ΔV /temperature data up to 400°C, seen in Figure 26, is due to recovery, it should be an irreversible change. This was investigated by conducting an identical experiment to the one that produced the

result seen in Figure 26 but, this time, the cold worked sample was also heat treated. This heat treatment was carried out for 15 minutes at 400°C (the temperature at which the part of the recovery stage of interest was presumed to have finished), and then allowed to cool slowly. The result of the experiment can be seen in Figure 29, and is compared to the result seen in Figure 26 (broken line). The profile of the data seen in Figure 26 below 400°C has disappeared as a result of the 400°C heat treatment, and the profile seen in Figure 26 can therefore be attributed to processes occurring during recovery.

The exact nature of the structural changes that cause this anomalous behavior could probably be determined, using reference standards that have been heat treated in a different way (e.g. heating to the annealing temperature and then quenching). By providing an annealed reference standard in which one particular aspect of its structure (e.g. the precipitation of carbides) changes during a heat treatment experiment, it was hoped that the structural changes occurring in the cold worked sample could be identified. The object of heat treating the reference standard, therefore, was to create a structure in the steel which, when used in a differential resistivity experiment, would exhibit similar changes in electrical resistivity (upto 400°C), as in a cold worked

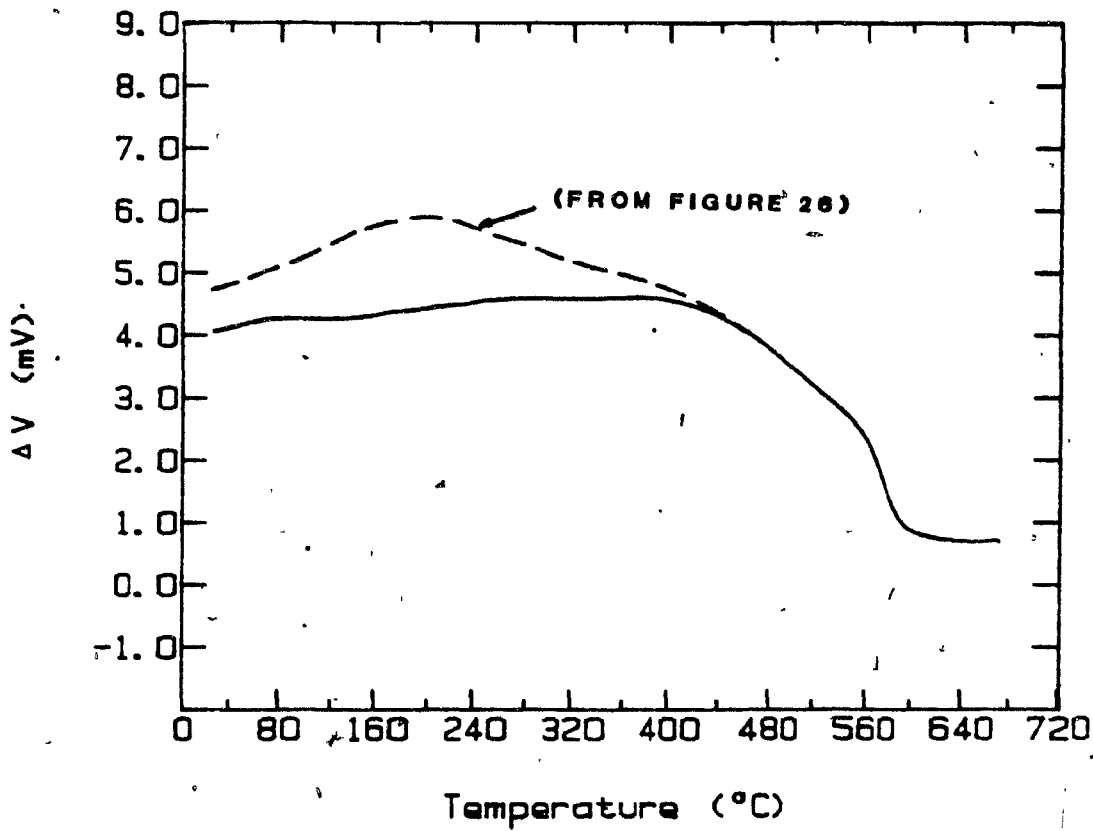


Figure 29. Reference Standard Annealed to Heat Treatment B.

sample. The behavior of the ΔV /temperature relationship in such an experiment during recovery would be expected to be constant.

The heat treatment of the reference standard that was able to give a result like that described above was heat treatment A in Table I. The reference standard was quenched from 700°C to produce: (1) a structure with a large proportion of the carbon content in solid solution at room temperature, and (2) to quench in vacancies which are formed at high temperatures.

The result gained from using the reference standard described above is shown in Figure 30, with the result illustrated in Figure 26 superimposed upon it (broken line). The entire curve has been displaced downwards by almost 2 mV from the broken line, because (i) the grain size of the reference standard is smaller than the reference standard used in the experiment that gave the result in Figure 26, and (ii) there was also more carbon in solid solution. The profile seen in Figure 26, thought to be due to recovery upto 400°C, is now no longer present, with the remaining profile of the curve almost unchanged. This implies that there are changes occurring in the reference standard that are similar to those occurring in the cold worked sample.

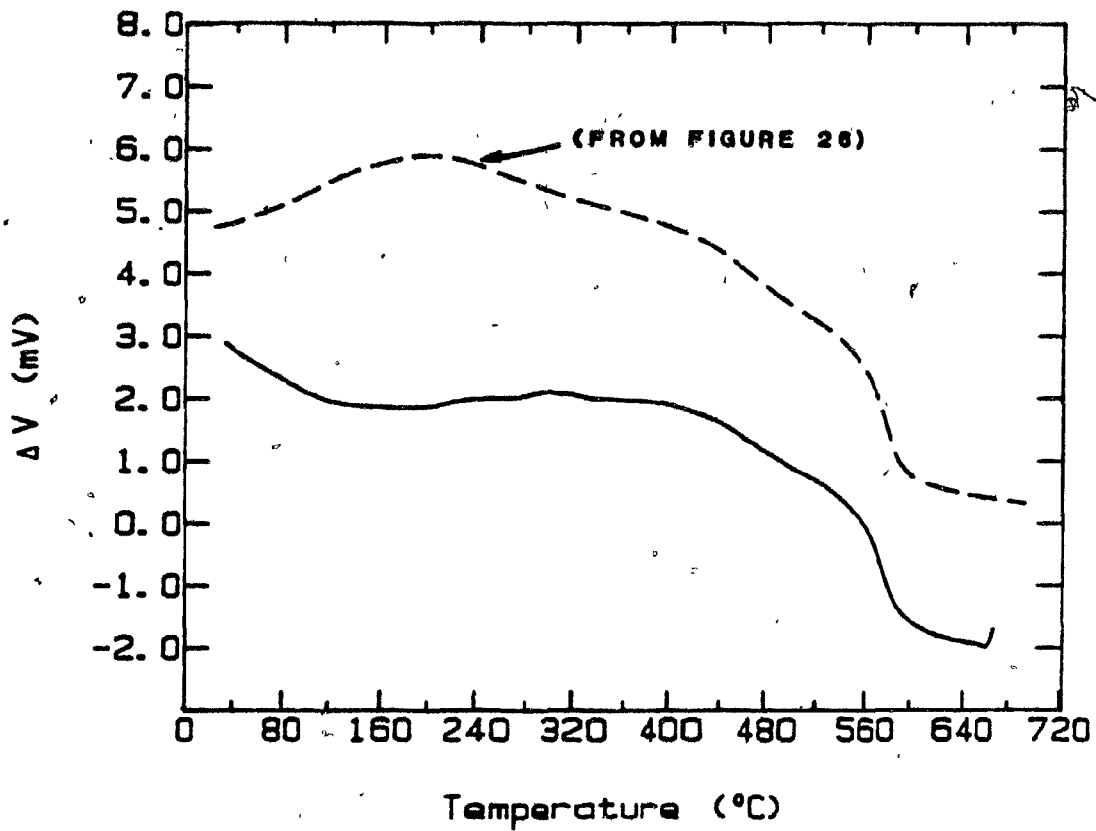


Figure 30. Reference Standard = Heat Treatment A.

4.3.1. EXPLANATION OF THE ANOMALOUS RECOVERY BEHAVIOR

The variation of the resistivity with temperature of a steel sample annealed to heat treatment A was investigated in the following experiment. Two samples of steel were annealed, one according to heat treatment A, the other to heat treatment B. These were then tested against each other, using the differential resistivity apparatus, under the same conditions as all the previous experiments. The result is seen in Figure 31, and shows a peak similar to that attributed to recovery in Figure 26.

The type of behaviour seen in Figure 31 has certainly been seen in aluminum-2% copper alloys by Federighi³⁶ (Figure 32). The peak seen in Figure 32 has been attributed to either of two processes: the retardation of the vacancy annihilation by the copper or the clustering of solute atoms, both of which would produce an increase in resistivity of the alloy. Similar atomic processes could apply in the annealing of the quenched steel reference standards and the cold worked steel samples, i.e. the clustering of carbon atoms in solid solution would produce an increase in electrical resistivity. Once the clusters reach a critical size, the matrix could no longer accommodate them, and thus the clusters would become incoherent precipitates of iron carbides. Once the precipitation starts, there would be a

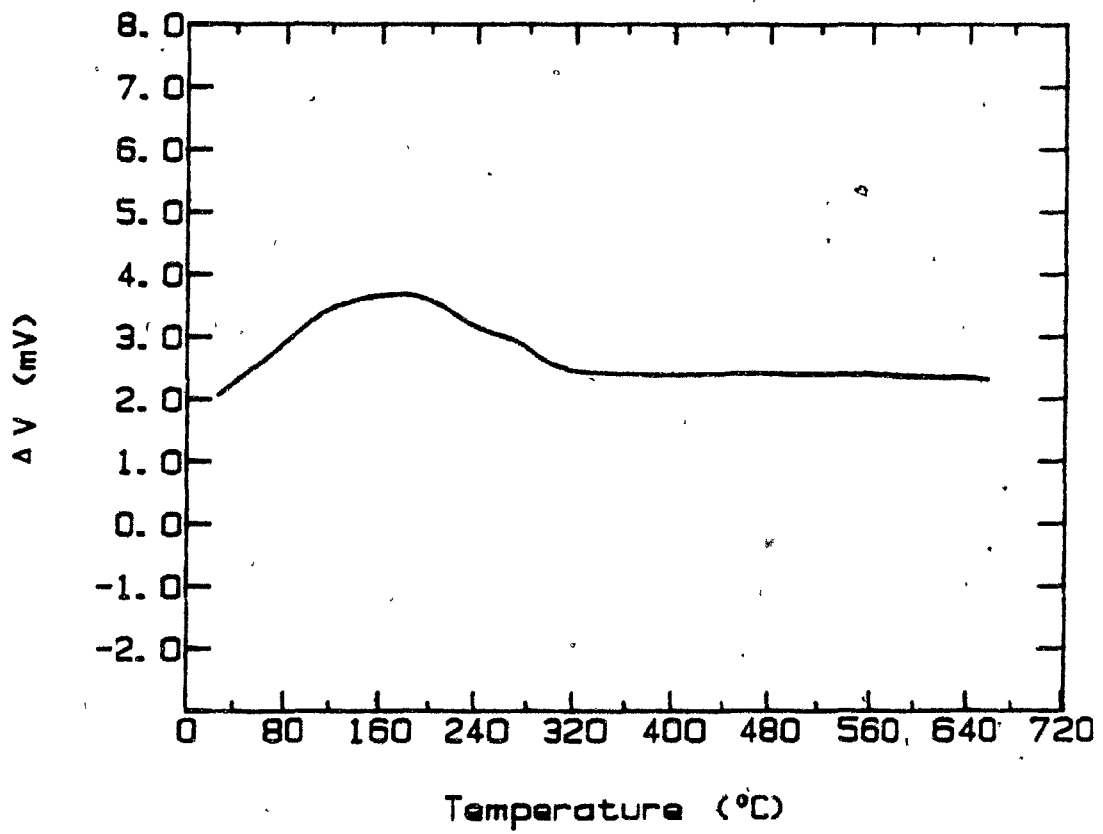


Figure 31. One Sample Annealed to Heat Treatment A, the Other Annealed to Heat Treatment B.

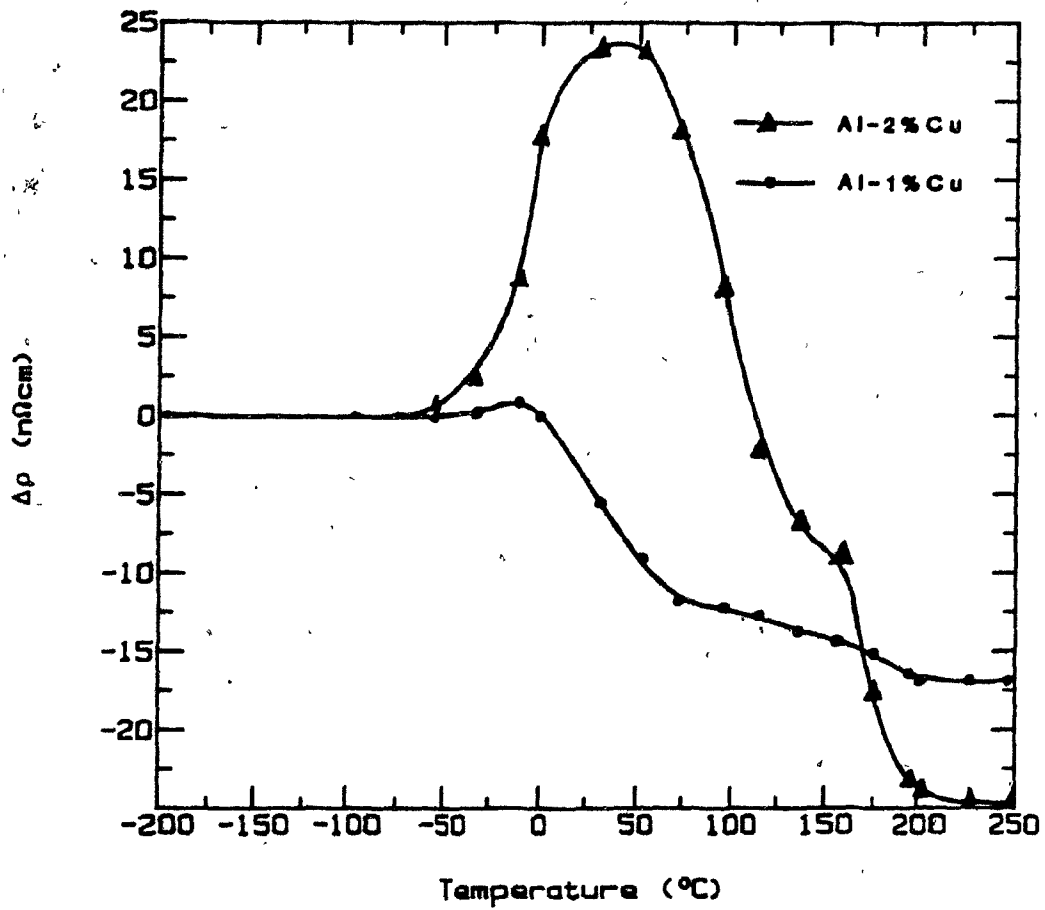


Figure 32. Change in Differential Resistivity ($\Delta\rho$) with Temperature for Al-Cu Alloys.

decrease in the electrical resistivity because of the decrease in the concentration of carbon atoms in the matrix which act as electron scattering points. In this case, the onset of precipitation would be at approximately 160°C, when the "recovery profile" seen in Figure 26 reaches a maximum.

Abe and Suzuki³⁷, using a thermoelectric power versus electrical conductivity plot, have identified three stages during recovery that would be consistent with the observations described above.

In the first stage, the dislocations rearrange themselves and a few will annihilate one another; the carbon atoms that become dissociated from the cementite segregate to the dislocations. As a consequence, the carbon is accommodated within the lattice interstices by virtue of the dislocations. These atomic processes, since they result in an increase in the number of electron scattering points, increase the resistivity of the steel.

The second stage begins when the dislocations are saturated with respect to carbon, and the dissociated carbon atoms occupy interstitial sites of the dislocation-free regions of the matrix.

In the final stage, the remaining cementite particles continue to dissolve into the completely recrystallized matrix.

These assumptions are consistent with the result seen in Figure 26. The resistivity of the cold worked sample therefore increases more rapidly than that of the reference standard because it has a higher dislocation density; hence the peak seen in Figure 26. Since it is the strain energy of the dislocations that provides the driving force for the dissociation of the carbon atoms, a higher dislocation density enhances this effect considerably. The rate of increase of the resistivity in the cold worked sample then decreases after about 230°C, due to decreases in the dislocation density and the number of vacancies during the rearrangement of dislocations in dislocation cells.

The behaviour explained above might also be attributed to the production and annihilation of vacancies. Pinned edge dislocations can only move out of their glide planes by climbing past the obstructions pinning them. Climb is carried out by the production of vacancies by dislocations which would, in turn, result in an increase in the resistivity. However, it is unlikely that climb takes place, since resistivity measurements show a greater response to changes in dissolved carbon than changes in the dislocation density³⁷.

4.4 RECRYSTALLIZATION

The successful observation of recrystallization has already been described in detail in Section 4.2. Particular reference was made to the derivative plot of ΔV which was able to determine the precise midpoint of recrystallization with a distinct peak.

4.5 GRAIN GROWTH

At present, the most important criteria for determining the end point of annealing for a fully annealed low carbon sheet steel is the end of recrystallization. This is primarily because there are no suitable "on-line" techniques available that are able to quantify the grain size of low carbon steel during batch annealing. A reliable grain size measuring device would be very beneficial for the purposes of quality control, and for the achievement of particular grain sizes required by various steel customers.

The differential resistivity technique, especially in the derivative/microprocessor/plotter form, is easily able to identify recovery and recrystallization as they occur but, so far, has not been able to clearly identify grain growth after recrystallization is complete.

Figure 33 shows the result of the change in ΔV as a function of time for a 4-hour isotherm at 700°C, using a reference standard annealed to heat treatment B.

Initially there is a small, but discernible, decrease in ΔV which, after about 10 minutes, does not change dramatically for the remainder of the isotherm. It was thought that if the initial decrease in ΔV was due to the grain size of the cold worked sample approaching the grain size of the reference standard, then this decrease could be enhanced by increasing the grain size of the reference standard. This was the principal object of heat treatments C, D, and E. These all produced large grain sizes, from 9μ to 31.5μ ; however, D and E did not provide the desired result for all the cycles of differential resistivity experiments, as will be shown below.

Figures 34(a) and 34(b) show the two results of the change in ΔV as a function of temperature, using reference standards annealed to heat treatments D and E respectively. Both of the results are compared with the result taken from Figure 26 (broken lines). The first point to note is that the room temperature value of ΔV in both cases is approximately 3 mV lower than that observed in Figure 26. This merely indicates that the resistivity of the reference standards has been increased due to the heat treatments they have received.

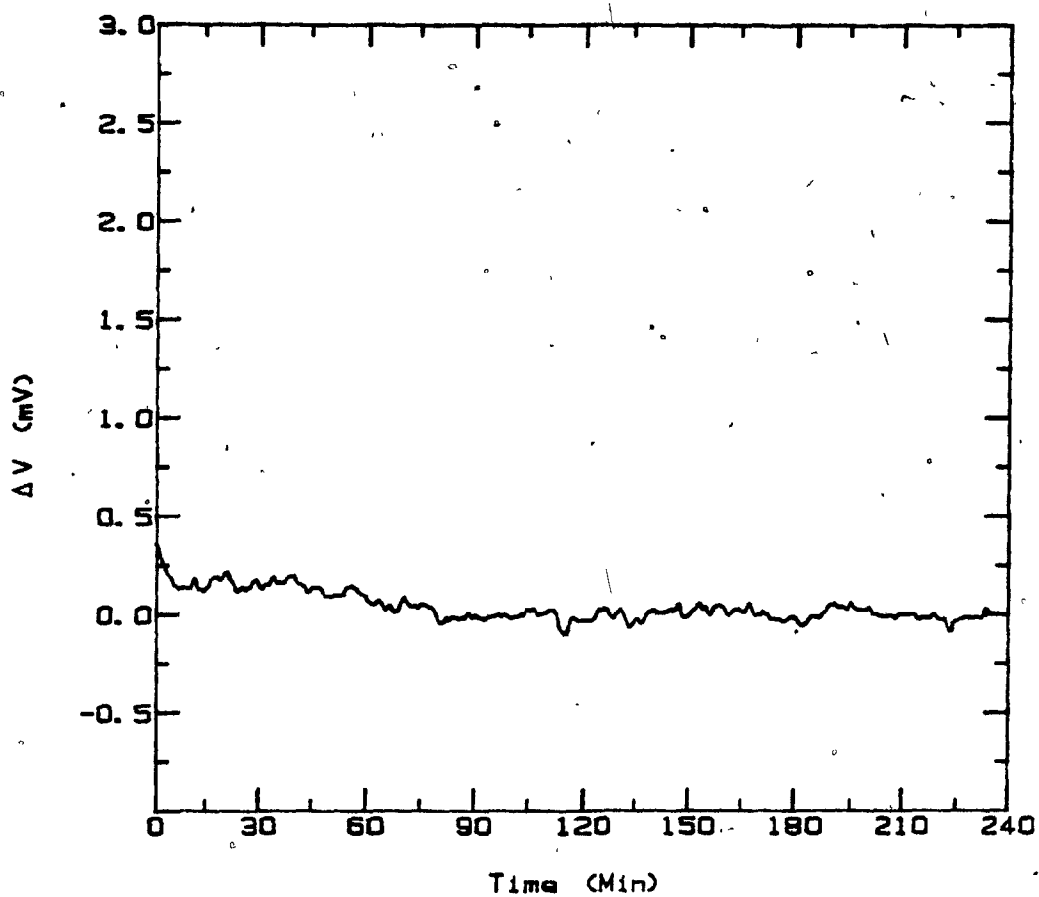


Figure 33. 4-Hour Isotherm Using a Reference Standard Annealed to Heat Treatment B.

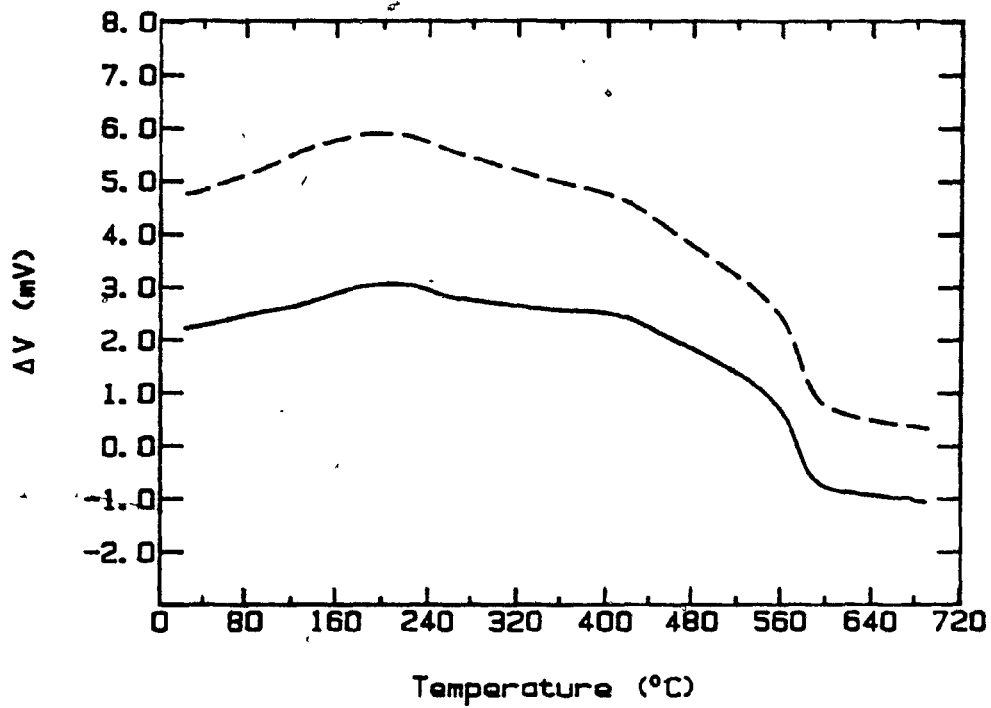


Figure 34(a). Reference Standard = Heat Treatment D.
(Grain size = 30.0μ)

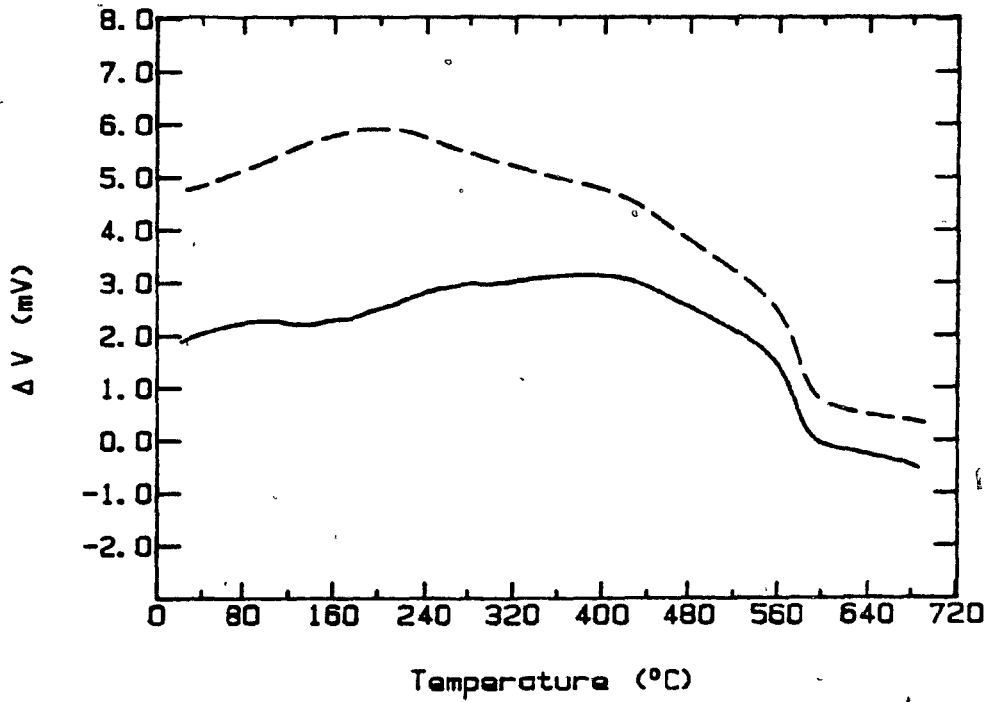


Figure 34(b). Reference Standard = Heat Treatment E.
(Grain size = 31.5μ)

The heat treatment of the reference standards took them up to 1100°C; at this temperature, their structure was austenite, which, when cooled, formed large grained ferrite and pearlite. This, however, is not the only consequence of austenitization, because the size of the magnetic domains (regions of unidirectional magnetic dipoles) is also increased when the steel is heated above the Curie temperature (770°C). The magnetic domain size has an important contribution to the overall electrical resistivity of steel³⁸, and it is thought that a significant increase in the magnetic domain size would result in an increase in this component. This would account for the decrease observed in ΔV values at room temperature, and subsequent temperatures in Figures 34(a) and 34(b).

Heat treatments D and E were investigated to determine their suitability for reference standards used for the investigation of grain growth. It was found that the change in ΔV with time during a 4-hour isotherm at 700°C, when using a reference standard annealed to heat treatment D, did not enhance the "visibility" of the grain growth. In this case, the decrease in ΔV was very small, approximately 0.25 mV (Figure 35), and it was thought that this was due to a combination of two opposing processes: grain growth occurring in the cold worked

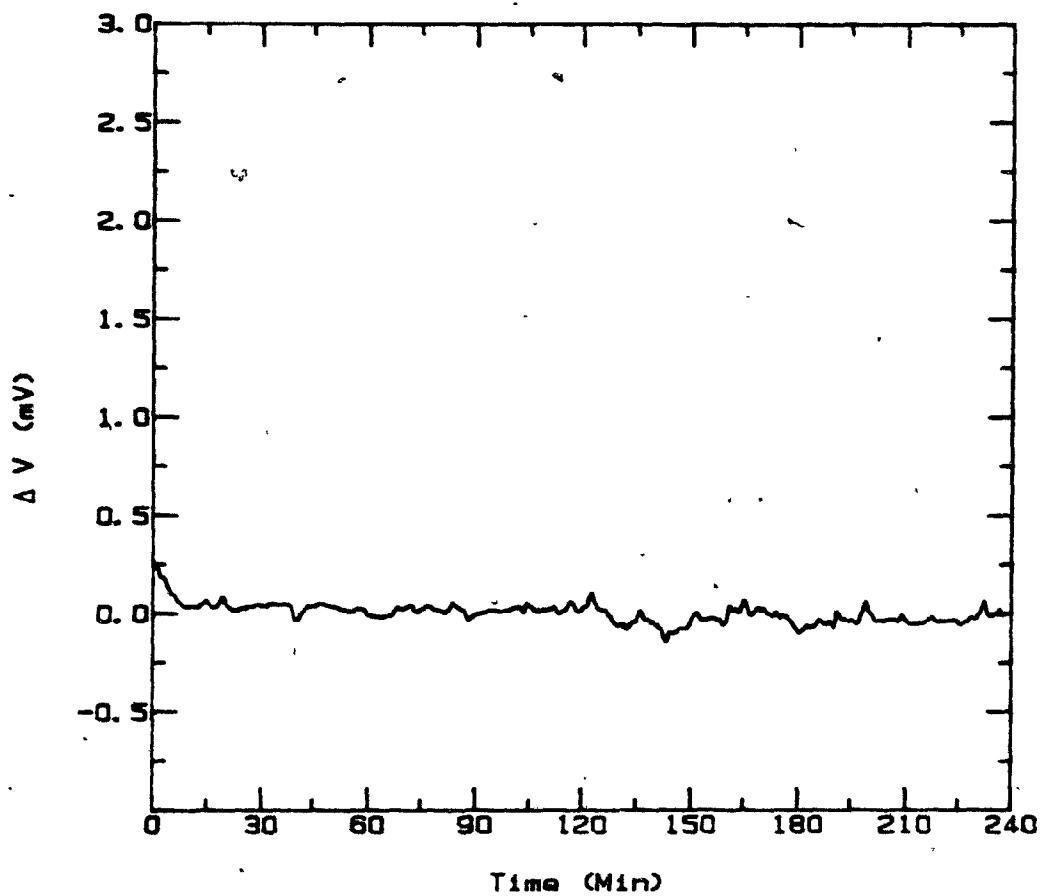


Figure 35. Change in ΔV over 4-Hour Isotherm
Reference Standard = Heat Treatment D.

sample, and spheroidization of the pearlite in the reference standard. The changes in resistivity that occur because of these processes are both very small. However, they are of the same order of magnitude and, since they are working in opposition, cancel each other out.

Similar experiments were carried out using reference standards annealed to heat treatment E (Figure 36). In this case, there was a much more noticeable decrease in ΔV during the first 30 minutes than was seen in Figure 35. However, the effect that the size of the magnetic domain had on the measurement of ΔV was not understood. Therefore, the decision was made to conduct the grain size investigation with reference standards annealed below the Curie temperature. Figure 37 illustrates the result obtained when using a reference standard annealed to heat treatment C.

Up until this point in the experimental program, the measurement of ΔV during isothermal annealing was severely clouded by a high degree of background noise. This was caused by the deposition of carbon on the probe and contact leads which, at 700°C, has a conductivity high enough to cause minor shorting of the leads. The carbon was deposited by the decomposition of traces of hydrocarbons that were present on the surface of the contact lead sheaths and the probe itself. The amount of

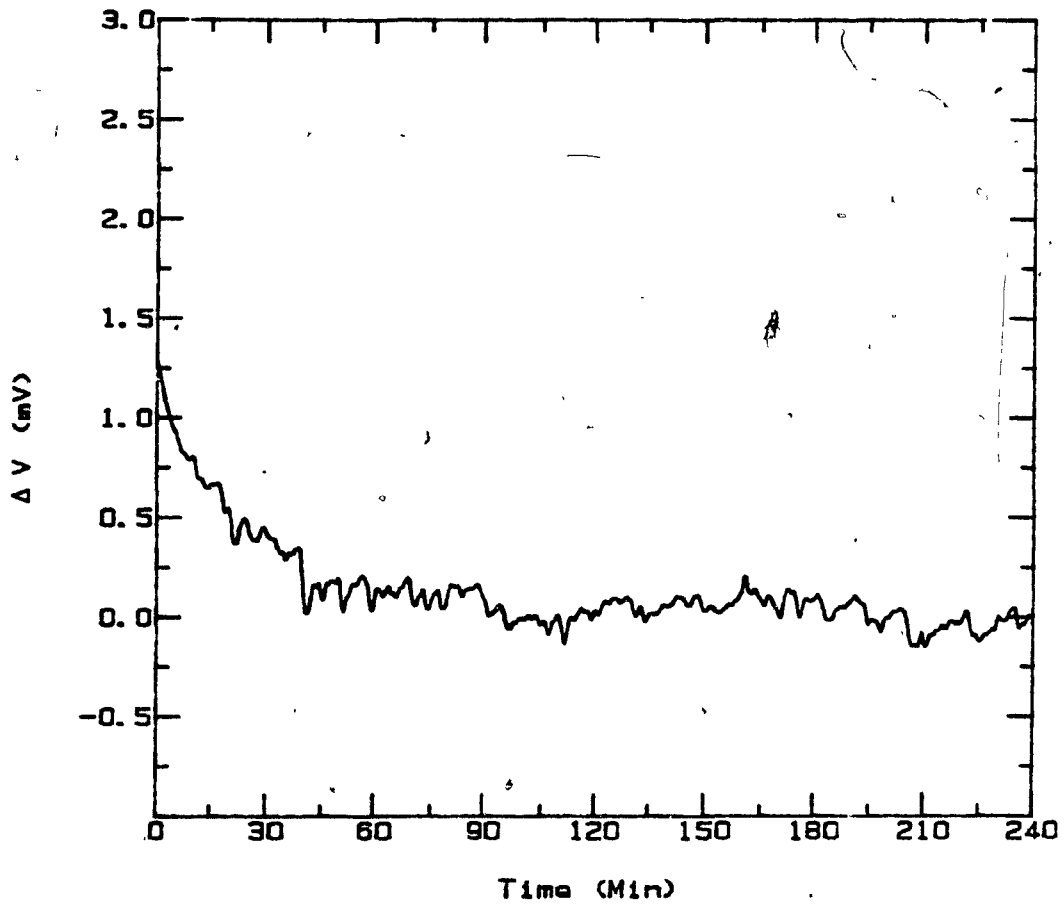


Figure 36. Change in ΔV Over 4-Hour Isotherm
Reference Standard = Heat Treatment E.

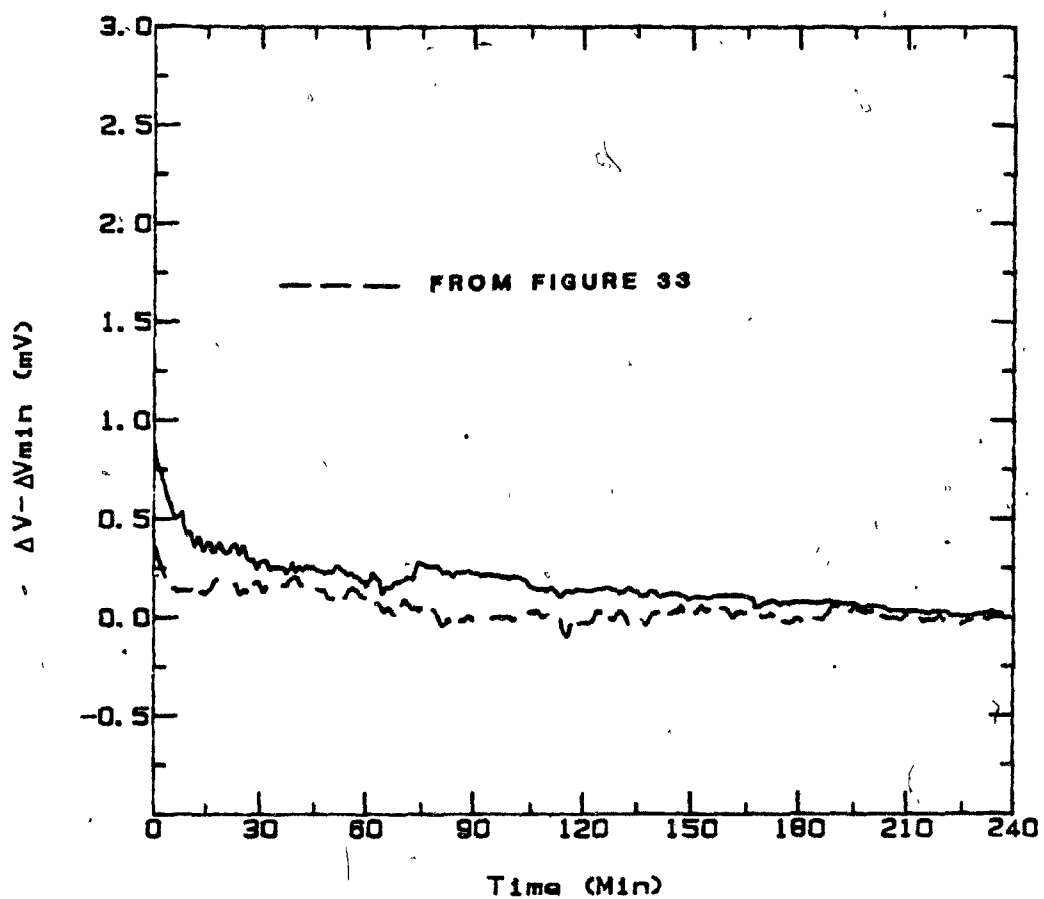


Figure 37. Change in ΔV Over 4-Hour Isotherm at 700°C.
Reference Standard = Heat Treatment C.

background noise was reduced, but not altogether removed, by ensuring that all the surfaces of the probe were grease-free. The noise level was reduced even more by mathematically smoothing the data during collection. The degree of smoothing, however, was limited so that it did not remove the real changes in ΔV that might be caused by a change in the grain size of the steel. As an example, Figure 37 shows how the variation of ΔV with time has been smoothed to remove as much background noise as possible.

The result illustrated in Figure 33 (broken line) was superimposed upon Figure 37, by taking the value of ΔV at the end of the isotherm in both cases, and using those points as reference point (ΔV_{MIN}). $\Delta V - \Delta V_{MIN}$ was then plotted against time to give the absolute change in ΔV during the isotherm. It is clear from Figure 37 that there is a more significant decrease in ΔV over the first 30 minutes, using reference standards annealed to heat treatment C than there is using those standards annealed to heat treatment B.

4.5.1 CORRELATION OF GRAIN GROWTH WITH DIFFERENTIAL RESISTIVITY MEASUREMENTS

The grain growth occurring within the steel during a 4-hour isothermal heat treatment at 700°C was determined from metallographic samples periodically

removed from the furnace. The change in grain size at 700°C is plotted as a function of time in Figure 38, along with the change in ΔV previously illustrated in Figure 37, over the same time period. The change in ΔV , ($\Delta V - \Delta V_{\text{MIN}}$) was then plotted as a function of the interfacial grain boundary area per unit volume (S_V) (Figure 39), using the equation³⁴ :

$$S_V = 2N_L \quad (10)$$

where N_L is the average number of intersections along a random line per unit length on a two-dimensional section. There appeared to be an approximately proportional relationship between the two measurements. By regression analysis on the data, a straight line with a correlation coefficient (r) of 0.973 (ideally this value should be 1), and a slope of 0.939×10^{-8} V.m. was obtained. From this value it was possible to calculate the specific resistivity for a grain boundary (i.e. the specific resistivity per grain boundary interfacial area), using the dimensions of the specimen, the current, and the amplification factor (see Appendix II for the calculation). The specific resistivity obtained was $167 \times 10^{-16} \Omega\text{m}^2$, which lies between the values of 140 to $230 \times 10^{-16} \Omega\text{m}^2$, reported by G. Lomard and M. Chevreton³⁹ for iron.

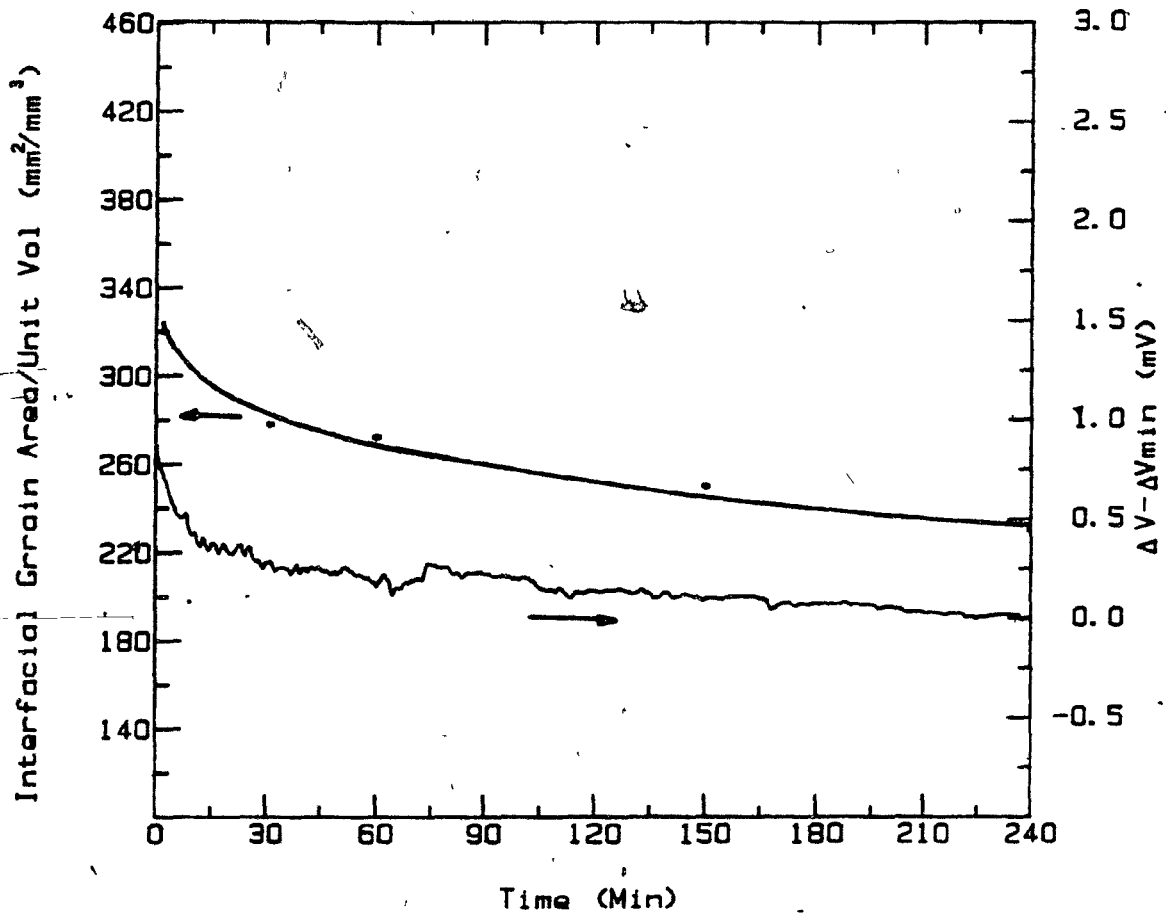


Figure 38. Change in ΔV and Grain Size During a 4-Hour Isothermal Heat Treatment at 700°C.

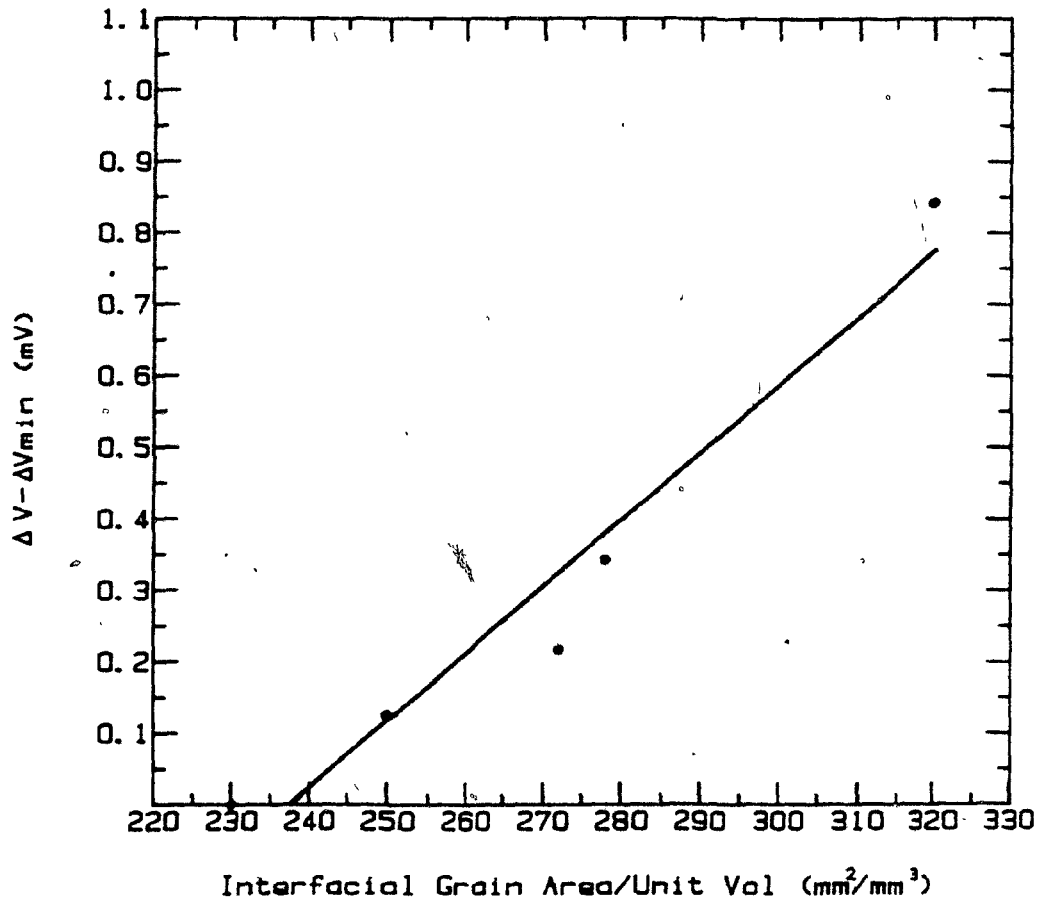


Figure 39. Change in ΔV as a Function of the Interfacial Grain Area.

Although the ΔV vs. time data (Figure 37) were mathematically smoothed to reduce the effect of background noise, the values of ΔV were still not as accurate as had been hoped. The measurement of ΔV would have been more precise if the amount of grain growth in the steel had been greater: the measurement of the change in ΔV would have been more prominent above the background noise. However, the low carbon steel used in this research project had a high inclusion content which obviously limited the amount of grain growth. It is therefore expected that the detection of grain growth using this technique would be more reliable with cleaner steels or with steels that recrystallized to a finer grain size (e.g. after very heavy cold rolling).

4.6 SIMULATION OF BATCH ANNEALING

Chapter 1 has already described the design and operation of a typical batch annealing furnace, and the long cycle times involved. The heating cycle, during which recrystallization takes place, and the soak times at temperature, are typically of the order of 16 and 8 hours respectively. It was hoped that the differential resistivity technique could be used (i) to detect recrystallization and particularly to identify its "end point" and (ii) to follow grain growth through to the end of the long cycle times involved in batch annealing.

Up to this point, all the experiments using the differential resistivity technique were carried out using a 2-hour heating cycle and a 4-hour isothermal anneal at 700°C, i.e. cycle times which are substantially shorter than those used industrially. To investigate any changes in the results that might be brought about by longer annealing times, experiments were carried out using a heating cycle time of 16 hours followed by an 8-hour isothermal anneal at 700°C. The reference standard that was used was annealed to heat treatment C, since this proved to be the most appropriate during the heating and isothermal cycles, and giving the best indication of grain growth. Figures 40 (a) and (b) are the results obtained for both cycles. These figures show that there is little difference between these and the experiments conducted with shorter cycle times. Thus, the results obtained and the comments made so far would apply to the long annealing times used in industrial annealing.

4.7 APPLICATION TO INDUSTRIAL ANNEALING

The studies indicate that a differential resistivity sensor could be applied to the batch annealing of steel. Chapter 2 pointed out that, as yet, there is no direct means by which the metallurgical (microstructural) state of the steel can be determined in a batch annealing

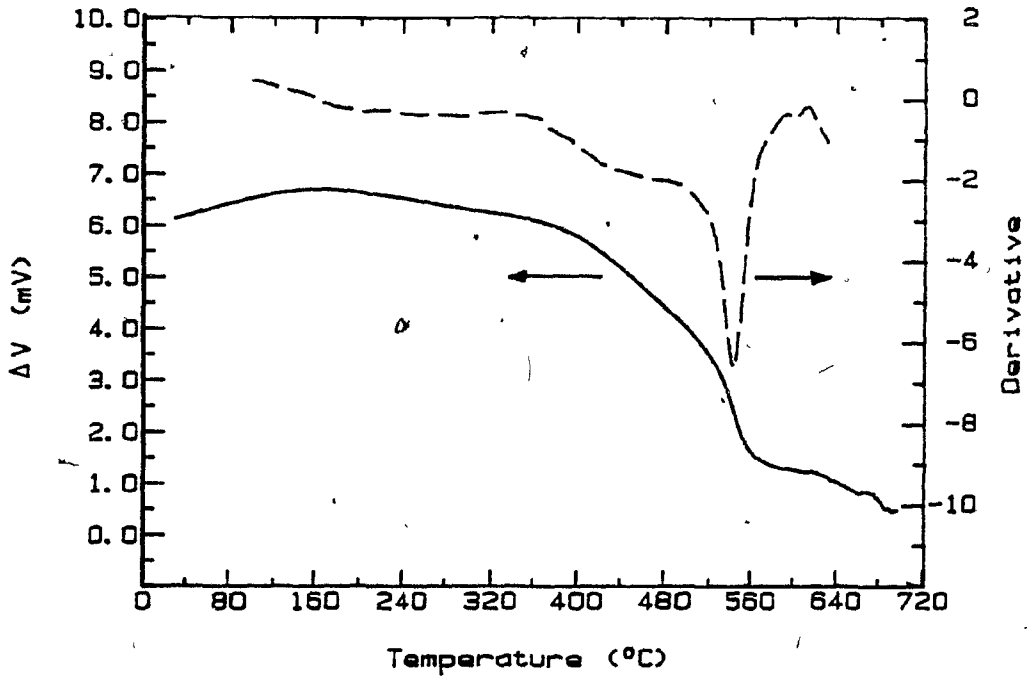


Figure 40(a). Change in ΔV and $d \Delta V/dT$ with Increasing Temperature (16-Hour Treatment)

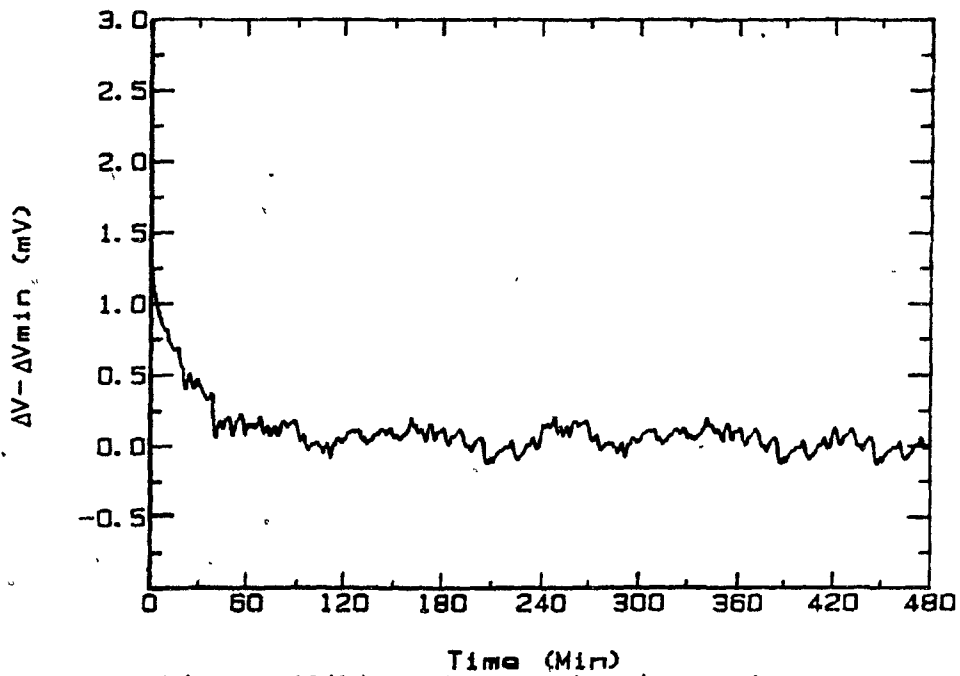


Figure 40(b). Changes in ΔV During 8-Hour Isothermal Anneal at 700°C.

furnace. The coils of steel within the furnace are tightly wrapped (except in the much less common technique of open coil annealing, in which the individual turns of the coils are kept slightly apart to allow for better heat transfer) and it would be most useful to know the stage of annealing of the steel, particularly within the coils situated at the coolest locations (if necessary using several sensors) in the furnace. However, the dimensions of the probe (approximately 1.5cm x 1.5cm x 6cm) might make this direct approach inconvenient (or at least less acceptable to operators who are used to dealing with much less bulky thermocouples). A possible solution to this difficulty is the arrangement shown in Figure 41. Here, a thermocouple is placed within the coil wraps (or wherever the microstructural information is needed) and is connected to a controller which precisely reproduces, with no time delay, the temperature/time cycle of this location in a remotely situated laboratory sized "slave" furnace. The differential resistivity probe is then placed in this slave furnace. Since the samples in the resistivity probe would be selected from the same material as that of the coils, the changes in resistivity, and hence microstructure, would correspond exactly with that of the steel adjacent to the sensing thermocouple in the batch annealing furnace.

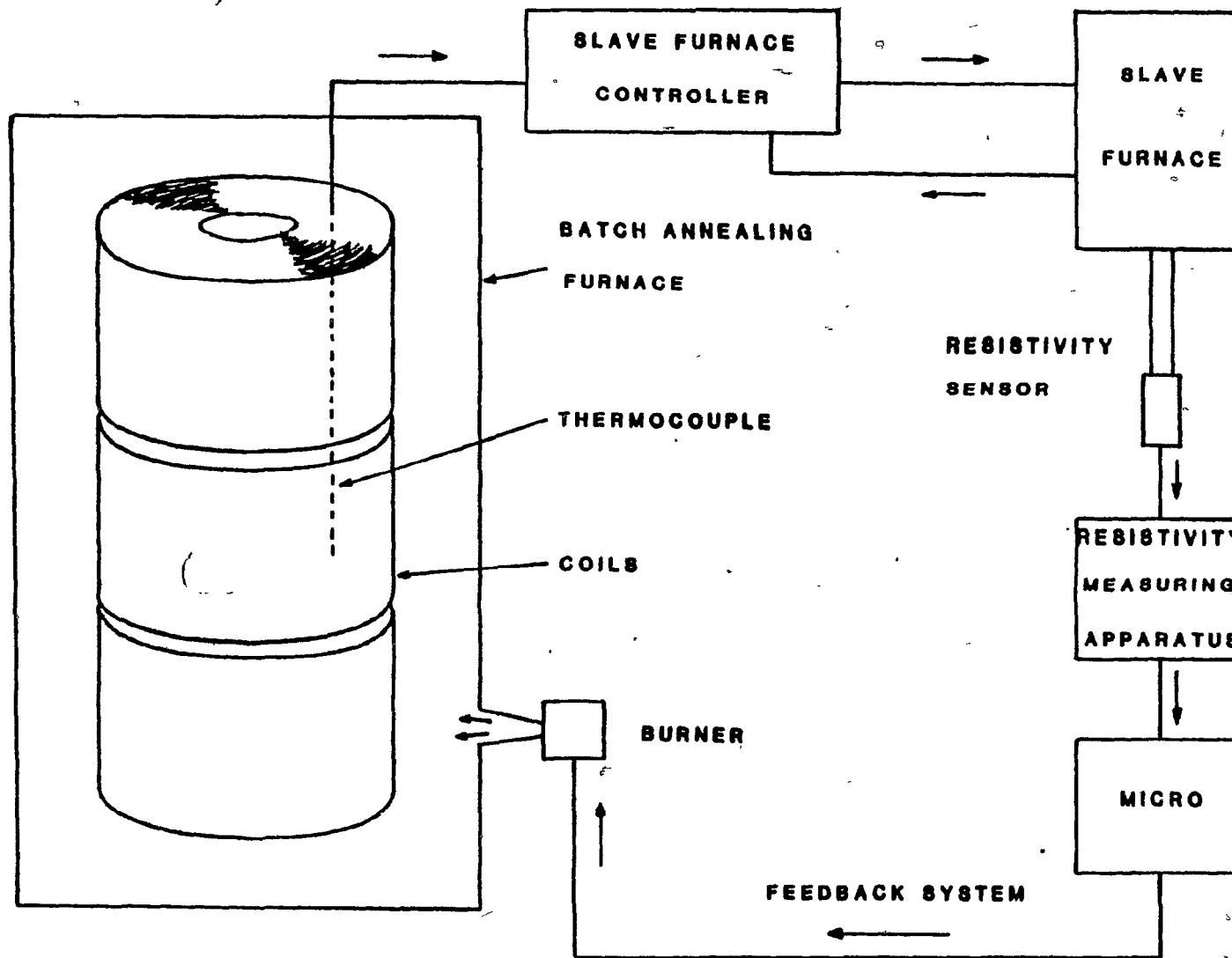


Figure 41. Schematic Diagram Showing How the Differential Resistivity Sensor Might Be Incorporated in a Batch Annealing Furnace Operation.

Recent discussions with representatives of major steel-making companies have indicated that their most important need is the knowledge of the end point of recrystallization and not the actual grain size of the steel. As this project has shown, the differential resistivity technique can clearly define recovery, recrystallization, the end point of recrystallization, and can at least indicate grain growth.

The derivative curve shows such a definite peak at the point of recrystallization that it would be an excellent parameter to use in the operation of an industrial batch annealing furnace. The operator of the furnace, or even a computer control unit, could act upon the occurrence of the derivative peak to shut down the burners of the furnace and commence the cooling cycle.

Determining the precise moment to shut down the furnace in this way would mean that the fastest turn-around time possible had been achieved which, in turn, would give improved efficiency of fuel usage. The ability to measure the grain size at the end of the annealing process (at least approximately) is an added bonus and would be particularly useful should the grain size of the steel have to be guaranteed.

Chapter 1.2 outlined the advancements that have been developed to make the batch annealing furnace a more

efficient and reliable process. However, it was pointed out that there was no sensor currently available that is capable of determining the actual progress of annealing. This research project has thus successfully developed a sensor capable of continuously monitoring the entire annealing process for low carbon steels with particular application to the control of batch annealing furnaces.

CHAPTER 5

5.1 CONCLUSIONS

1. Differential resistivity measurements have been used to continuously monitor the microstructural and property changes which occur during annealing of a cold worked low carbon steel at temperatures up to 700°C.
2. The recovery, recrystallization, and grain growth stages can all be clearly identified during annealing.
3. The initial increase in the differential resistivity during recovery is attributed to the dissociation of carbon atoms, and their subsequent segregation to dislocations.
4. The recrystallization stage is particularly well defined in the form of a derivative ΔV plot.
5. Grain growth could be followed after recrystallization, and a value of $167 \times 10^{-16} \Omega m^2$ was obtained for the specific resistivity per interfacial grain boundary area for the low carbon steel.
6. The differential resistivity technique is thought to be easily adaptable to industrial, batch furnace control, particularly using the idea of a "slave furnace".

CHAPTER 6

6.1 SUGGESTIONS FOR FURTHER WORK

1. Test the response of the technique to a variety of commercial grade low carbon steels.
2. Improve the accuracy of the technique for the continuous monitoring of grain growth during annealing.
3. Carry out industrial trials using the differential resistivity technique to monitor a batch annealing furnace and evaluate its suitability as a means of furnace control.
4. Adapt the technique to the heat treatment of other high volume production alloys such as copper, nickel, and aluminum alloys.

APPENDIX I

```

LIST RECRYST.BAS
10      X1%=1250      :      X2%=9200
20      Y1%=1164      :      Y2%=7163
30      OPEN 'PRINT' AS 0
40      SZ = -200      :      BZ = 600
50      PRINT 'FIRST AND LAST DELTA V      = -200 , 600'
60      PRINT
70      S1%= 0.0      :      L1% = 720
80      PRINT 'FIRST AND LAST TEMPERATURE = 0 , 720'
90      PRINT
100     S2% = -10      :      B2% = 1
110     PRINT 'FIRST & LAST DERIVATIVE      = -10 , 1'
120     PRINT
130     PRINT 'DO YOU WISH TO CHANGE ANY OF THE ABOVE ?'
140     INPUT A1$
150     IF A1$ .EQ. 'Y' THEN GOTO 200
160     INPUT 'INPUT FIRST & LAST DELTA V';S2%;B2%
170     INPUT 'INPUT FIRST & LAST SLOPE ' ;S1%;L1%
180     INPUT 'INPUT FIRST & LAST TEMP ' ;S1%;L1%
190     PRINT
200     REM LINE TYPE IS NULL
210     LET LT$ = ''
220     M3=1700./(B2%-S2%)
230     M2=1700./(B%-S%)
240     B1%=(L1%-S1%)*10
250     DIM X(21),Y(21)
260     I1% = HEX('7E04')
270     PRINT 'INPUT TEMPERATURE VS. DELTA V FILENAME'
280     INPUT LINE F$
290     PRINT 'INPUT TEMPERATURE VS. D(DELTA V)/DT FILENAME'
300     INPUT LINE G$
310     OPEN NEW F$ AS 1
320     OPEN NEW G$ AS 2
330     PRINT 'CHANNEL LIMITS ENTERED ARE 3,4'
340     LET C1%=3
350     LET C2%=4
360     POKE HEX ('B002'),C1%
370     POKE HEX ('B003'),C2%
380     INPUT 'INPUT INTERVAL BETWEEN SAMPLES IN SECONDS';N%
390     I1% = 1000*N%
400     REM *****BEGIN DATA ACQUISITION FROM ASSEMBLER*****
410     DPOKE HEX ('B004'),I1%
420     INPUT 'INPUT DURATION OF EXPERIMENT IN MINUTES';M1
430     M1 = M1 * 60
440     LET J = 0
450     DPOKE HEX ('BFFD'),HEX ('B085')

```

```

460 LET Z = 0
470 AA = USR(0)
480 IZ = IIZ
490 X$ = " "
500 Y1$ = " "
510 Y$ = CHR$(PEEK(IZ))
520 IZ = IZ + 1
530 IF Y$ = ':' THEN 610
540 IF Y$ = '/' THEN 590
550 X$ = X$ + Y$
560 IF X$ = '+OVLOAD' THEN GOSUB 1700
570 IF X$ = '+OVLOAD' THEN GOTO 470
580 GOTO 510
590 LET V3 = VAL(X$)
600 GOTO 490
610 LET V2 = VAL(X$)
620 Z = Z + 1
630 V1 = V3 * 1000
640 IF V1 < 45150. THEN 680
650 IF V1 < 64927. THEN 750
660 IF V1 < 76358. THEN 820
670 REM CAN PUT A THERMOCOUPLE OVERLOAD MESSAGE HERE
680 REM E TYPE COEFFICIENTS FROM 0 TO 600 CENTIGRADE
690 A0 = 0.0
700 A1 = 1.6410783E-2
710 A2 = -1.3560189E-7
720 A3 = 1.8630042E-12
730 A4 = -8.5535337E-18
740 GOTO 890
750 REM 600 TO 850 CENTIGRADE
760 A0 = 2.5192188E+1
770 A1 = 1.3909529E-2
780 A2 = -4.7201133E-8
790 A3 = 5.5638781E-13
800 A4 = -1.7775228E-18
810 GOTO 890
820 REM 850 TO 1000 CENTIGRADE
830 A0 = -7.1102114E+2
840 A1 = 5.6554599E-2
850 A2 = -9.7013068E-7
860 A3 = 9.3938146E-12
870 A4 = -3.3333675E-17
880 REM THERMOCOUPLE POLYNOMIAL
890 T1 = (((((A4*V1+A3)*V1+A2)*V1+A1)*V1+A0)
900 LET V2 = V2 * 1000
910 LET V2$ = STR$(V2)
920 LET T1$ = STR$(T1)
930 X1$ = T1$ + Y1$ + V2$
940 REM STORE TEMPERATURE & VOLTAGE DATA ON DISC
950 PRINT #1, X1$
960 PRINT USING '###.## ###.##', TAB(20) T1, TAB(30) V2

```

```

470 REM ON FIRST DATA POINT INITIALIZE PLOTTER
980 IF Z <= 1 THEN GOSUB 1610
990 TX = M2 * (V2-SZ)
1000 KZ = 10 * (T1-S1Z)
1010 IF T1 < S1Z THEN 1060
1020 IF T1 < L1Z THEN 1060
1030 PRINT #0, 'SP1;'
1040 REM PLOT TEMP & VOLTAGE DATA
1050 PRINT #0, 'PA;'KZ;TZ;'PD;PU;PA';
1060 J = J + 1
1070 IF J > 20 THEN GOSUB 1740
1080 X(J) = T1
1090 Y(J) = V2
1100 M1 = M1 - NZ
1110 IF M1 <= 0 THEN 1500
1120 IF J > 20 THEN GOTO 470
1130 IF Z > 1440 THEN 470
1140 IF Z > 144 THEN 470
1150 IF J > 20 THEN 470
1160 REM BEGIN CALCULATING THE DERIVATIVE
1170 FOR J = 1 TO 20
1180 S1 = S1 + X(J)
1190 S2 = S2 + Y(J)
1200 S3 = S3 + (X(J) * Y(J))
1210 S4 = S4 + (X(J)^2)
1220 NEXT J
1230 REM S5 = THE SLOPE OR DERIVATIVE AT THE POINT S1/20
1240 S6 = ((20 * S3)-(S1 * S2))
1250 S7 = ((20 * S4)-(S1^2))
1260 IF S7=0 THEN 1390
1270 S5 = S6/S7
1280 T2 = S1/20
1290 S5%=STR$(S5)
1300 T2%=STR$(T2)
1310 X7%=T2%+Y1%+S5%
1320 REM STORE TEMPERATURE & DERIVATIVE ON DISC
1330 PRINT #2,X7%
1340 PRINT USING '###.## ###.##',TAB(40)T2,TAB(50)S5
1350 TX = M3 * (S5-S2Z)
1360 PRINT #0, 'SP2;'
1370 REM PLOT TEMP & DERIVATIVE
1380 PRINT #0, 'PA;'KZ;TZ;'PD;PU;PA';
1390 FOR K = 6 TO 20
1400 LET X(K-5) = X(K)
1410 LET Y(K-5) = Y(K)
1420 NEXT K
1430 LET J = 15
1440 LET S1 = 0
1450 LET S2 = 0
1460 LET S3 = 0
1470 LET S4 = 0

```

```

1480 LET S5 = 0
1490 GOTO 470
1500 DPOKE HEX('BFFD'),HEX('BOE0')
1510 REM STOP ALL INTERRUPTS
1520 PRINT #0, 'SPO;'
1530 PRINT #0, 'IN;' : CLOSE 0,1,2
1540 AA = USR(0)
1550 PRINT 'EXPERIMENT IS OVER';CHR$(07)
1560 DPOKE HEX('BFFD'),HEX('CD03')
1570 AA = USR(0)
1580 END
1590 REM *****
1600 REM INITIALIZE PLOTTER
1610 TZ = M2 * (V2-SZ)
1620 KZ = 10 * (T1-S1Z)
1630 PRINT #0, 'IN;IP';X1Z;Y1Z;X2Z;Y2Z;
1640 PRINT #0, 'IW';X1Z;Y1Z;X2Z;Y2Z;
1650 PRINT #0, 'SCO';E1Z;'0,';1700;
1660 PRINT #0, 'PA';KZ;TZ;'PU;PD;PA';
1670 PRINT #0, 'LT';LT$;'PA';
1680 RETURN
1690 REM *****
1700 PRINT
1710 PRINT '*****OVERLOAD OUTPUT*****'
1720 RETURN
1730 REM *****
1740 FOR K = 6 TO 20
1750 LET X(K-5)=X(K)
1760 LET Y(K-5)=Y(K)
1770 NEXT K
1780 J = 15
1790 RETURN

```

+++

APPENDIX II

Dimensions of specimen seen in Figure 18(b)

Length between contacts	(L)	=	25.7	x	10 ⁻³	m
Width	(W)	=	2.70	x	10 ⁻³	m
Thickness	(t)	=	0.43	x	10 ⁻³	m
Current	(I)	=	0.05A			
Amplification factor*	(A _f)	=	507			
Slope of line (Figure 39)	(V _m)	=	0.939	x	10 ⁻⁸	V.m.

Specific Resistivity/Interfacial grain boundary area

$$\begin{aligned}
 &= \frac{V_m}{I} \times \frac{Wt}{L} \times \frac{1}{507} \\
 &= \frac{V_m \times (2.7 \times 10^{-3}) \times (0.43 \times 10^{-3})}{0.05 \times (25.7 \times 10^{-3}) \times 507} \\
 &= V_m \times 1.782 \times 10^{-6} \\
 &= \underline{167 \times 10^{-16}} \Omega m^2
 \end{aligned}$$

* The amplification factor was the amplification of the potential drop across the contact points on the samples by the transformers T₁ and T₂ in Figure 18(a).

Dimensions of specimen seen in Figure 18(b)

Length between contacts (L) = 25.7×10^{-3} m

Width (W) = 2.70×10^{-3} m

Thickness (t) = 0.43×10^{-3} m

Current (I) = 0.05A

Amplification factor* (A_f) = 507

Slope of line (Figure 39) (V_m) = 0.939×10^{-8} V.m.

Specific Resistivity/Interfacial grain boundary area

$$\begin{aligned}
 &= \frac{V_m}{I} \times \frac{Wt}{L} \times \frac{1}{507} \\
 &= V_m \times \frac{(2.7 \times 10^{-3}) \times (0.43 \times 10^{-3})}{0.05 \times (25.7 \times 10^{-3}) \times 507} \\
 &= V_m \times 1.782 \times 10^{-6} \\
 &= \frac{167 \times 10^{-16}}{\Omega m^2}
 \end{aligned}$$

* The amplification factor was the amplification of the potential drop across the contact points on the samples by the transformers T₁ and T₂ in Figure 18(a).

APPENDIX III .

PATENT PROTECTION

Patent protection is presently being sought for the differential resistivity technique and its possible applications.

REFERENCES

1. J. Frenckel, Z. Physik 37 (1926), 572
2. Thomas, "Electron Microscopy and Strength of Crystals" (1963), Interscience, p. 793
3. Silcock, Heal & Hardy, J. Inst. Metals 82 (1953-54), 239
4. W.G. Burgers, C.A. Verbraak, Acta Met 5 (1957), 765
5. W.G. Burgers, C.A. Verbraak, Acta Met 6 (1959), 580
6. W.J.H. Slarkhorst, Acta Met, 23 (1975), 301
7. Fujita, J. Physics Soc., Japan, 16 (1961), 397
8. C.J.E. Smith, J. Inst. Metals, 74 (1948), 747
9. C.J.E. Smith, I.L.Dillamore, Metal. Sci., 4 (1970), 161
10. P. Faivre, Ph.D. Thesis, University of Sussex, (1973), P. Faivre, R.D. Doherty submitted to J. Mat. Sci.
11. P.A. Beck, 'Metal Interfaces', A.S.M. Metals Park Ohio (1952), p. 208
12. Bailey Hirsch, Proc. Roy. Soc. A 267 (1962)
13. C.S. Smith, Trans AIME 75 (1948), 15
14. Chase Econometrics World Steel Outlook, February 1983
15. P.R. Mould, J. of Metals, May 1982, 18-28
16. Iron & Steel International, June 1980, 149-163
17. Industrial Heating, October 1980, 8-12
18. Terzic, Archiv fur das Eisenhüttenwesen, Jan. 1971, 1-5
19. D.S. Harries, R.I.L. Guthrie, CIM Bulletin 75 (1975), 117-121

20. H.P. Wittler, *Stahl und Eisen* 100 (1980)
21. D. Preston, N.J. Grant, *Trans AIME* 221 (1961), 164
22. L.M. Clareborough, M.E. Hargreaves, and G.W. West, *Phil. Mag. Ser. 8*, 1, No. 6 (1956), 528-536
23. B.F. Decker, D. Harber, *Trans AIME* 188 (1950) 887
24. A. Lucci, G. Riontino, G. Venturello, *Thermochemie C.N.R.S., Paris* (1972), p. 391
25. R.L. Smith, W.N. Reynolds, H.N.G. Wadley, *Met. Sci.* 15 (1981), 554
26. H.J. Hansen, *J. Metals* 18 (1966), 1131
27. I.B. MacConnack, B.K. Tanner, *J. Appl. Cryst.* 11 (1978), 40
28. S.D. Dlubec, O. Brummer, N. Meyendorf, *Solid State Communications* 27 (1978), 40
29. K. Tanaka, T. Watanabe, *J. App. Phys.* 11 (1972), 1429-1439
30. Y. Meyzaud, P. Parriere, *Man. Sci. Rev. Met.* 7-8 (1974), 416-422
31. R.A.L. Drew, B. Muir, W.M. Williams, *Met. Trans. A* 14, 175-182
32. B. Muir, J. Strom-Olsen, *J. Phys. Ed.* 9 (1976), 163
33. *Metals Handbook*, 9th Edition, Vol. 2, p. 284, ASM 1979
34. S.A. Argyropoulos, R.S. Valiveri, B.M. Closset, *J. Metals* 35 (1983), 30-35
35. L.J. Cuddy, *Phil. Mag.* 12 (1965), 855
36. T. Federighi, "Resistometric Researches on Point Defects in Quenched Al and Al-Rich Alloys," Conference on "Lattice Defects in Quenched Metals," Academic Press, Ed. R.M.J. Cotterill, M. Doyama, J.J. Jackson, M. Meshii (1965)

37. H. Abe, T. Suzuki, Trans. ISIJ 19 (1979), 689
38. S. Araj, B.F. Oliver, J.T. Michalak, J. App. Phys. 38 (1967), 1676
39. G. Lormand, M. Chevreton, Phil. Mag. B 44, No. 3 (1981), 389-404